FZR

FZR
129

Forschungszentrum Rossendorf

Institute of Ion Beam Physics and Materials Research

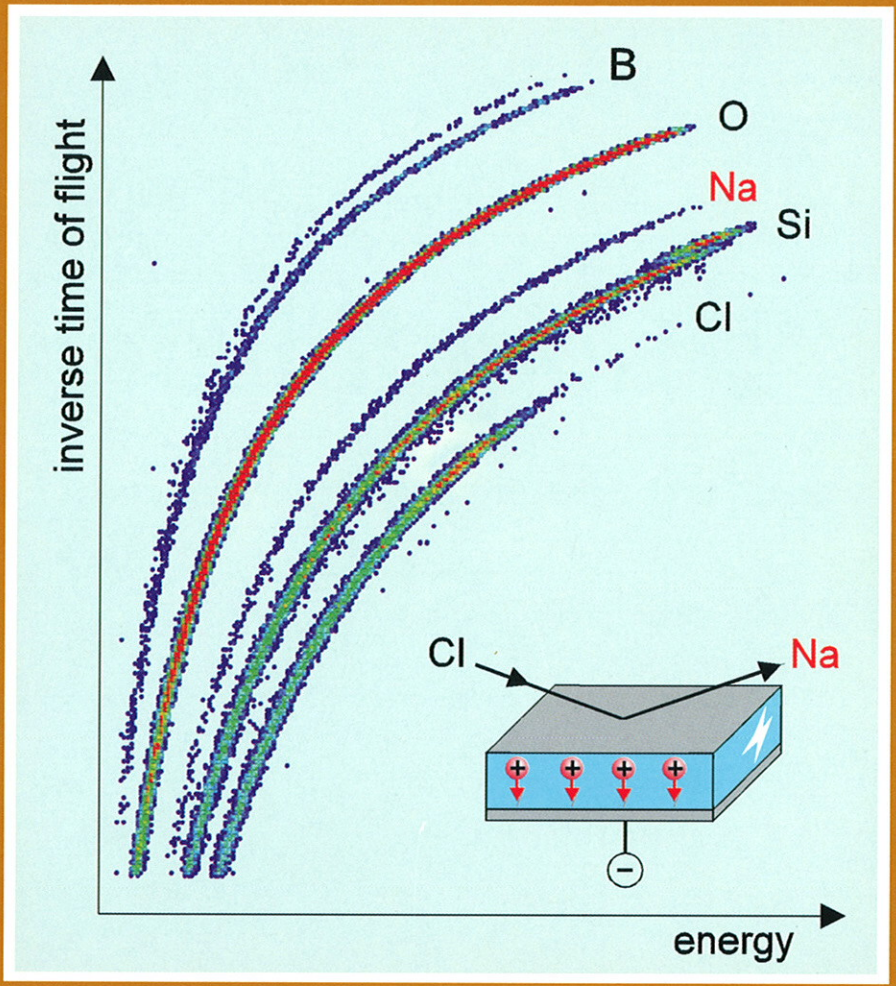

Annual Report 1995

Postfach 510119
D-01314 Dresden, Germany
Tel. +49-351-260-22 45
Fax +49-351-260-32 85

Forschungszentrum
D 120
-Bibliothek-
Rossendorf e.V.

BRD

FORSCHUNGSZENTRUM ROSSENDORF
INSTITUT FÜR IONENSTRAHLPHYSIK UND
MATERIALFORSCHUNG

Annual Report 1995

Editors:
W. Möller, E. Wieser, J. von Borany

FZR-129
März 1996

For further information on the research projects described in the present annual report, please address the director or one of the authors at the institute.

Front cover:
Using in situ elastic recoil detection analysis (with 30 MeV Cl ions), near surface transport phenomena in glasses can be monitored in real time. From a sequence of mass discriminated multielement spectra the evolution in time of the glass stoichiometry is determined within a 1 µm thick surface layer. The measurements were performed to investigate the fundamental processes of anodic glass-silicon bonding (see page 45).

Postal address:

Postfach 51 01 19
D-01314 Dresden
Germany

Telecommunication:

Tel.: +49 351 260 2245
Fax: +49 351 260 3285
E-mail moellerw@fz-rossendorf.de

Contents

Statistics

Preface

The Research Center Rossendorf (Forschungszentrum Rossendorf, FZR) represents the largest governmental research organization in the "new" states of Germany. A total staff of about 600 employees (440 permanent) is devoted to the main directions of research in the fields of materials science and biomedicine-chemistry, and additionally nuclear physics. Correspondingly, the center houses five institutes of Ion Beam Physics and Materials Research, Safety Research, Radiochemistry, Bioinorganic and Radiopharmaceutical Chemistry, and Nuclear and Hadron Physics. Based on former activities before the foundation of FZR in 1992, the institutes have developed in the recent years towards a high scientific and technical standard also on an international scale, and established themselves in their communities by a rising number of external contacts and collaborations.

The Institute of Ion Beam Physics and Materials Research (about 120 employees in total), is devoted to the application of ion beams for the modification and the analysis of near-surface layers of solids. The research activities aim at combining closely basic studies and investigations of technological application. For the modification of materials, a broad range of ion-based techniques is available, such as ion implantation, and ion- and plasma-assisted thin film deposition. Correspondingly, characteristic ion energies are available from about 10 eV for plasma processes to several 10 MeV for heavy ion implantation and ion beam analysis. With ions provided in this energy range, the institute represents the largest organization of this kind in Germany. Therefore, the German Science Council confirmed its role as a national ion beam center in the 1994 recommendation for the future of the FZR.

Fast ions are employed to form new phases and structures in near-surface layers of solids, which in connection with the deliberate generation of radiation defects, determine or modify the surface properties of conventional or new materials. Correspondingly, new fields of application open in electronics, optics, mechanics, and medical technology.

High energy ion beam analysis is employed as an important tool for the characterization of near-surface layers, both for the institute's scientific program and for external services. The institute offers a broad range of such methods and is continuously improving the corresponding facilities and data reduction techniques.

Technical process development is accompanied by experiments which improve the understanding of the basic physical and chemical mechanisms. For this purpose, in-situ diagnostics play a prominent role. In connection with the experimental studies, theoretical investigations are being performed, in particular using computer simulation programs.

The scientific progress of the institute in 1995 is in particular documented by a significantly increased number of publications in the most renowned international journals. The first PhD theses of the institute have been finished, and one of the PhD students received an international award.

In 1995, further relations were established both with industry and within regional, national and international programs. The institute is a member of the Dresden Materials Research Community, which represents about 300 professional scientists at the Technical University of Dresden, the Max-Planck and Fraunhofer societies, and other research institutions. Within programmes by the German Federal Minister of Education, Science, Research and Technology

the institute offers its facilities to scientists in particular from universities. From the European Human Capital and Mobility program, long-term visitors contribute to its scientific program. Members of the institute played a leading role in the definition of a proposal for a new national program of ion beam application, and in different European networks on ion beam processing of semiconductors, analysis of art objects, and deposition of hard coatings. Services of ion beam modification and analysis were performed for about 50 different organizations from universities, research institutes, and industry.

In 1995, the institute has completed its basic local equipment for research during the forthcoming years. A 500 kV implanter from HIGH VOLTAGE ENG. was successfully commissioned. First encouraging results are also available from a 300 keV transmission electron microscope (TEM) from PHILIPS including sample preparation. The detailed design has been commenced for the extension building of the institute, which will allow the combination of the different ion accelerators and implanters and the TEM.

For the Rossendorf Beamline (ROBL) at the European Synchrotron Radiation Facility, the final specification of the beam line optics was made. The design of a goniometer for materials science experiments was finalized. The contract for the construction phase of ROBL, which will be operated in common with the Institute of Radiochemistry, was signed by FZR and ESRF.

Appreciable progress in science and application has been achieved by the institute, which shall be displayed below. The present annual report will first address some "highlights", and after that give a complete overview in form of short displays of the results of the individual activities.

Crystal-GRID: A new Method for the Investigation of Atomic Interaction in Solids

M. Jentschel, K.H. Heinig and H.G. Börner*
*Institute Laue-Langevin, Grenoble, France

The **G**amma **R**ay **I**nduced **D**oppler-broadening method gives the unique opportunity to measure an effect, which is directly related to the interatomic potentials in solids. In 1995 a very important step has been made in order to improve the application of the GRID method for the investigation of interatomic potentials in solids: For the first time there were carried out Crystal-GRID experiments using single crystalline targets.

The GRID method [1] uses the fact that, following neutron capture, a recoiling excited nucleus is produced by emission of a high energetic primary γ-quantum γ_1. The recoil velocity is determined by the momentum conservation

$$v_0 = E^0_{\gamma_1} / Mc,$$

where $E^0_{\gamma_1}$ is the energy of γ_1, M the mass of the recoil nucleus and c the velocity of light. The recoil energies are in the order of 10 eV up to 1000 eV, depending on M and $E^0_{\gamma_1}$. The recoils loose this energy by collisions with the surrounding lattice atoms and are thermalized within a certain time. During their slowing down, the still excited recoiling nuclei continue to deexcite by secondary γ_2-emission, where the emission probability is defined by the lifetime τ of their intermediate nuclear state, being populated by the γ_1 emission

$$P_{\gamma_2} \propto \exp(-t/\tau).$$

Since the γ_2-quanta are emitted in flight, their energy is Doppler shifted in a laboratory system

$$E_{\gamma_2} = E^0_{\gamma_2}(1+\frac{\vec{v}(t)\vec{n}}{c}),$$

where $\vec{n}$ is a unit vector parallel to the axis of observation (spectrometer axis). The measurement of E_{γ_2} leads to a Doppler-broadened line shape, the intensity distribution of which is given by

$$I(E)dE \propto \sum_i \int_0^\infty dt \exp(-t/\tau)\delta[E - E^0_{\gamma_2}(1+\frac{\vec{v}_i(t)\vec{n}}{c})]dE,$$

where $\vec{v}_i(t)$ is the velocity of the i-th recoiling atom at time t [2]. The time $t=0$ starts for each individual recoil at the moment of γ_1-emission, and the summation is done over all registered recoil events. For single crystalline targets the projection $\vec{v}(t)\vec{n}$ depends on the alignment of the target with respect to the spectrometer axis [2]. This results in different line shapes for different target-spectrometer alignments. Each of these line shapes has a characteristic structure, which is more sensitive to the details of the potentials than the line shapes from polycrystalline targets.

The first Crystal-GRID measurements, carried out in 1995, had the aim to prove experimentally the predicted dependence of the line shapes on the spectrometer-target alignment. Furthermore they allow to establish criteria on resolution and intensities needed to be sensitive to interatomic potentials. For this purpose it was decided to use a nucleus, which is well investigated from the nuclear physics point of view. As a good candidate ^{49}Ti was chosen, the level scheme of which is shown in Fig. 1. The lifetime of the 3260 keV state has been carefully studied by a series of GRID measurements with different chemical compounds and the value of $\tau = 17.5^{(0.8)}_{(1.7)}$ fs was adopted [3]. The level is populated to 95% by a primary γ-transition from the capture state, leading to a sharp distribution of the recoil energies around 261 eV. The 1498 keV line, depopulating this level, is strongly Doppler-broadened due to the short lifetime and the strong recoil. As target compound $SrTiO_3$ was chosen, such crystals are commercially available at a moderate price. For them the <100>, <110> and the <111> crystal orientations were expected to show strongly different structure.

The experimental line shapes of the 1498 keV line for the <100> and the <111> directions are shown in Fig. 2, together with the instrumental response function (dashed line) [4]. A comparison of both line shapes shows that the predicted dependence on the crystal direction could be verified experimentally. A first comparison of the experimental data to profiles resulting from MD-simulation has been done. Here two approaches were used, which give a first idea of agreement/disagreement between simulation and experiment: One way is to use a potential, which is fitted to reproduce in simulations the equilibrium properties of solid $SrTiO_3$ and then to extrapolate it to higher energies. The other way is to take potentials, successfully used in simulations of high energetic (> 1 keV) ion-solid interaction, and to extrapolate them to lower energies. Both extrapolations might be bad approximations, but they give a starting point to correct the potentials in such a way that they describe the behaviour from low up to very high energies correctly. For the first approach a potential developed by Kawamura et.al. [5] was used, which gives correct atomic positions and elasticity constants of $SrTiO_3$ in MD simulations. This is an ionic potential with Born-Mayer repulsion, which describes the low energy behaviour, but has not been tested for higher energies. The best fit to the experimental data from a simulation with this potential results in lifetimes $\tau = 5.4 \pm 0.6$ fs for the <100> and $\tau = 8.6 \pm 1.1$ fs for the <111> directions, respectively (of course, they should be equal). It is

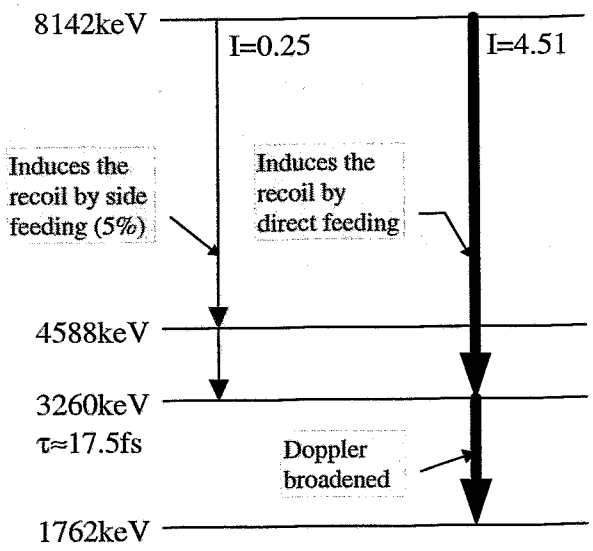

Fig. 1: Nuclear level scheme of ^{49}Ti with transitions, which were used in the experiment. The 3260 keV state is mainly populated by the 4882 keV transition from the 8142 keV capture state. The Doppler broadening of the 1498 keV transition was measured.

highly probable that these values are by far shorter than the adopted value. From that one can conclude that the repulsive part of the potential is to steep above 10 eV.
In the second approach one assumes that during the time period, which is relevant for the slowing down, the lattice appears to be static. This means that only the interaction of the recoiling atom with the lattice atoms is relevant for the slowing down, which allows the use of purely repulsive potentials [6]. Line shape fits to the experimental data based on such simulations are shown in Fig. 2 as a thick solid line. The corresponding lifetime values are $\tau = 12.8 \pm 1.2 fs$ and $\tau = 17.2 \pm 1.3 fs$ for the <100> and the <111> directions, respectively. These values are in much better agreement with the expectations, but they are still too different for these two directions.

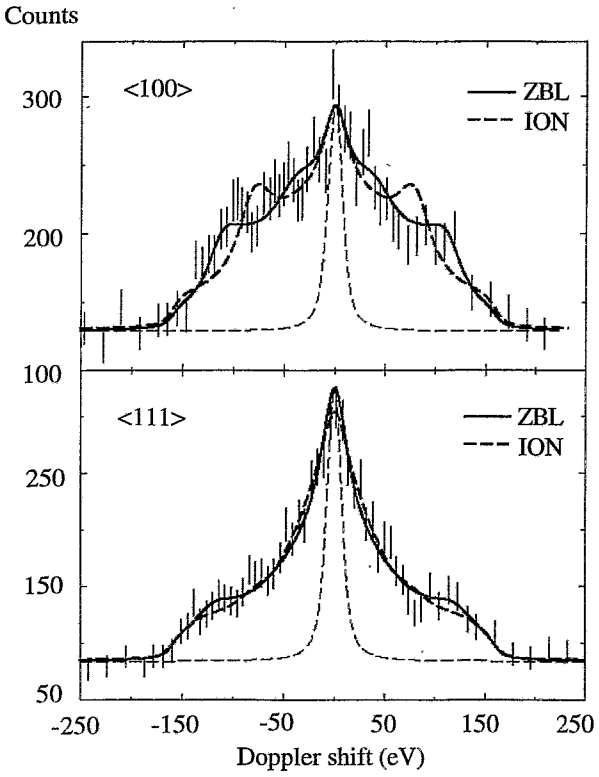

Fig. 2: The Doppler broadened lineshapes of the 1498 keV line, obtained from the <100> and <111> directions, respectivelly. The thick lines result from MD-simulations with the ZBL and an Ionic potential. The thin lines correspond to the instrumental response function.

Exactly this fact must be used as the basic criterion for the further modification of the potentials, since the lifetimes must be the same for each direction. As free parameters for the modification one should use in a first step the ionic charge number of the recoiling atom and the corresponding screening length of the electron cloud. This is motivated by the fact, that the Ti-atom has an ionic charge number of *+4* before the recoil happens. This enters also into the potential of Kawamura. However, as the simulation seems to indicate, a neutral atom gives better results. The question of charge transfer during the recoil acceleration and/or during further collisions is a point, which has now to be investigated further by this method. Once the potential is determined such that all lifetimes are equal for arbitrary directions, one will have extracted the lifetime and the potential from the same target. This is a qualitatively new step in the Crystal-GRID technique. Further improvements in the instrumental setup (development of the new spectrometer GAMS5) and in the target selection should result in reduced error bars, which gives additional hope to obtain more decisive information about interatomic potentials.

Acknowledgements

This work was performed by financial support from the Sächsische Ministerium für Wissenschaft und Kunst.

References

[1] H.G.Börner, J.Jolie, J.Phys.G: Nucl. Part.Phys. 19 (1993) 217

[2] K.H.Heinig, D. Janssen, in: Workshop on Application of High Resolution Gamma Spectroscopy in Studies of Atomic Collissions and Nuclear Lifetimes, Grenoble Oct.5-7, 1992, eds H.G.Börner *et.al.*

[3] A. Kuronen, J. Keinonen, H.G.Börner,J.Jolie, S. Ulbig, Nuclear Physics A549 (1992) 59

[4] M.Jentschel, K.H.Heinig, H.G.Börner, J.Jolie, E.G.Kessler, Nucl.Instr.&Meth. B, 1996 (in print)

[5] Kawamura in F.Yonezawa, "Molecular Dynamics Simulations", Springer Series in Materials Science 103

[6] F.J. Ziegler, J..P. Biesack, U. Littmark, The Stopping and Ranges of Ions in Matter, Vol.1, New York Pergamon , 1985

Random and Channeling Stopping Power of Heavy Ions in Silicon

W. Jiang, R. Grötzschel, W. Pilz and B. Schmidt

The growing technological interest in MeV ion implantation and the theoretical modeling of dopant depth profiles as well as the usage of heavy ion beams for thin film analysis demand accurate data of heavy ion stopping in solids. Whereas the stopping of light ions (H, He) is investigated extensively both experimentally and theoretically [1,2], much less reliable data are available for heavy ions, where experiments are rather sparse. The theory of stopping bases on a velocity dependent effective charge [3], but the theoretical understanding of this ionization fraction is still limited ([4,5] and the refs. therein). Thus further refinements of the theoretical description and a comparison with experimental results are desirable. It is furthermore of interest to include channeling effects into the modeling, but stopping data for channeled particles are rare.

In this report we present measurements of stopping power in monocrystalline silicon for various heavy ions in the energy range from 0.2 to 1.4 MeV/amu. The experiments were performed in transmission geometry both for random and aligned (axial and planar) incidence.

The schematic layout of the experiment is shown in Fig.1. MeV heavy ions from the 5 MV tandem accelerator are well collimated to a divergence of 0.01° by a cross collimator slit (0.8×0.8 mm^2) and a small hole of 0.2 mm diameter at a distance of 4.5 m, about 80 mm in front of the target. This hole is placed in the center of the bottom plate of a Faraday cup (Cup1) with an entrance collimator of 2 mm, which allows an easy normalization of the measurements. The small beam diameter reduces the influence of the lateral inhomogeneity of the thickness of the target foils. The target, mounted on a precision two-axes goniometer, was a 0.71 μm thick crystalline Si foil, prepared by an electrochemical etch technique [6]. Typical ion beam currents through the foil ranged from 5 to 20 pA, depending on ion energy and crystal direction. It was found that the damage caused by the energetic ions was negligible even for several ten hours of bombardment. A 100 mm^2 silicon detector in the chamber was applied for crystal alignment. To achieve an energy resolution of $< 3\times10^{-3}$ we used an electrostatic energy analyser (ESA), which consists of the entrance slit (0.5×0.5 mm^2), the 30° deflector plates with a maximum bending power of 4 MeV/q (DANFYSIK) and the vertical exit slit (0.2 mm). The acceptance angle for the transmitted ions amounts to 0.02°. At the exit of the ESA a Faraday

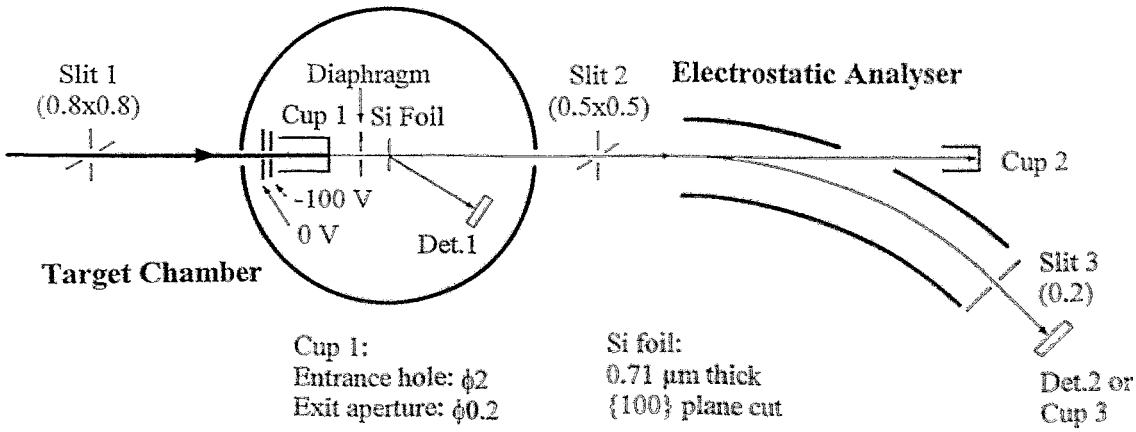

Fig. 1: Experimental arrangement.

cup or a surface barrier detector (SBD) were interchangeable for the measurements of direct beam and transmitted ions, repectively. During the measurements the vacuum inside the target chamber and the ESA was kept below 10^{-4} Pa. The experiment is PC controlled via CAMAC and serial ports. The software for crystal alignment and data acquisition was written in FORTRAN77.

A typical ESA spectrum obtained with 11 MeV $^{14}N^{3+}$ ions under <100> axial channeled incidence is shown in Fig.2. Each peak represents one charge state of emergent ions, as labeled in the figure. Unlike in random case, where the peaks are nearly of Gaussian shape, the peaks in the aligned case show marked low energy tails corresponding to the detection probability of particles with different trajectories in the channel at the extreme forward angle. Similar asymmetric peak shapes have been observed for planar channeling incidence when the off-plane angle ϕ_{in} is much less than the critical angle Ψ_c. At tilt angles ϕ_{in} of about $\Psi_c/2$, only discrete trajectories with an even number of reflections in the planar potential can be observed, resulting in a distinct multiple peak structure in the energy loss [7]. Fig.3 shows the {110} ESA transmission energy-loss spectrum for the 5^+ emergent charge state of a 11 MeV N^{3+} beam for an off-plane angle of 0.12°, where five peaks can be clearly resolved. For lighter ions like lithium we observed similar trajectory effects.

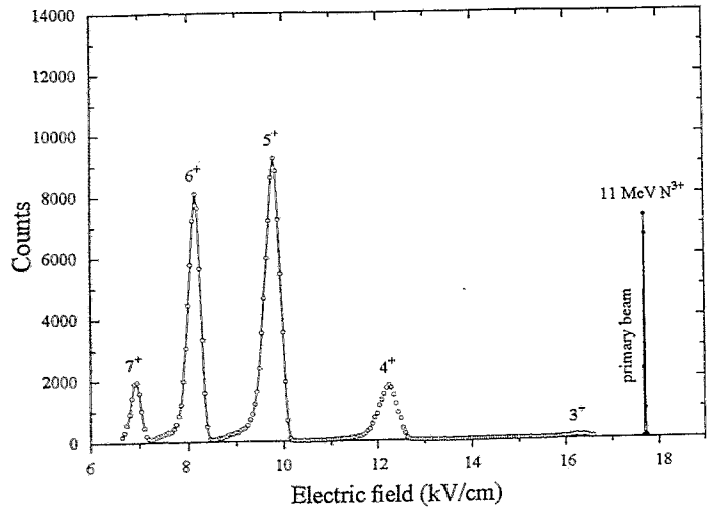

Fig. 2:
ESA spectrum for 11 MeV N transmission through a 0.71μm thick Si <100> channel.

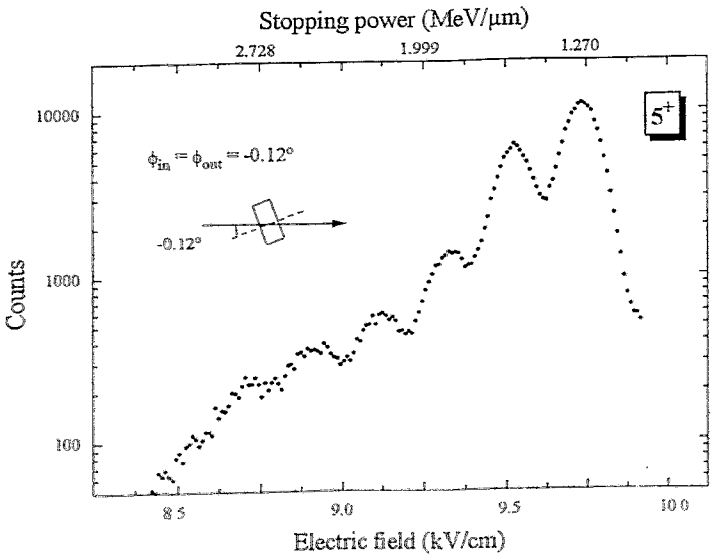

Fig. 3:
ESA energy-loss spectrum of 11 MeV N ions transmitted through a 0.71 μm thick Si {110} plane.

To calculate the stopping power values in the random case, each charge state peak was fitted by a Gaussian and the corresponding energy loss was assigned to a mean energy $E_n = 0.5(E_{in} + E_{out})$. Since the energy loss was found to be independent of the charge state, the stopping values were obtained by arithmetic averaging over the measured charge states, weighted by the percentage of the peak intensity. This procedure is not applicable for the channeling spectra due to the asymmetric peak shape. Here we determined for each charge state the center of gravity of the peak. The mean stopping defined in this way is generally greater than the most likely stopping defined by the peak maximum position or the stopping for the hyperchanneled particles, which can be derived from the leading edge. In no case any significant dependence of the stopping power on the emergent charge states was observed. It has been reported earlier [8] that at 3 MeV/amu heavy channeled ions show a charge-state dependence of the energy loss even for more than 1 μm pathlength in Si <110>. In order to check this dependence in our energy range, 2^+, 3^+ and 4^+ N ions with 11 MeV, channeled in 0.71 μm thick Si, were investigated. The results show practically the same stopping for the different primary charge states of the N ions. This indicates that the stripping process is very efficient and the statistical equilibrium ($\sim 5^+$) is reached very soon in every case. A similar behavior for nitrogen ions at lower energies in Si has also been reported [9].

Stopping results for nitrogen ions from E_n= 4.5 MeV to 19.5 MeV in silicon along <100> axis, {110} plane and in the random case are presented in Fig.4. The plotted solid line is the theoretical curve calculated with TRIM95. The comparison of the measured random stopping with the calculation shows a systematic deviation of about 5% near the stopping power maximum. At higher energies deviations seem to be larger. As shown by this figure, there

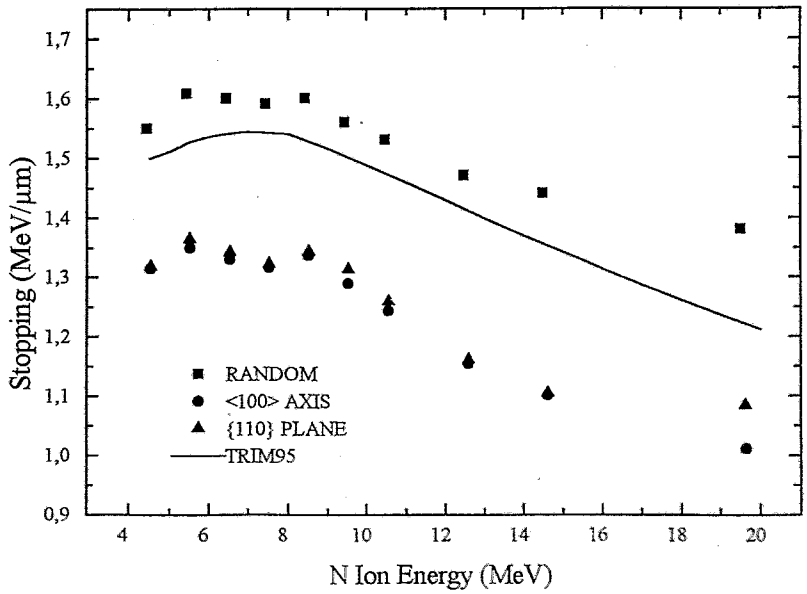

Fig. 4: Mean stopping for nitrogen ions in silicon.

exists no significant difference of stopping between ions channeled in the {110} plane and in the <100> axis, respectively. Only at the highest measured energy of 20 MeV the observed planar stopping was about 10% higher than in the <100> axial case. As mentioned above the absolute stopping power values are related to the data for He stopping, since the foil thickness was determined by 1.5 MeV He RBS. Although the relative error of the single data sets was as low as 2%, a wedge inhomogeneity of the foil of about 8 % over the full usable width of 1.0 mm may have contributed another 2% due to the uncertainty in the target position.

In the table the random and the mean channeling stopping powers of Li, B, N and P ions in silicon are listed. The random values of B, N and P deviate from the TRIM95 calculations by less than 5%, in the case of Li the measured values are generally 10% higher in the energy range from 2.8-5.8 MeV. The energy dependence of the stopping for channeled ions is similar to the random case. Except for nitrogen at 20 MeV, all kinds of ions in the measured energy ranges have almost equal energy losses in <100> and {110} orientations. For the light ions the channeling stopping values are found to be 70% to 80% of the random values in the investigated energy range. In the case of P a comparable factor was found at the low energy end, at energies above 10 MeV differences seem to disappear. Further experiments and a more detailed data evaluation considering the energy straggling are in progress.

Table: Mean stopping powers of Li, B, N and P ions in Si crystal.*

Ion	Energy (MeV)	TRIM95 (MeV/μm)	Random (MeV/μm)	<100> (MeV/μm)	{110} (MeV/μm)
^{7}Li	2.8	0.51	0.58	0.47	0.48
	3.8	0.47	0.56	0.44	0.45
	4.8	0.44	0.52	0.38	0.40
	5.8	0.41	0.47	0.32	0.35
^{11}B	3.7	0.98	0.92	0.83	0.81
	5.7	0.97	0.94	0.85	0.80
	7.7	0.94	0.90	0.77	0.77
	9.7	0.88	0.91	0.70	0.70
	11.7	0.82	0.87	0.65	0.65
^{14}N	4.5	1.50	1.55	1.32	1.32
	5.5	1.53	1.61	1.35	1.36
	6.5	1.54	1.60	1.33	1.34
	7.5	1.54	1.59	1.32	1.32
	8.5	1.53	1.60	1.34	1.34
	9.5	1.50	1.56	1.29	1.31
	10.5	1.47	1.53	1.24	1.26
	12.5	1.41	1.47	1.15	1.16
	14.5	1.36	1.44	1.10	1.10
	19.5	1.23	1.38	1.01	1.08
^{31}P	5.0	2.76	2.65	2.19	2.14
	8.0	3.05	3.09	2.82	2.67
	11.0	3.30	3.27	3.01	2.92
	13.8	3.56	3.47	3.28	3.17
	18.8	3.79	3.60	3.44	3.35

* Measurements were made by an Electrostatic Analyser.
Si foil was 0.71 μm thick, determined by 1.5 MeV He RBS.
Relative error of stopping powers at different energies is about 2%.

References

[1] H.H. Andersen, J.F. Ziegler, Hydrogen Stopping Powers and Ranges in All Elements, Plenum Press, New York, 1977

[2] J.F. Ziegler, Helium Stopping Powers and Ranges in All Elements, Plenum Press, New York, 1977

[3] J.F.Ziegler, J.P.Biersack, U.Littmark, The Stopping and Range of Ions in Solids, Pergamon Press, New York, 1985

[4] R.J.Mathar, M.Posselt, Phys. Rev. B 51 (1995) 107

[5] R.J.Mathar, M.Posselt, Phys. Rev. B 51 (1995) 15798

[6] B. Schmidt, J. von Borany, U. Todt, A. Erlebach, Sensors and Actuators A41/42 (1994) 689

[7] S. Datz, C.D. Moak, T.S. Noggle, B.R. Appleton, H.O. Lutz, Phys. Rev. 179 (1969) 315

[8] J.A. Golovchenko, A.N. Goland, J.S. Rosner, C.E. Thorn, H.E. Wegner, H. Knudsen, C.D. Moak, Phys. Rev. 23 (1981) 957

[9] G.G. Bentini, M. Bianconi, Nipoti, Nucl. Instr. and Meth. B80/81 (1993) 33
G.G. Bentini, M. Bianconi, R. Nipoti, F. Malaguti, E. Verondini, Nucl. Instr. and Meth. B53 (1991) 1

Self-Organization in Buried Layers of Precipitates Due to Ostwald-Ripening

S. Reiss and K.-H. Heinig

Ion Beam Synthesis (IBS) of well-defined structures by high dose ion implantation, followed by high-temperature annealing, has a large potential for mirco- and optoelectronic applications. However, although the successful fabrication of several types of structures – e.g., buried SiO_2 layers in Si, buried silicide layers and wires in Si, or Si and Ge nanoclusters in SiO_2 – by IBS has been reported, the broad application of IBS is hindered by some problems: (i) high prices of the samples, caused by the high ion doses necessary to form regions of a new phase in the substrate, (ii) problems with the quality of the synthesized structures, and (iii) defects in the substrate, resulting from the implantation of such high ion doses.

To overcome these problems and to optimize IBS a better theoretical understanding of the underlying physical processes is required. One key process controlling the quality of the formed structure is the redistribution of the implanted material during annealing. This redistribution is due to OSTWALD-ripening of precipitates of the newly synthesized phase, which have been formed during the implantation. The driving force of OSTWALD-ripening is the presence of a surface tension at the phase boundary between the new phase and the substrate. This surface tension gives a large contribution to the free energy of the system. The system can diminish this part of the free energy by dissolving smaller precipitates and transferring their mass into larger ones.

The OSTWALD-ripening of spatially inhomogeneous and open systems – like precipitates, formed during IBS – is still not very well understood. Therefore we developed a model and a computer code, which allow the simulation of the OSTWALD-ripening of an large ensemble (e.g., a few thousand) of precipitates during the annealing step of IBS. In the simulation we compute the evolution of each precipitate of the ensemble in discrete time steps [1]. To take into account collective effects in the ensemble, for each time step the individual material balance of each precipitate is determined within a *local* Mean-Field-Approximation. Thus, one has to solve for each time step a huge coupled system of linear equations for the material balances. The initial stage in the simulation of the ripening is adjusted to the results of experimental investigations. This is necessary, because up to now no reliable theory of the nucleation and growth of precipitates during IBS exists.

One of the first systems, investigated by us with this method, was the ripening of a layer of SiO_2 precipitates buried under the Si surface [2,4]. Avoiding the geometrical approximation used in ref. [2], we modeled the buried layer (which we assumed to be infinite in two dimensions), by a finite rectangular unit cell with periodic boundary conditions parallel to the surface [4]. For such a geometry, a formal divergence occurs within the set of equations for the material balance (see e.g., eq. (6) in ref [3]). To overcome this problem, we extended EWALD's method of summation to a 2D lattice. The surface itself – which is a sink for the implanted oxygen – was modeled by the introduction of a "'mirror source"' for each precipitate above the surface. Finally, based on the result of experimental SEM investigations of short annealed, bevelled samples, we assumed, that the initial state of the ripening consists of equal sized precipitates with a depth-dependent number density of Gaussian shape.

Fig. 1 shows the simulated evolution of such a buried layer of SiO_2 precipitates in Si during

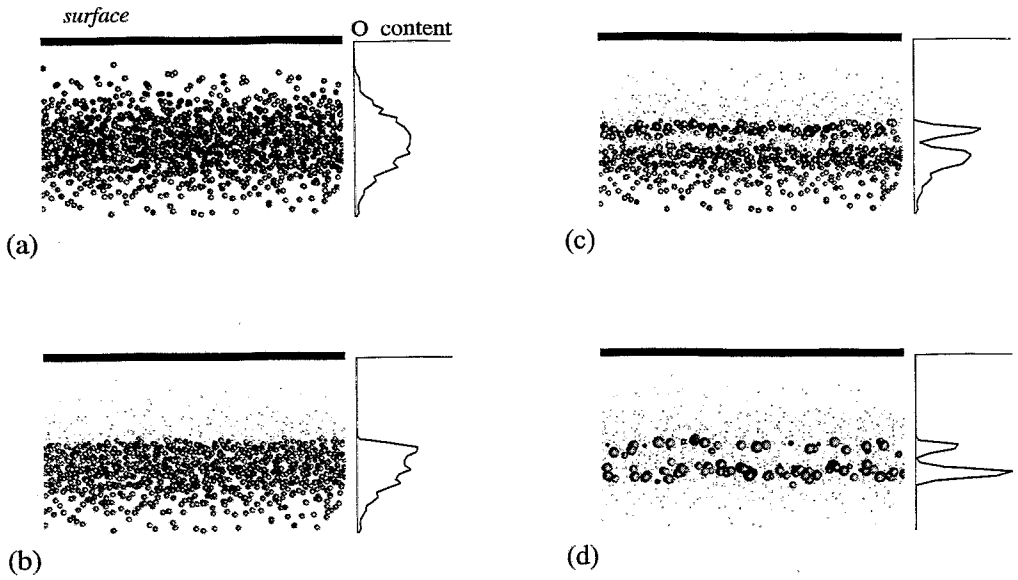

Fig. 1: Cross sections through a buried precipitate layer, showing the evolution from an initially Gaussian-distributed precipitate layer (a) towards a double layer structure (d).

annealing. As found in our previous work [2], the initial layer breaks during the ripening into two (or even more) sublayers of precipitates. The resulting structure is very similar to an experimental result of Hemment et. al. [5], These authors observed the formation of double layers of precipitates during annealing. The distance between the sublayers – called structure wavelength λ – is proportional to the initial diffusional screening length κ of the precipitate ensemble. For homogeneously filled buried layers the proportionality constant was found to be the same as for the finite precipitate ensembles, investigated in [3]. The structure formation during the ripening, observed for the given initial conditions, can be explained by a self-organization process [1]. The driving force is the material loss of the system to a large sink, e.g. the surface or any other large inhomogeneity in the ensemble.

A second system investigated recently [4] is the ripening of an ensemble of buried SiO_2 precipitates in Si, distributed within an elliptical cylinder. As described above, the influence of the surface is modeled by mirror sources. The cylinder (assumed to be infinite along its axis) is described by a unit cell with periodic boundary conditions parallel to its axis. Because also for this geometry a formal divergence occurs in the evolution equations, an appropriate extension of the EWALD-summation method to a 1D lattice was used. Fig. 2 shows cross

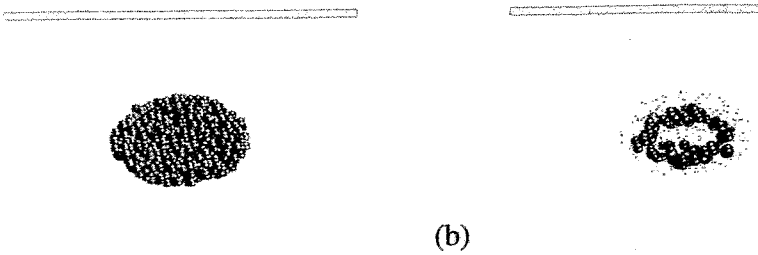

Fig. 2: Cross sections through a buried cylinder of precipitates at the beginning (a), and the end (b) of the simulation, showing the evolution to a "nanopipe".

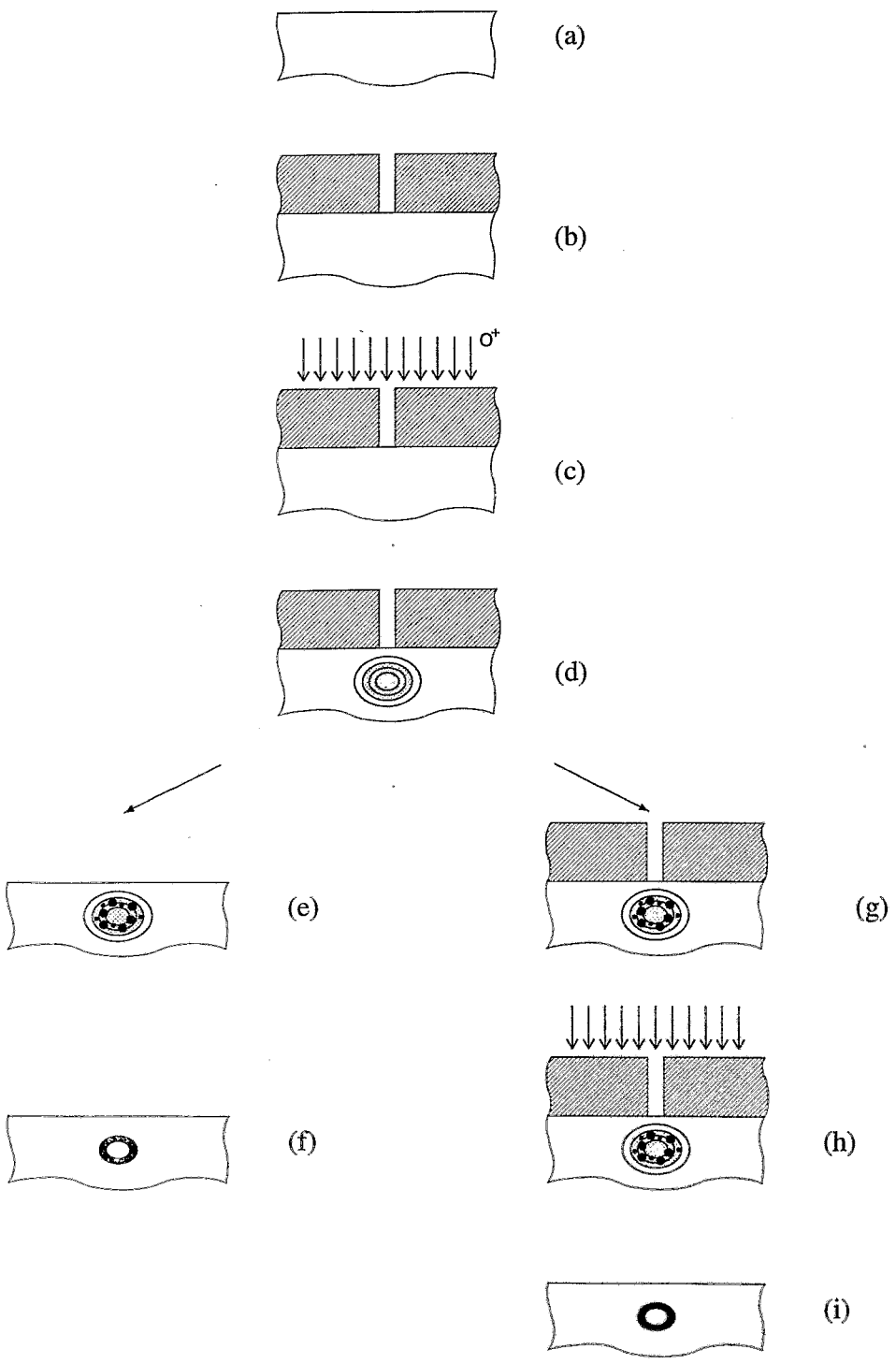

Fig. 3: Scheme of the proposed method of manufacturing a buried nanotube by IBS (explanation in the text) [6].

sections perpendicular to the cylinder axis through the ensemble at the beginning (Fig. 2a) and after (Fig. 2b) the annealing. Due to the material loss of the precipitate ensemble in all directions, the structure formation leads to the formation of a buried hollow cylinder of precipitates, filled with pure silicon.

Based on this result, we predicted an interesting method to form a new type of structure – a "'nanotube"' [4,6]. If one takes a wafer (Fig. 3a), puts on it a slit mask (Fig. 3b) and implants a certain dose of ions, one obtains a (in a first approximation elliptical) buried cylinder of precipitates (Fig. 3c). If this as-implanted state fulfills the conditions nessecary for the self-organization, a hollow cylinder of precipitates will form during the annealing (Fig. 3e). If the dose is high enough, the precipitates will finally coalesce to a buried nanotube (Fig. 3f). Alternatively, if coalescense cannot be reached one can add a second implantation and annealing sequence (Fig. 3h). The large precipitates, formed during the first implantation and annealing sequence, can now grow at the expense of the additionally implanted ions until they coalesce to the nanotube (Fig. 3i).

However, only experiments can decide, whether the manufacturing of a buried nanotube by IBS is possible or not.

References

[1] S. Reiss, K. H. Heinig, Nucl. Instr. and Meth. B 84 (1994) 229

[2] S. Reiss, K.-H. Heinig, R. Weber, W. Skorupa, Mat. Res. Soc. Symp. Proc. 316 (1994) 819

[3] S. Reiss, K. H. Heinig, Nucl. Instr. and Meth. B 102 (1995) 256

[4] S. Reiss, K. H. Heinig, "Self-Structuring of Buried SiO_2-Precipitate Layers During IBS – A Computer Simulation", Nucl. Instr. and Meth., in press

[5] P. L. F. Hemment, K. J. Reason, J. A. Kilner, R. J. Chater, C. Marsh, G. R. Booker, G. K. Celler, J. Stoemenos, Vacuum 36 (1986) 877

[6] K. H. Heinig, S. Reiss, B. Schmidt, W. Skorupa, Euro-patent EP 94106815.7.

Room-Temperature, Short-Wavelength (400 - 500 nm) Photoluminescence from Silicon-Implanted Silicon Dioxide Films

W. Skorupa, R.A. Yankov, I.E. Tyschenko, T. Böhme*, H. Fröb* and K. Leo*
*Institut für Angewandte Photophysik, TU Dresden

Bulk single-crystal silicon as a basic electronics material is of limited use for optoelectronic applications because of its low intrinsic recombination probability. Recently it has been demonstrated that Si-based nanostructures can yield high-intensity photoluminescence (PL) at room temperature (RT). After the pioneering work on PL from porous Si produced by wet etching [1], various techniques of fabricating Si nanosystems have been employed, these include microwave plasma decomposition of SiH_4 and H_2 [2], rf-magnetron sputtering of Si and SiO_2 [3], laser breakdown of silane gas [4] and crystallization of amorphous Si [5]. One promising method of forming nanometer-sized structures relies on ion implantation of either Si [6-9] or Ge [10,11] into an SiO_2 matrix and subsequent heat treatment (ion-beam synthesis). Important advantages of this approach are the precise control over the quantities and depth distributions of the implanted ions and its full compatibility with Si technology. In most cases single-energy implantation has been employed for the synthesis of semiconductor nanoclusters. Such implantation, however, results in a Gaussian-shaped depth distribution of the implanted ions and provides largely unequal conditions for the nucleation and growth of second-phase inclusions, so that nucleation occurs preferentially around the peak of the implant depth profile. The use of multiple-energy implantation would be preferable as it would enable the production of a thicker impurity-rich layer of better uniformity to increase the number of clusters/emitting centres. Furthermore, both the mean cluster size and the width of the cluster-size distribution have been observed to increase with raising substrate temperature [12,13]. The wavelength values of the luminescence maxima reported up to now are about 500 nm or higher [6,9,12]. For the purpose of producing luminescence with shorter wavelengths (blue light), the cluster growth process could be circumvented by using low (< RT) wafer temperatures to ensure a retarded rate of nucleation and/or growth during implantation. As far as the post-implantation heat treatment is concerned, to date the attempts at formation of semiconductor nanoclusters in an oxide layer have only been made via furnace annealing (FA) at temperatures ranging from 400 °C to 1300 °C and times from 0.5 to 5 h [6,8,9]. Clearly, a reduction of annealing time and temperature would be an apparent benefit to lower the cluster size. On the other hand, a high annealing temperature enables a better removal of radiation damage, both in the clusters and the surrounding oxide. Short-time annealing using Rapid Thermal Annealing (RTA) and Flash Lamp Annealing (FLA) with duration ranges of 1-30 sec and 2-20 ms, respectively, could solve this contradiction.

In this report we describe first experiments to study the PL from an Si/SiO_2 nanocrystal system produced by low-temperature, multiple-energy implantation and subsequent short-time thermal processing. The goal of this experiment is the formation of small clusters to produce luminescence with short wavelength and a narrow intensity distribution. For the purpose of comparison, furnace annealing (FA) was also performed.

Thermally-grown, 500 nm-thick SiO_2 films on (100) Si wafers were implanted with Si^+ ions over a central region of 9 cm^2. Double implantation with silicon ions at energies of 200 keV and 100 keV was used to create concentration profiles of excess silicon atoms in the silicon dioxide layer. At first, 200 keV Si^+ ions were implanted to doses of $1x10^{16}$ cm^{-2} (low dose

or LD), $3x10^{16}$ cm^{-2} (medium dose or MD), and $1x10^{17}$ cm^{-2} (high dose or HD). The doses implanted at the lower energy of 100 keV were equal to 60% of those implanted at 200 keV. According to TRIM calculations, under these implantation conditions the resulting silicon atom distributions are fairly flat-topped in a depth region of 100-300 nm below the oxide surface. The maximum silicon concentration is $6.3x10^{20}$ cm^{-3} for LD, $2x10^{21}$ cm^{-3} for MD, and $6.3x10^{21}$ cm^{-3} for HD. The substrate temperature during implantation was maintained at about -20 °C by mounting the wafers on a LN_2-cooled stage. After implantation the wafers were cut into segments. Three of the segments containing the implants with the above-specified total doses (LD, MD and HD, respectively) were left untreated, these are further referred to as reference samples. The others were subjected to transient heat treatment using either RTA at 1050 °C for 1 s in an Ar ambient or FLA at 1050 °C for 20 ms in an N_2 ambient. Comparative anneals were performed for LD, MD and HD implants employing conventional FA at 600 °C for 0.5 h in an N_2 ambient. Finally, the reference samples together with the heat-treated ones were all given a routine furnace anneal at 400 °C for 0.5 h in an ambient of N_2 with 5% H_2 to improve the quality of the interfaces between the Si clusters and the surrounding oxide. PL measurements were performed using a Spex Fluoromax spectrometer at RT. The excitation wavelength was varied over the range of 325 to 488 nm and the emitted light was detected by means of a photomultiplier R928 (Hamamatsu). The PL data were corrected to the photomultiplier sensitivity and the blank substrate background.

PL measurements revealed no visible emission from the unimplanted thermally-grown SiO_2 layer, neither before nor after the final routine anneal. The three reference samples exhibited quite different PL behavior depending on the implant dose (Fig.1). More specifically, the LD specimen did not yield any discernible PL signal. In contrast, pronounced short-wavelength PL was recorded from the MD sample whose spectrum shows a distinct double-peak structure with maxima at 417 and 438 nm. Moreover, this short-wavelength emission occurs over a narrow range of wavelengths giving rise to a steep-fronted signal to the side of higher wavelengths. There are also indications of a low-intensity peak at 467 nm and another broad peak of much reduced intensity at 650 nm. The PL spectrum from the HD sample exhibited two broad, separated peaks of largely attenuated intensity centered at 470 and 658 nm with the greater intensity at the longer wavelength. From a practical viewpoint, most important is the fact that under the experimental conditions used in this study, the medium-dose implant appears to have produced efficient short-wavelength PL without resorting to any post-implantation heat treatment other than the final routine anneal carried out for 0.5 h at a temperature as low as 400 °C. The inference is that this dose is either very close or equivalent to the optimum fluence for which best short-wavelength PL results can be obtained by the shortest route.

Rapid thermal annealing regimes influenced the emission behavior of the structures in a rather complex manner. Fig. 1 is a composite of PL spectra recorded from the LD, MD and HD implants after FLA and RTA. In order to obtain semiquantitative information as to the individual role of each annealing regime, the relative intensities of the respective PL spectra were compared and plotted together with the signals from the reference samples. In the case of the LD implant (see the upper part of Fig. 1) both transient annealing methods resulted in blue emission with the distinctly stronger PL signal being due to RTA. For the MD implant, apparent changes in the PL behavior occurred depending on the manner of annealing, as shown in the central part of Fig. 1. The highest-intensity PL signal was recorded from the reference sample. The PL signal after FLA is also of rather high intensity

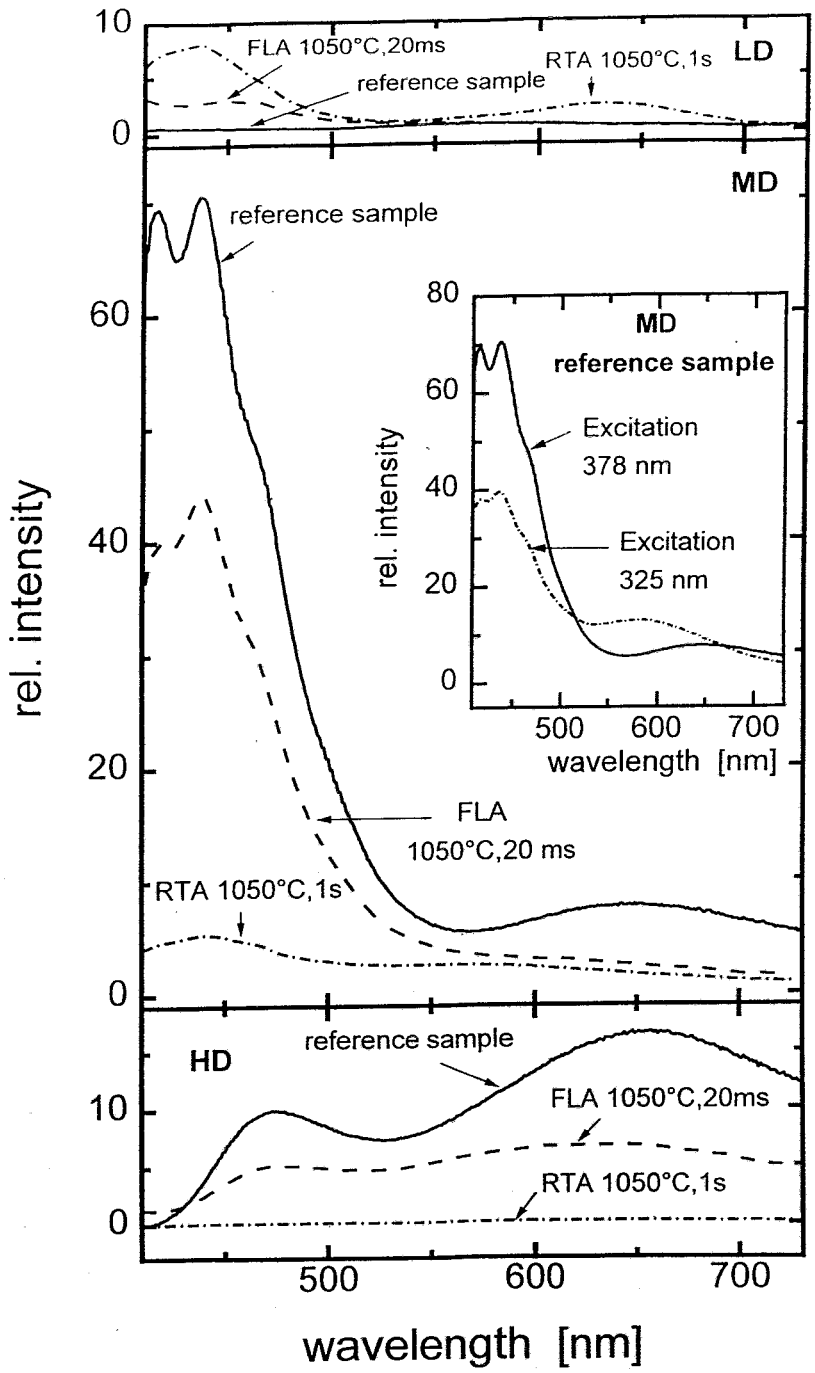

Fig.1: The relative intensity of PL from SiO_2 films implanted with Si^+ ions to total doses of $1.6\times10^{16}cm^{-2}$(LD), 4.8×10^{16}(MD) and $1.6\times10^{17}cm^{-2}$(HD) after rapid thermal annealing at 1050°C for 1s or flash lamp annealing at 1050°C for 20 ms followed by routine annealing at 400°C for 0.5 h in forming gas. The spectra labelled as "reference sample" got only this routine anneal step. The inset shows changes in the PL signal upon reducing the excitation wavelength from 378 nm, normally used, to 325 nm.

and of similar shape as the spectrum from the reference sample retaining in particular the specific bimodal structure over the short-wavelength range, but showing a featureless tail beyond 550 nm. The PL spectrum after RTA is of considerably reduced intensity and the bimodal tendency at short wavelengths has completely vanished. As for the HD implant (lower part of Fig. 1), once again the reference sample exhibited the highest intensity while FLA led to two broad signals of reduced intensity merging into one another. Surprisingly, RTA in this case appears to have totally quenched the emission over the wavelength range studied. A reduction of the excitation wavelength to 325 nm leads to a decrease of the blue PL signal and does not cause any significant change of the energetic position of the three PL peaks described above. However, this reduction causes a shift of the shallow peak located

at 650 nm toward shorter wavelengths (inset to Fig.1, MD). This can only be explained by a different luminescence mechanism for the two bands. More detailed investigations are in progress.

The comparative heat treatment by FA at 600 °C for 0.5 h produced the following PL results (not shown here): For the LD sample the intensity was almost indistinguishable from the background level of the original thermal oxide being about an order of magnitude lower than that obtained after RTA; for the MD sample the intensity was comparable with that recorded after RTA; and for the HD sample the intensity was commensurate with that measured after FLA.

As is evident from the results described above, the PL efficiency over the short-wavelength range is highest for the MD reference sample (Fig. 1). It is interesting to note that the positions of the blue PL peaks in our case correlate with those of the maxima in the PL spectra from nanocrystalline thin Si films fabricated by crystallization of amorphous Si, as described in ref. [5]. In most cases, however, Si nanocrystals formed by different methods do not exhibit uniform PL behavior and hence various PL spectra have been reported in the literature. Depending on the processing conditions, PL peaks have been observed at 415, 437 and 645 nm [5], over the range of 490 to 540 nm and at 750 nm [9], at 570 and 630 nm [14], at about 600 nm [12], at 750 nm [4], at 750 and 470 nm [3], as well as in the range of 710 to 800 nm [2].

Referring back to our study, one can make the following supplementary comments. At present there is not yet full agreement on the mechanisms responsible for the PL in nanometer-sized Si structures. Taking into account both the experimental fact that the nanocrystal size increases with increasing implant dose [6,12] and the quantum-confinement arguments, the appearance of distinct PL peaks over different ranges of the emission spectrum could be rationalized by the varying size of the Si inclusions formed within the oxide, since the only difference among the reference samples is the volume concentration of the implanted Si atoms. An alternative interpretation could be made in terms of the different nature of the emitting centers which, according to [9,12], are believed to be implantation-induced defects in Si and/or in SiO_2 as well as defects associated with the Si/SiO_2 interfaces. The density of these defects should also depend on the Si^+ ion dose. The absence of the 417 and 438 nm peaks in the spectra from both the HD annealed implants and the LD reference sample (Fig. 1) implies that Si-O-H compounds are not expected to be the emitting centers, which is consistent with the results reported in [5]. At the same time the preservation of the positions of these peaks in the PL spectra from the annealed MD implants could be taken as evidence that radiative recombination is not caused by quantum-confined excitons in the Si nanocrystals. Furthermore, the fact that shorter-wavelength excitation causes a blue shift only in the 650 nm PL peak (inset to Fig. 1) can serve as another piece of evidence for the different nature of the emitting centers.

In conclusion, an optimum of silicon atom concentration and the overall thermal budget given to the silicon implanted silicon dioxide layer is necessary for the formation of blue PL emitting centres. In the reported experiments a room temperature short wavelength PL band of high intensity was produced by low temperature, multiple energy implantation to a total dose of 4.8×10^{16} cm^{-2} (atomic concentration about 2×10^{21} cm^{-3}) and subsequent annealing at 400 °C for 0.5 h or at 1050 °C for 20 ms. Investigations of the origin of the blue PL band are in progress.

Acknowledgements

One of the authors (I.E.T.) would like to acknowledge research support by a grant from Deutscher Akademischer Austauschdienst, Ref.No. 325.

References

[1] L. T. Canham, Appl. Phys. Lett. 57 (1990) 1046
[2] H. Takagi, H. Owada, Y. Yamazaki, A. Ishizaki, T. Nakagiri, Appl. Phys. Lett 56 (1990) 2379
[3] K. Kohno, Y. Osaka, F. Toyomura, H. Katayama, Jpn. J. Appl. Phys. 33 (1994) 6616
[4] Y. Kamemitsu, T. Ogawa, K. Shiraishi, K. Takega, Phys. Rev. B48 (1993) 4883
[5] X. Zhao, O. Schoenfeld, J. Kusano, Y. Ayogai, T. Sugano, Jpn. J. Appl. Phys. 33 (1994) L649
[6] H. A. Atwater, K. V. Shcheglov, S. S. Wong, K. J. Vahala, R. C. Flagan, M. L. Brongersma, A. Polman, Mat. Res. Soc. Symp. Proc. 321 (1994) 363
[7] J. G. Zhu, C. W. White, J. D. Budai, S. P. Withrow, and Y. Chen, Mat. Res. Soc. Symp. Proc. 358 (1995) 175
[8] T. Komoda, J. P. Kelly, A. Nejim, K. P. Homewood, P. L. F. Hemment, B. J. Sealy, Mat. Res. Soc. Symp. Proc. 358 (1995) 163
[9] P. Mutti, G. Ghislotti, S. Bertoni, L. Bonoldi, G. F. Cerofolini, L. Meda, E. Grilli, M. Guzzi, Appl. Phys. Lett. 66 (1995) 851
[10] C. M. Yang, K. V. Shcheglov, M. L. Brongersma, A. Polman, H. A. Atwater, Mat. Res. Soc. Symp. Proc. 358 (1995) 181
[11] K. V. Shcheglov, C. M. Yang, K. J. Vahala, H. A. Atwater, Appl. Phys. Lett. 66 (1995) 745
[12] T. Shimitzu-Iwayama, K. Fujita, S. Nakao, K. Saitoh, T. Fujita, N. Itoh, J. Appl. Phys. 75 (1994) 7779
[13] C. W. White, D. S. Zhou, J. D. Budai, R. A. Zhur, R. H. Magruder, D. H. Osborne, Mat. Res. Soc. Symp. Proc. 316 (1994) 499
[14] H. A. Atwater, K. V. Shcheglov, S. S. Wong, K. J. Vahala, R. C. Flagan, Mat. Res. Soc. Symp. Proc. 316 (1994) 409

Nanocrystallites of Silver Halides Encaged in Host Matrices of SiO_2

M.T. Pham, W. Matz, D. Möller and A. Mücklich

In the nanometer size range, metals and semiconductors exhibit surface mediated plasmon resonance and quantum confinement effects [1]. Size dependent changes in band gap energy, excited-state electronic behavior, and optical spectra are generated which differ drastically from those known for molecular and bulk solid-state limits. Other properties are caused by the large fraction of reactive atoms in grain boundaries [2], and the architecture of the material assembly [3]. The new characteristics make this material class attractive for a number of technologies, including photonic devices, catalysis, corrosion protection, solar energy conversion, and chemical/biochemical sensors [3-7].
Preparation and characterization of nanocrystallites are critical for a fundamental understanding and tailoring of material properties of practical use. Metallic silver and semiconducting silver halides are widely used as model material for studying the size quantization effects and surface photochemistry of finely dispersed semiconducting particles. Mostly, colloidal solutions have been studied. A wide range of particle size is adjustable by various forms of arrested precipitations, including particle fractionating [6-10]. The highly reactive particle surface is favorable for modification by adsorption/reaction of/with dissolved species [8], but responsible for the instability of colloid solutions, resulting in time dependent variation of particle size and concentration [8-11], the critical parameters of interest. The surface complexation is useful in stabilizing colloids, and in some cases even yielding quantum powders [12]. But the liquid phase is impractical for many respects. The encagement in solid hosts has been described for some matrices, e.g. glasses, polymers, and zeolites [6,7,9,13,14]. The problems have been the limitation in concentration level and profile, the susceptibility to decomposition of compounds e.g. in the melt-quenching processes, and the incompatibility with the standard planar technologies. Furthermore, the detailed mechanisms that govern the particle size, shape, concentration, and stoichiometry are not yet fully understood.

We report the preparation of nanocrystallites of silver halides by ion implantation. The method involves the formation of silver halides following a sequential implantation of silver and halogens into a host matrix of SiO_2. The great reactivity of halogens with silver, in competition with the high quenching rate of the implantation process and the insolubility of silver halides in SiO_2 results in forming silver halide particles embedded in the matrix host. Thin chemical vapour deposited (CVD) SiO_2 films were used in a three-layer system on a Si substrate (p-type, <100>, 10-15 Ohm cm): CVD-SiO_2(100 nm)/Si_3N_4(100 nm)/SiO_2(70 nm)/Si. This substrate structure was chosen to show the process compatibility with the silicon technology and in order to probe the surface chemistry of the implanted layer using the field effect ion sensitivity (FEIS). Implantation energies for silver (40 keV) and halogen ions (25 keV Cl; 42 keV I) were selected according to TRIM simulations to produce overlapping concentration profiles within the matrix layer. The ion dose of 6×10^{16} cm^{-2} was applied for both components to form AgX. Thermal treatment following ion implantation was conducted in N_2 for 10 minutes at temperatures ranging from 400 to 900 °C. Studies of crystallinity, particle size and shape, and compound formation were performed by X-ray diffraction (XRD), transmission electron microscopy (TEM), atomic force microscopy (AFM), and FEIS.

The FEIS technique [15] is usually used to determine the ion concentration in electrolyte solutions from the interfacial potential developed between the latter and the surface of a thin film material. Experimentally, the interfacial potential is measured with a field effect structure of the type: electrolyte / thin film material / insulator / semiconductor. For thin films of silver halides, the generation of interfacial potentials depends on the concentration of halide or silver ions in

solution. This technique was used here in an inverse manner to verify the presence of a silver halide phase expected to be formed due to ion implantation. Such measurements show e.g. changes in interfacial potentials in response to variation of iodide ion concentration in the solution for a sample implanted with Ag and Cl and heat treated at 600 °C. The maximum response reaching values of 52 - 56 mV per concentration decade is strong evidence for the presence of the chemical compound AgCl at/in the implanted surface layer (Fig. 1). Depending on the amount of the silver halide phase, the response value can vary theoretically between zero and 59 mV. This ion sensitivity, with varying magnitude, was observed also at greater depths from the surface by measuring in combination with successive layer etching and for all three anion types I^-, Br^-, and Cl^-. For samples implanted with Ag and I, similar results were obtained with responses smaller in magnitude, suggesting that the quantity of implantation-produced AgI is small compared with that of AgCl (Fig. 1).

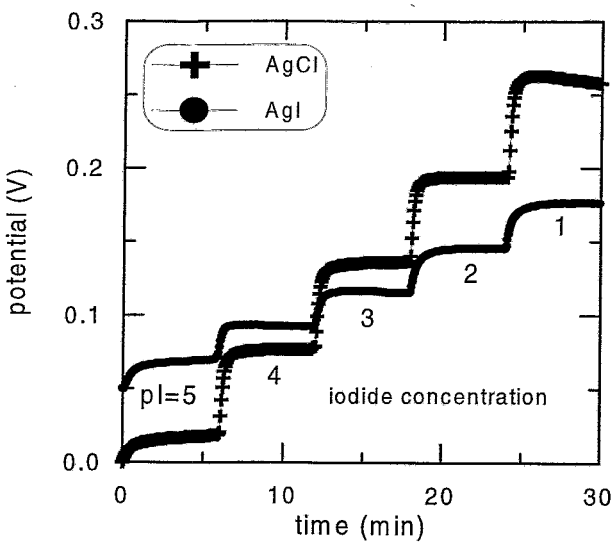

Fig. 1:

Ion implantation-produced AgCl and AgI embedded in SiO_2, as evidenced by FEIS measurements: changes in interfacial potentials in response to iodide ion concentration variation in solution. Differences in the signal magnitude indicate different amounts of AgCl and AgI formed under the same preparation conditions. Ag and Cl/I were implanted in SiO_2 to a dose of 6 x 10^{16} cm^{-2} each. Annealing at 600°C in N_2 for 10 min.

TEM and AFM images conclusively show that the implanted layer consists of spherical particles with a size distribution. Fig. 2 is a bright field TEM image of the cross sectional view of an Ag and I implanted sample. Similar results were obtained for Ag and Cl implanted surfaces. In the as-implanted state larger particles are observed near the surface while smaller particles are distributed deeper into the implanted layer. The bottom region of the SiO_2 layer is nearly free of particles (Fig. 2a). With increasing annealing temperature, a growth in diameter and a more uniform distribution of larger particles were observed (Fig. 2b). There appear smaller particles in the bottom region of SiO_2 but no particles cross the border to the Si_3N_4 layer. The SiO_2/Si_3N_4-interface is a diffussion barrier. The largest particles observed for the as-implanted state and after annealing at 600 °C are approximately 12 and 20 nm, respectively. The EDX analysis shows mostly silver for the particles, I was detected only in a minor amount. From the TEM images thickness reduction of the top layer was seen to occur both after implantation and as a result of the heat treatment. The former can be attributed dominantly to a sputtering-related phenomenon and the latter is believed to correlate with a densification based on the collapse of open structures present in the implanted layer.

Fig. 3 shows an AFM image of the planar view of the same sample as in Fig. 2a. The largest structures, visible as spheres, are approximately 100 - 120 nm in diameter, thus well exceeding that derived from TEM and XRD measurements. Generally, objects seen by AFM appear greater than their real size, because the cantilever tip can scan the surface only from a distance and are due to the tip size- and shape-limited resolution.

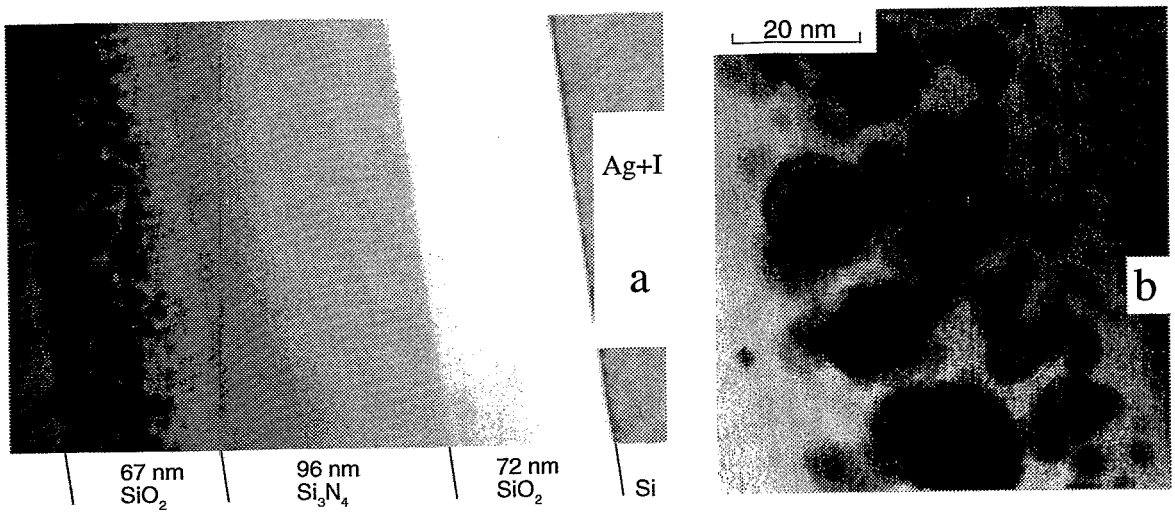

Fig. 2:

TEM images of the as-implanted sample (a) and after annealing (b) at 600°C for 10 min. Implantation of Ag and I up to doses of $6x10^{16}$ cm^{-2} into SiO_2 layer.

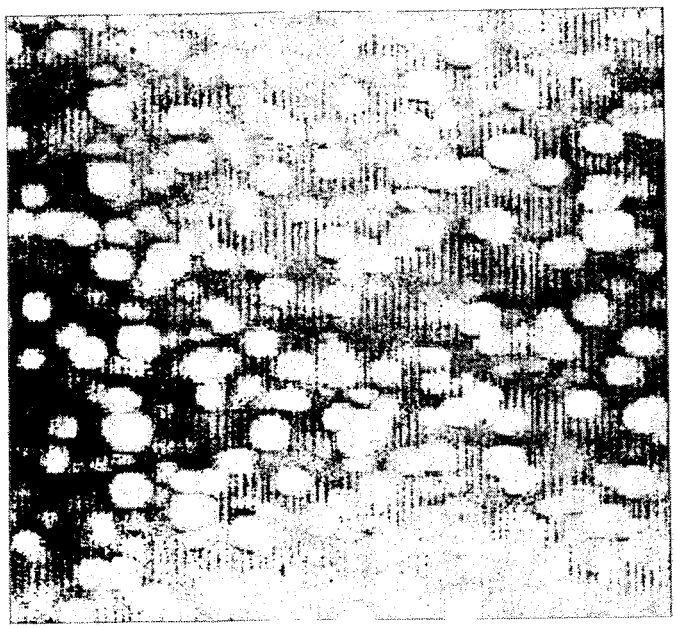

Fig. 3:

Planar view AFM image of the same sample presented in Fig. 2b. The imaged area was 2000 x 2000 nm^2.

For samples implanted with Ag and Cl, XRD pattern reveals the crystalline cubic AgCl phase Chlorargyrite. All Bragg reflections expected to appear from AgCl were found: (111), (200), (220), (311), (222), and (420). These diffraction features were found for all samples, including as-implanted and heat-treated (up to 900 °C) samples, suggesting that AgCl is formed already during ion implantation. For the ion dose rates used, the substrate heating due to ion bombardment was estimated to be 140-170 °C, hence the as-implated state is assumed to correspond to this temperature level. In contrast, after implantation of Ag and I crystallites of silver were conclusively observed, but no AgI. All four Bragg reflections in the examined θ range, i.e. (111), (200), (220), and (311) were identified. During annealing a formation of crystalline AgI was also not observed. The absence of AgI may be explained by a lower percentage of I entering the SiO_2. For samples with ion ratio Ag:Cl = 10 the formation of only silver crystallites was observed by XRD too.

The mean particle size estimated from the XRD peak broadening using the Scherrer' s formula confirms qualitatively the TEM and AFM results. Fig. 4 shows the mean particle size as estimated from the resolution corrected line width of the Bragg peaks (left scale). The Scherrer formula contains a scaling factor depending on particle form. We can overcome the size differences from XRD and TEM by applying the scaling factor 0.5 to the XRD data (right scale). The general trend observed is that the particle size increases with the annealing temperature. The largest change was seen for Ag and I implantations with particle diameter being more than double at 600 °C compared to that at ~ 150 °C.

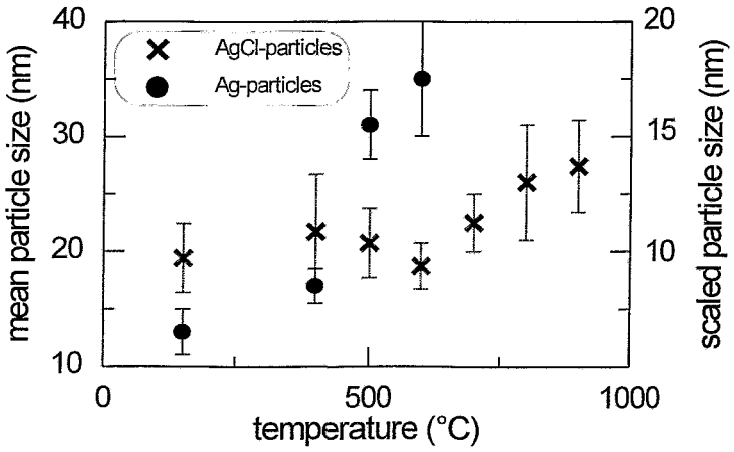

Fig. 4:

Mean particle sizes deduced from the line broadening of Bragg peaks in XRD (left scale). The SiO_2 matrix was implanted with Ag and Cl/ I with the dose of $6x10^{16}$ cm^{-2} each. In the case of Ag and Cl AgCl crystallites were observed. In the case of Ag and I only silver crystallites were detected by XRD.

The right hand scale is from the correction of the particle size according to the TEM observations (scaling factor 0.5).

Silver implanted in silica and glass is known to form spherical particles [16,17], the behaviour of which due to thermal treatment, however, is quite different. Heat treatment following implantation has been shown to lead to splitting into smaller units and even to atomic dispersion [18]. The thermal behavior observed in the present work after an additional implantation of halogens provides further strong evidence for chemical reactions of silver with halogens. The repulsive forces acting between Ag particles are increasingly screened by silver halides as a result of this compound formation, thus supporting the particle growth and aggregation. Weak screening resulting from insufficient silver halide formation is evidenced by Cl implantation with Ag in excess, leading to a decrease of diameter with rising temperature. At the surface and in the sub-surface region, particles occur in large concentration. The inter-particle spacing is accordingly small and the tendency to aggregation increases. This effect was observed by AFM, but being less apparent in the cross sectional views by TEM. The larger diameter derived from XRD for Ag and I implanted samples is reasonably consistent with this result, since it presents the aggregate size.

The peculiar situation encountered here is a heterogeneous reaction system resulting from the two-step implantation, Ag followed by halogen: silver particles reacting with a beam of halogen ions. The reaction conditions are characterized by high quenching rates. Taking into consideration this fact, the results from various analytical techniques presented above suggest favourably a model of thin shells of silver halide enveloping a metallic silver core in the case where no silver halide crystals were observed by XRD. In principle, a monolayer of silver halide is sufficient to generate an interfacial potential to be measurable by FEIS. With an ion dose ratio of Ag:Cl = 1, both XRD and FEIS confirmed the formation of crystalline AgCl. In contrast, AgI, although formed according to FEIS, escaped XRD, EDX, and SAD measurements, indicating a small amount and a very limited spatial extent. Also for a ion dose ratio of Ag:Cl = 10, the

formation of AgCl was identified by FEIS, but not by XRD. XRD requires crystalline objects with three-dimensional extension, thus being insensitive in the case of thin shells around a nucleus. Model calculations indicate that AgI shells of about 3 nm thickness around the Ag crystallites produce XRD peak heights for AgI about 200 times less than the silver peaks. This is not detectable by XRD.

In conclusion, semiconducting silver halides crystallites can be encaged in a solid host matrix by ion implantation. With thin SiO_2 film matrices, the method involves implanting silver and halogens followed by a thermal treatment. In the sequential implantation mode with Ag as first implantion followed by halogen, spherical particles of metallic silver are formed which then react with halogens. The resulting material was identified to form spherical crystallites consisting either directly of silver halide or probably of a silver halide shell enveloping a metallic silver core. The formation of crystallites or shells depends on the ion dose ratio in the matrix, on the nature of halogen species but not on the heat treatment. There is a size distribution with a maximum of about 20 and 15 nm in diameter for Ag (in Ag and I) and AgCl, respectively. The heat treatment following ion implantation increases the particle diameter. The coupling of this composite material, as thin films below 100 nm, to a silicon substrate via a nitride layer has been demonstrated. The latter has proved to be an efficient barrier to the movement of silver and silver halides.

References

[1] M.G. Bawendi, M.L. Steigerwald, L.E. Brus, Annu. Rev. Phys. Chem. 41 (1990) 477

[2] R.W. Siegel, Mater. Res. Soc. Bull. 15 (1990) 60

[3] Katherine C. Grabar, R.G. Freeman, M.B. Hommer, M.J. Natan, Anal. Chem. 67 (1995) 735

[4] R.F. Haglund Jr., Li Yang, R.H. Magruder, III, C.W. White, R.A. Zuhr, Lina Yang, R. Dorsinville, R.R. Alfano, Nucl. Instrum. Methods B 91 (1994) 493

[5] C. Flytzanis, F. Hache, M.C. Klein, D. Ricard, Ph. Roussignol, Prog. Opt. 29 (1991) 321

[6] A. Hagfeldt, M. Grätzel, Chem. Rev. 95 (1995) 49

[7] P.V. Kamat, Chem. Rev. 93 (1993) 267

[8] A. Henglein, Top. Curr. Chem. 143 (1988) 113

[9] H. Weller, Angew. Chem. 105 (1993) 43

[10] A. Henglein, Chem. Rev. 89 (1989) 1861

[11] K.P. Johansson, A.P. Marchetti, and G.L. McLendon, J. Phys. Chem. 96 (1992) 2873

[12] A. Fojtik, H. Weller, U. Koch, A. Henglein, Ber. Bunsenges. Phys. Chem. 84 (1988) 969

[13] G.A. Ozin, A. Kuperman, A. Stein, Angew. Chem. 28 (1989) 359

[14] X. Liu, J.K. Thomas, Langmuir 5 (1989) 58

[15] J. Janata, R. J. Huber, Eds., Solid State Chemical Sensors, Academic Press 1985.

[16] P. Mazzoldi, L. Tramontin, A. Boscolo-Boscoletto, G. Battaglin, G.W. Arnold, Nucl. Instrum. Methods B 80/81 (1993) 1192

[17] N. Matsunami, H. Hosono, Appl. Phys. Lett. 63 (1993) 2050

[18] R.A. Wood, P.D. Townsend, N.D. Skelland, D.E. Hole, J. Barton, C.N. Afonso, J. Appl. Phys. 74 (1993) 5754

Dynamic Simulation of Damage Accumulation During Ion Implantation into Single-Crystalline Silicon

M. Posselt

Increasing attention is paid to experimental and theoretical investigations on the alteration of the shape of as-implanted profiles with growing dose due to enhanced dechanneling caused by the defect evolution during ion bombardment. The modeling of the damage accumulation is the most important issue in the simulation of this effect.

Ballistic processes in collision cascades created by the implanted ions produce a complex defect structure. After the collisional phase, prompt in-situ relaxation processes change the damage structure. Depending on the target temperature and other external conditions, recombination and recrystallization take place and result in a reduction of damage. At ion current densities typical for the most implantation experiments considered in connection with investigations on the dose dependence of the shape of implantation profiles, the interaction of collision cascades generated by different ions can be neglected. Therefore, only the defect structure formed after the prompt in-situ annealing has an influence on the ions implanted subsequently.

The nature of the as-implanted damage is not fully understood. The available experimental methods yield only certain details of the puzzle. Molecular dynamics (MD) simulations were recently used to study elementary processes of defect evolution during ion bombardment [1,2]. Since they need a considerable amount of computing time, MD simulations are limited to single ion impacts at low energies, and to the beginning of the damage relaxation. In practical investigations on the interdependence of defect evolution and channeling, dynamic binary collision (BC) simulations prove to be very useful. Due to the lack of quantitative microscopic informations, the damage buildup during ion bombardment and the dynamic change of the target structure are described by phenomenological models. For silicon different models were used. Recent MD simulations have shown that during single ion impact not only point defects but also a considerable amount of submicroscopic amorphous pockets are formed [1,3]. Since the dechanneling of implanted ions is strongly affected by the extension of the defects, amorphous pockets are more relevant than point defects. Therefore, in dynamic BC simulations the assumption of the accumulation of submicroscopic amorphous pockets is more realistic than the consideration of point defect accumulation. At sufficiently high doses certain regions of the target are completely amorphized. The abrupt transition to total amorphization cannot be described in the framework of the simple accumulation model. It is rather assumed to take place if density or size of amorphous pockets exceeds a critical value.

In the statistical approach used in the dynamic binary collision code Crystal-TRIM [4,5] the motion of recoiled target atoms in subcascades is not simulated. Instead, it is assumed that the nuclear and electronic energy deposition of the subcascades takes place at the position where the collision between the ion and the primary-knock-on-atom (PKA) occurs. This approximation has been proved to be reasonable for the present purposes even in the case of heavy ion implants like arsenic where subcascades have considerable extensions [6]. The neglect of recoil motion renders the program fast and efficient. The implanted dose D_o is simulated by N pseudoprojectiles which correspond to dose increments $dD = D_o/N$. The probability p_{ak} that in a certain depth interval k of the target a pseudoprojectile is moving in amorphous material is determined by the total nuclear energy deposition per target atom deposited in

this depth interval by all previous pseudoprojectiles. p_{ak} is defined by the following damage accumulation function

$$p_{ak} = \left\{ \begin{array}{c} c_a N_{dk}^A \\ 1 \end{array} \right\} \text{ if } c_a N_{dk}^A \left\{ \begin{array}{l} \leq c_c \\ > c_c \end{array} \right. \tag{1}$$

where the number of displacements per target atom, N_{dk}^A, is related to the nuclear energy deposition per target atom via the modified Kinchin-Pease formula [7]. The two empirical parameters c_a and c_c characterize the in-situ annealing of amorphous pockets and the onset of total amorphization, respectively. Equation (1) can be considered as the simplest expression to model statistically independent accumulation of amorphous pockets and the onset of total amorphization by only two parameters. The motion of a pseudoprojectile in amorphous material is simulated in the same manner as in the standard TRIM code using the mean atomic distance l as the free flight path and $l/\sqrt{\pi}$ as the maximum impact parameter of a binary collision. Based on the probability p_{ak} at each binary collision it is decided whether the target is amorphous or crystalline. Due to the statistical model, the size and the location of the amorphous pockets are not fixed but change from one pseudoprojectile to another.

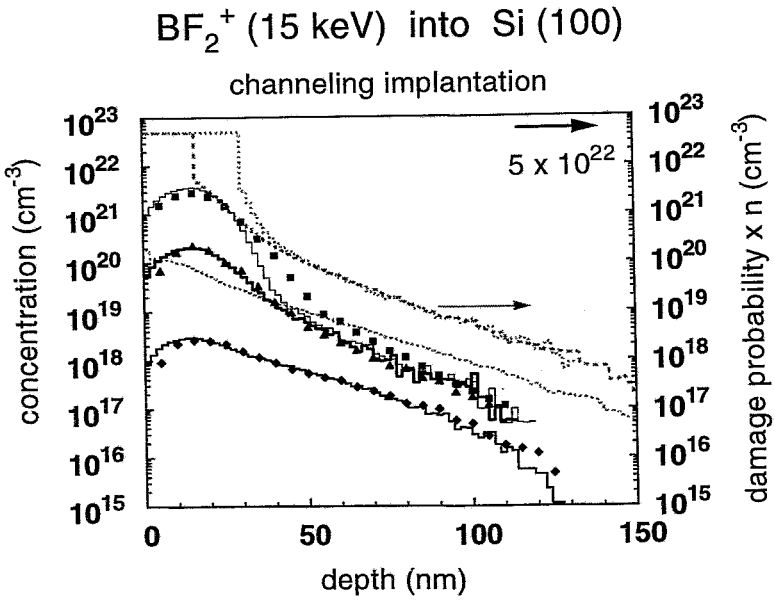

Fig. 1:
Boron range profiles and damage distributions for 15 keV BF_2^+ implantations into (100) Si, into the ⟨100⟩ axial channel direction, for three different doses: 10^{13} (bottom curves), 5×10^{14}, and 8×10^{15}cm^{-2} (top curves). The SIMS data (diamonds, triangles and squares) were taken from [8]. The histograms were obtained by Crystal-TRIM simulations. The damage profiles, given by the damage probability multiplied by the atomic density of Si, are shown by gray dashed and dotted curves.

Fig. 1 shows range and damage profiles for 15 keV BF_2^+ implants. The agreement of the simulated range distributions with SIMS profiles is reasonably good. With growing dose the dechanneling of the implanted ions increases. This leads to the saturation of the channeling

component of the depth profile, but to a further increase of its "random" component. In the simulation of BF_2^+ implants the dissociation of the molecular ions immediately after ion impact is assumed, since the binding energy of the molecules is much smaller than the implantation energy. The trajectories of boron and fluorine projectiles and their range distributions were calculated separately. However, the damage produced by fluorine was taken into account in the simulation of the boron trajectories and vice versa. Note that in Fig. 1 the damage profiles show a weaker decrease with increasing depth than the range profiles. This is due to fluorine which has a somewhat deeper range distribution than boron. The thickness of the amorphous layer can be obtained from the damage profiles shown in Fig. 1. Unfortunately, only a few experiments have been hitherto performed to measure both range and damage distributions. One example is given in Fig. 2. The range profile was determined by SIMS, the thickness of the amorphous layer was measured by cross-sectional transmission electron microscopy (XTEM). The depth dependence of the experimental range profile as well as the thickness of the amorphous silicon layer are reproduced satisfactorily. However, the experimental dose was probably slightly higher than given by Walker et al. [9]. In Crystal-TRIM simulations the empirical parameters c_a and c_c were found to be independent of the ion energy, dose and direction of incidence. They only depend on the ion species and probably on the target temperature. For BF_2^+ implants $c_a = 0.17$ and $c_c = 0.1$ was used.

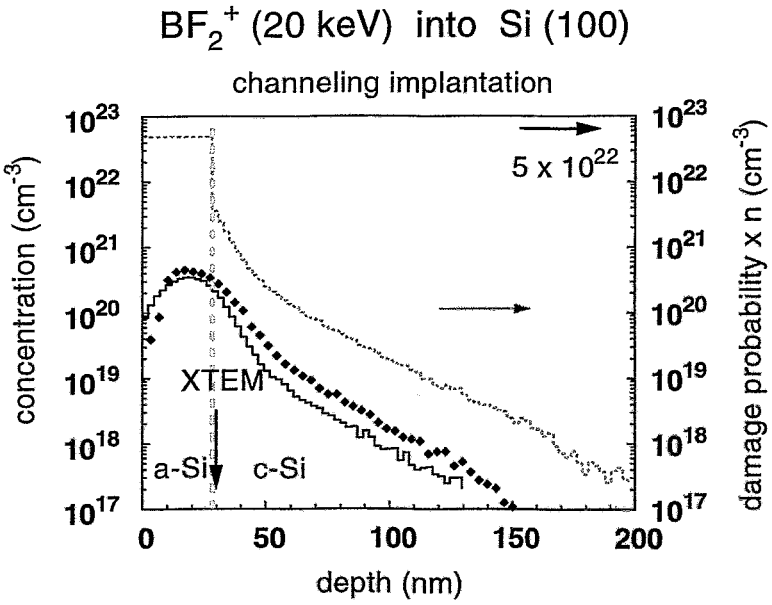

Fig. 2:
Boron range distribution and damage profile for 20 keV BF_2^+, $10^{15}cm^{-2}$ implantation into (100)Si, into the ⟨100⟩ axial channel direction. The SIMS (diamonds) and XTEM data are from Walker et al. [9]. The thickness of the amorphous layer predicted by Crystal-TRIM was 28 nm, in XTEM investigations 30 nm was obtained.

In summary, a statistical approach which assumes the accumulation of amorphous pockets and the formation of extended amorphous zones was introduced into the BC code Crystal-TRIM. Using the simple expression (1) for the damage accumulation function with only two empirical parameters, the change of the shape of range distributions with growing dose as well as the formation of amorphous layers during ion bombardment can be simulated.

Acknowledgements

The author is grateful to Dr. T. Feudel (Swiss Federal Institute of Technology, Zürich), Dr. C. S. Murthy (IBM Semiconductor Research and Development Center, East Fishkill), B. Schmidt, Dr. K.-H. Heinig and Dr. H.-U. Jäger for valuable discussions.

References

[1] T. Diaz de la Rubia, G. H. Gilmer, Phys. Rev. Lett. 74 (1995) 2507
[2] D. M. Stock, G. H. Gilmer, M. Jaraiz, T. Diaz de la Rubia, Nucl. Instr. and Meth. B102 (1995) 207
[3] T. Diaz de la Rubia, M. J. Caturla, private communication
[4] M. Posselt, Nucl. Instr. and Meth. B96 (1995) 163
[5] M. Posselt, Radiation Effects and Defects in Solids 130/131 (1994) 87
[6] A. Simionescu, S. Herzog, G. Hobler, R. Schork, J. Lorenz, C. Tian, G. Stingeder, Nucl. Instr. and Meth. B100 (1995) 483
[7] P. Sigmund, Radiation Effects 1 (1969) 15
[8] A. F. Tasch, S. H. Yang, S. J. Morris, D. Lim, J. Vac. Sci. Technol. B12 (1994) 166
[9] A. J. Walker, P. H. Woerlee, H. G. Pomp, N. E. B. Cowern, J. Appl. Phys. 73 (1993) 4048

Proximity Gettering of Transition Metals in SIMOX (Separation by IMplanted OXygen) Structures

W. Skorupa, N. Hatzopoulos, R.A. Yankov and A.B. Danilin*
*Center for Analysis of Substances, Moscow, Russia

Although a great deal of effort has gone into the development of ion beam synthesized silicon-on-insulator (SOI) structures of high quality [1], the important topic of gettering of transition metals in these advanced materials has received little attention in comparison with bulk silicon. The successful application of ion beam synthesized substrates to the large scale fabrication of improved performance integrated circuits depends on various factors and, in particular, on the ability to control the diffusion of unwanted impurities. Therefore, further research along this line is needed to gain deeper insight into the gettering phenomena in such complex systems.

The first evidence that the damage around an ion beam synthesized buried nitride layer can act as a proximity gettering sink [2] for metal contaminants was given by Skorupa *et al.* [3]. This was inferred from the appreciable increase in the generation lifetime of minority carriers within the implanted region. Kamins and Chiang [4] studied gettering of Cr and Cu in SIMOX material. This material was synthesized according to the conventional fabrication procedure of the early 1980´s and still of poor quality concerning the microstructure. They observed that Cr tends to segregate predominantly to the upper Si/SiO_2 interface whereas Cu segregates to the damage on both sides of the buried oxide. Moreover, it was shown that the buried oxide does not prevent the diffusion of Cu during the anneal. Similar studies of Cu gettering were also carried out by Delfino *et al.*[5]. Recently, Jablonski *et al.*[6] investigated this same phenomenon in more detail using high quality SIMOX substrates and verified, in agreement with the earlier work, that the buried oxide is not a barrier to the movement of the contaminants from the top Si layer into the bulk and *vice versa*. The authors observed that marked segregation of both Cu and Ni occurs to the immediate region below the lower SiO_2/Si interface. It should be noted however, that the presence of metal impurities in the close vicinity of the buried oxide is undesirable as there is a probability of their diffusing back to the active device region during subsequent thermal processing. In recent years, it has been established that both C and He, when implanted in Si at high energies, can form strong gettering sites for metal impurities [7-9]. The proximity gettering method has the added advantages of meeting the requirement for low thermal budget processing and being compatible with IC technology.

In this report it will be demonstrated that by using C or He induced proximity gettering in high quality SIMOX wafers it is possible to remove and stabilize metal contaminants not only away from the silicon top layer, but also remote from the damage region adjacent to the lower interface of the buried oxide where they are normally gettered.

The starting material was commercially available, device grade SIMOX wafers produced by SOITEC [10]. The thicknesses of the silicon overlayer and the buried oxide are 0.2 and 0.4 μm, respectively. To create gettering sites for metal impurities, either C or He ions were implanted into the frontface of the SIMOX substrates. The implant energies were 1 MeV for C and 360 keV for He ions and were estimated by means of the TRIM-92 [11] code in such a way as to position the gettering regions at a depth of about 1.5 μm from the surface. The doses necessary to achieve efficient gettering were chosen to be $1x10^{16}$ cm^{-2} for C ions [8]

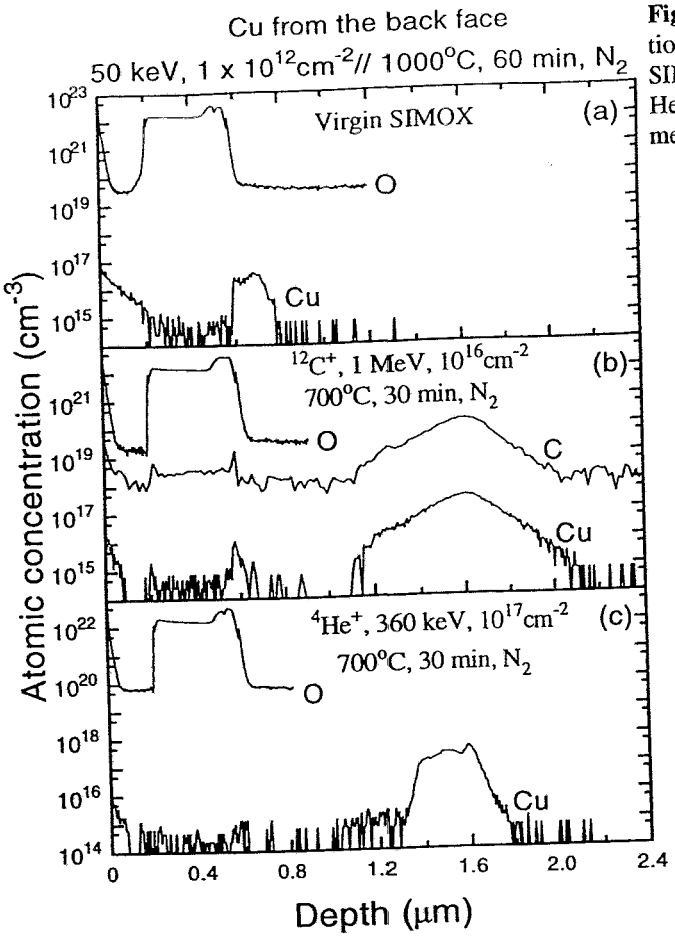

Fig.1: SIMS profiles of SIMOX samples intentionally contaminated with Cu: (a) reference SIMOX sample, (b) C-gettering implantation, (c) He-gettering implantation. For further experimental details, see text.

and $1x10^{17}$ cm^{-2} for He ions [9]. Subsequent to implantation, the samples were annealed in a flowing nitrogen ambient at 700 °C for 30 min. This anneal allows the He gas, which was effectively trapped in the form of bubbles during implantation, to outdiffuse towards the surface leaving empty cavities [9], and would reduce also the density of defects generated in the top Si layer by the gettering implants. The contaminants, Cu or Fe, were introduced from the backface of the SIMOX wafers using 50 keV implants to a dose of $1x10^{12}$ cm^{-2}. In order to diffuse the impurity metals through the whole of the sample thickness, an anneal at 1000 °C was performed for 1h in flowing nitrogen. SIMS analysis was performed on all the samples using a CAMECA IMS *4f* instrument. (For further details of the SIMS data aquisition, see Refs.[12,16].)

The SIMS analyses of the implant experiments designed to study the proximity gettering of Cu and Fe are given in the composite diagrams of Figs.1 and 2, respectively. In all cases, the O profile is of comparable shape and has the characteristic flat-topped appearance due to the presence of the buried oxide. The small peak on the back edge of the O plateau where the O level exceeds that for stoichiometric silicon dioxide is a SIMS artefact typical of the SiO_2/Si interface [13] and is not associated with the microstructure of the buried oxide. Fig.1(a) shows the Cu concentration depth profile in virgin SIMOX. Cu is detected primarily in the region next to the lower interface, consistent with what is known about the gettering behaviour of this impurity in SIMOX material [6], presumably because of the supersaturation of silicon self-interstitials therein [14]. The peak height of the Cu distribution corresponds to a Cu concentration of about $5x10^{16}$ cm^{-3}. Fig.1(b) shows the SIMS results of

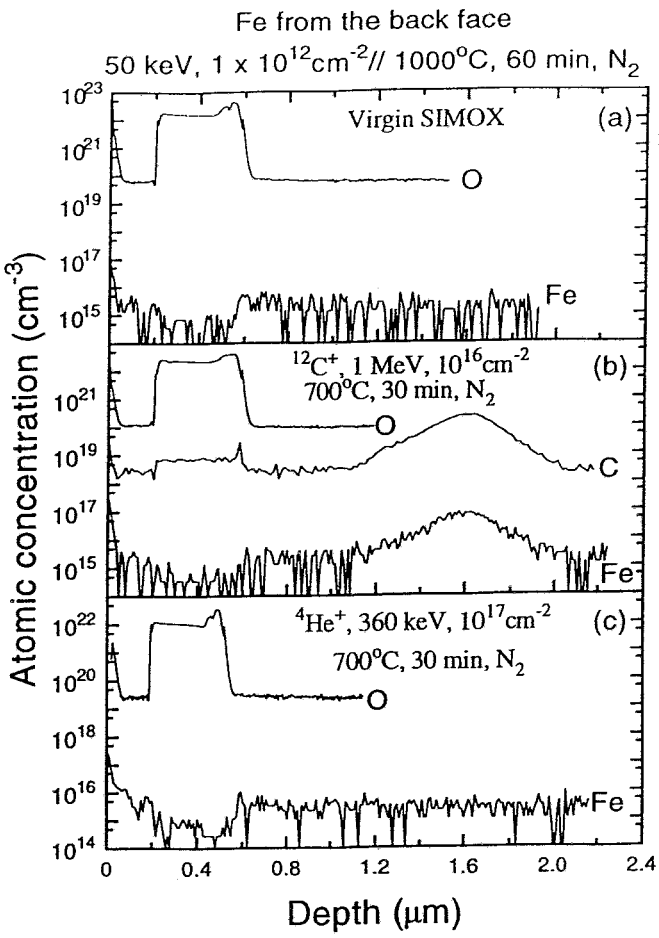

Fig.2: SIMS profiles of SIMOX samples intentionally contaminated with Fe: (a) reference SIMOX sample, (b) C-gettering implantation, (c) He-gettering implantation. For further experimental details, see text.

the experiment involving the implantation of C. The shape of the C implant follows a Gaussian distribution typical of this species when implanted in Si. Of particular interest is the Cu profile which is distinctly different to that in virgin SIMOX samples. Within the detection limit of SIMS, no Cu is found in the region adjacent to the lower interface, neither are traces of Cu detected in the Si overlayer. Instead, the Cu distribution is proven to closely mirror the C profile down to the sensitivity threshold of 10^{18} cm^{-3} for C and 10^{16} cm^{-3} for Cu indicating that Cu has been trapped entirely by the C rich layer. Clearly, the gettering efficiency of the C implant is much stronger than that of the damage below the SiO_2/Si interface. Moreover, the peak height of the Cu profile is an order of magnitude larger than in the case of virgin SIMOX, reaching a value of about $4x10^{17}$ cm^{-3}. For the He implanted SIMOX sample (Fig.1(c)), similar gross features are apparent as in Fig.1(b). Again, like in the C implanted material, no Cu is found around the interfaces of the buried oxide. The Cu has segregated to the projected range of the He ions which means that the metal impurity must have been gettered by the void containing layer resulting from the He implant [9]. The only difference to be noted in this case is related to the width of the Cu profile which is less than that in the C implanted specimen, presumably due to the voids present within a narrow band with a minimum He concentration of 10^{21} cm^{-3} in the as-implanted state [9].The peak height of the Cu depth profile is commensurate with that in Fig.1(b). It is worth noting that although the maximum concentration of gettered Cu is about the same for the two gettering procedures, the amount of implanted C is an order of magnitude lower than that of He. This reinforces the inference that C related defects have a much higher gettering efficiency compared with He.

As far as the Fe contaminated SIMOX material is concerned, there is a complete lack of gettering in both the virgin SIMOX (Fig.2(a)) and the He implanted sample (Fig.2(c)). Distinct gettering of Fe is only observed in the case of C implantation, as previously reported for bulk silicon wafers [15]. Apparently, Cu and Fe have a rather different gettering behaviour, but the reason for this difference is obscure at present. On the basis of the results obtained, the following correlation can be made. Cu segregates to the region below the buried oxide and does so to the He implant. Fe does not segregate to the region below the buried oxide and is not gettered by the He implant. At the present stage one can only speculate as to the nature of the internal "free" surface of the voids formed by the He implantation and annealing. It is likely that O is released from various sources, both internal and external, such as the CZ Si wafer itself, the buried oxide as well as the annealing atmosphere, and may therefore diffuse to the voids, thus oxidizing their internal surfaces. As a result, the SiO_2/Si interfaces so formed become gettering sinks for Cu but not for Fe. In other words, there is an implicit similarity between the "microscopic" gettering efficiency of the voids and the "macroscopic" efficiency of the regions adjacent to the buried oxide.

References

[1] Proc. 6th Int. Symp. SOI Technology and Devices, edited by S. Cristoloveanu (The Electrochemical Soc., Pennington, 1994) Vol. 94-11

[2] In this sense the term "proximity gettering" means gettering caused by a damage layer located very close to the active device region.

[3] W. Skorupa, U. Kreissig, E. Hensel, H. Bartsch, Electron. Lett. 20 (1984) 426
W. Skorupa, P.Knothe, R. Groetzschel, Electron. Lett. 24 (1988) 464

[4] T.I. Kamins, S.Y. Chiang, Mat. Res. Soc. Symp. Proc. 53 (1986) 239

[5] M. Delfino, M. Jaczynski, A.E. Morgan, C. Vorst, M.E. Lunnon, P. Maillot, J.Electrochem. Soc. 134 (1987) 2027

[6] J. Jablonski, Y. Miyamura, M. Imai, H. Tsuya, in: Proc. 6th Int. Symp. SOI Technology and Devices, The Electrochemical Soc. Proc. Vol. 94-11 (1994) 28

[7] H. Wong, N.W. Cheung, P.K. Chu, Appl. Phys. Lett. 52 (1988) 889

[8] W. Skorupa, R. Koegler, K. Schmalz, H. Bartsch,
Nucl. Instr. Methods B55 (1991) 224

[9] S.M. Myers, D.M. Follstaedt, D.M. Bishop,
Mat. Res. Soc. Symp. Proc. 316 (1994) 33

[10] SOITEC, Site Technologique ASTEC, BP 85X, Grenoble, 38041, France.

[11] J.F. Ziegler, J.P. Biersack, U. Littmark, The Stopping and Ranges of Ions in Solids, edited by J.F. Ziegler (Pergamon, New York, 1985) Vol. 1.

[12] S.W. Novak, R.G. Wilson, J. Appl. Phys. 69 (1991) 463

[13] J.A. Kilner, R.J. Chater, P.L.F. Hemment, R.F. Peart, E.A. Maydell-Ondrusz, M.R. Taylor, R.P. Arrowsmith, Nucl. Instr. Methods. B7/8 (1985) 293

[14] A. De Veirman, K. Yallup, J. Van Landuyt, H.E. Maes,
Mat. Science Forum 8-41 (1989) 207

[15] W. Skorupa, R. Koegler, M. Voelskow, K. Schmalz, G. Morgenstern, P.Gaworzewski, Nucl. Instr. Methods B68 (1992) 408

[16] W.Skorupa, N.Hatzopoulos, R.A.Yankov, A.B.Danilin,
Appl.Phys.Lett.67 (1995) 2992

Layered Growth of Boron Nitride Thin Films

M.F. Plass, W. Fukarek, A. Kolitsch and M. Mäder

Cubic boron nitride (c-BN) has remarkable properties, i.e. high hardness, good thermal conductivity, chemical inertness, and a large band gap. c-BN containing thin films are mainly reported to exhibit a layered growth, i.e. cubic BN on top of hexagonal BN next to the substrate [1]. After the first few nanometers, where the c axis is randomly oriented, the hexagonal planes of the h-BN erect, i.e. the c axis is aligned parallel to the substrate surface. On top of this non-cubic material the nanocrystalline c-BN starts growing. The c-BN grain boundaries are sp^2 bonded BN [2].

Transmission electron microscopy (TEM) yields quantitative information about the transformation of non-cubic to cubic growth [1]. As high resolution TEM is very difficult and expensive, it is not practicable as a standard technique. The aim of this work is to resolve the layered growth of c-BN containing films with three different ex situ characterisation techniques, polarised infrared reflection (PIRR), surface sensitive electron energy loss spectroscopy (EELS), and Rutherford backscattering (RBS).

Three samples were synthesised by ion beam assisted deposition on silicon wafers heated to 400 °C, using an ion energy of 500 eV and different ion (nitrogen and argon) to boron atom arrival ratios I/A = 1.6, 1.8, or 2.0. The cubic fraction increases with increasing ion bombardment. No growth of c-BN was detectable with IR spectroscopy for the lowest I/A ratio. Ex situ EELS on the as-deposited samples was performed with an primary electron energy of 3 keV. A contaminated BN surface was probed with an exponential declining information depth of approximately 5 nm. The simulation of the RBS measurements enables an estimation of the elemental contamination profiles. Stoichiometry was assumed for all BN films, which appears to be justified by elastic recoil detection (ERD) results [3].

The IR measurements were performed with s- and p-polarised light in the range between 800 and 7000 cm^{-1}. The angle of incidence ϕ was either 45 or 60 degrees. The PIRR set-up and the data acquisition and reduction has been described in Refs. [3, 4]. The computer program WVASE™ [5] was used to analyse the reflection spectra. The dielectric function $\varepsilon_1(\omega) + i\,\varepsilon_2(\omega)$ is composed of single oscillators, characterised by square function broadened Lorentzians obeying the Kramers-Kronig relation and a frequency independent constant ε_∞ representing the electronic contribution.

The optical properties of h-BN are anisotropic with respect to the c axis, $\varepsilon(E\|c) \neq \varepsilon(E\perp c)$ [6]. To simulate the IR spectra the contribution of the sp^2 bonded BN was separated in an h-BN interlayer and in threefold isotropic BN at the grain boundaries of the nanocrystalline c-BN toplayer. As both structures exhibit different vibrational properties [3], this procedure promises success. The h-BN interlayer is distinguished in two parts concerning the orientation of the c axis. Near the substrate the c axis is randomly oriented, which means this layer with a few nanometers thickness is an isotropic effective medium consisting of the $E\|c$ and $E\perp c$ contributions. Next, the c axis is assumed to be oriented parallel to the substrate. For the c-BN containing films the model was expanded by a third layer with a thickness $d_{c\text{-}BN}$. This toplayer was assumed as an effective medium with a content f_c of the cubic phase and isotropic threefold coordinated BN, which forms the grain boundaries [2]. The model calculations give the different layer thicknesses and various phonon parameters of the BN coatings.

The recorded PIRR spectra and the calculated data are presented in Fig. 1. The spectra exhibit the transverse optical (TO) near 1400 cm^{-1} and the very sharp longitudinal optical (LO)

stretching band of sp^2 bonded BN near 1600 cm^{-1}, and occasionally the c-BN TO mode at 1100 cm^{-1} and the LO mode at 1300 cm^{-1}. The two LO peaks can only be detected with p-polarised light. The correlation of the experimental and the calculated data is reasonably good. The results indicate that with increasing I/A ratio the total h-BN layer thickness decreases, whereas the cubic content of the toplayer remains almost constant.

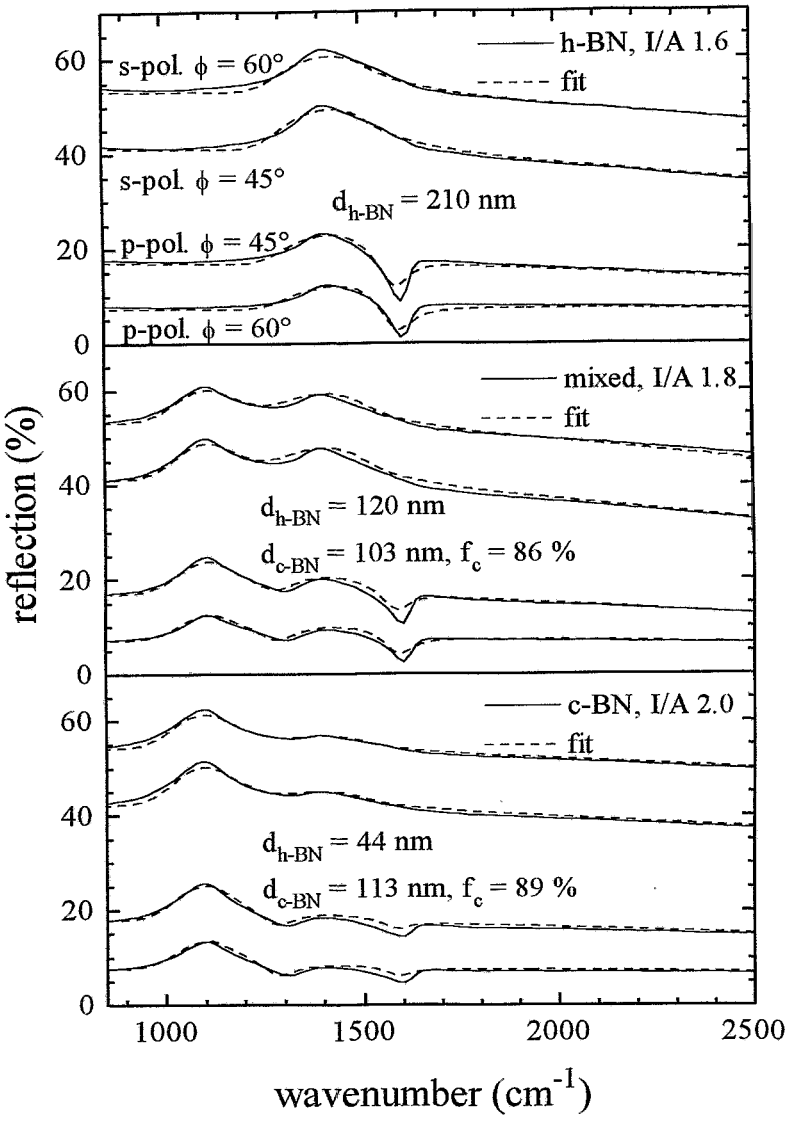

Fig. 1:

PIRR spectra and calculated data: The obtained fit parameters, i.e. the different thicknesses d and the cubic fraction of the toplayer f_c are listed.

The spectra of the EELS measurements are shown in Fig. 2. The spectrum of the non-cubic film exhibits the π plasmon peak at 8 eV and the σ loss peak at 26 eV. The intensity of the π plasmon decreases for the almost pure c-BN sample (I/A = 2.0). The remaining features at an energy loss smaller than 30 eV are due to several monolayers of sp^2 bonded BN or contaminations at the surface. Furthermore, the spectrum exhibits an additional shoulder near 34 eV. Because this kink is a pure σ loss and not a (π + σ) contribution, the peak position indicates a high atomic density comparable to crystalline c-BN. As the spectrum of the mixed sample (I/A = 1.8) shows only marginal differences compared to the cubic sample (I/A = 2.0), the near surface regions of both films are mainly cubic.

The RBS spectra are presented in Fig. 3. The samples are contaminated with Ar, Fe, and W. The metal contaminations caused by the ion source are of the order of 0.05 %. The peak of the Ar incorporation is enlarged in Fig. 3b). A nearly constant Ar incorporation of 4 % is found throughout the non-cubic film (I/A= 1.6). The almost pure c-BN sample (I/A= 2.0) exhibits a smaller Ar content (2.5 %), but an enrichment near the Si interface. The mixed film (I/A= 1.8) shows a clearly detectable alteration of the Ar incorporation at approximately half the film thickness. Near the Si substrate the Ar content is equal the value of h-BN (4 %), but it drops to 2.5 % which is the value in the cubic sample. This observation clearly indicates the layered growth, i.e. the change of the h-BN to c-BN phase. Albeit, the Ar bombardment is essential for the c-BN formation, the Ar incorporation in the denser c-BN is smaller than in the non-cubic phase.

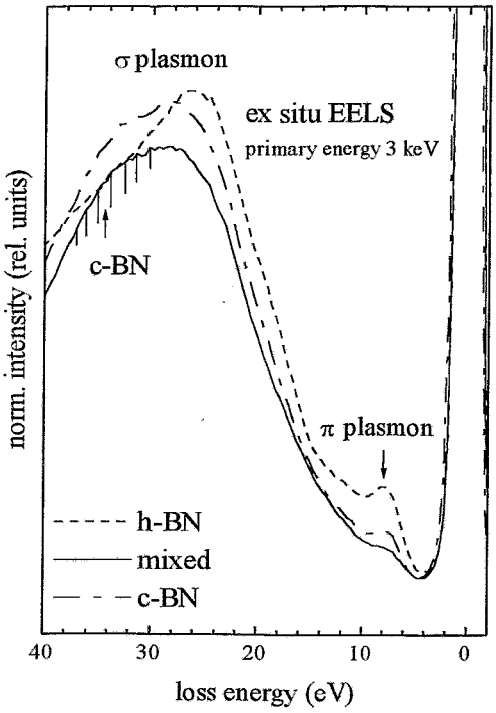

Fig. 2:

EELS spectra of the BN samples deposited with three different I/A ratios (I/A = 1.6: non-cubic, 1.8: mixed, 2.0: cubic).

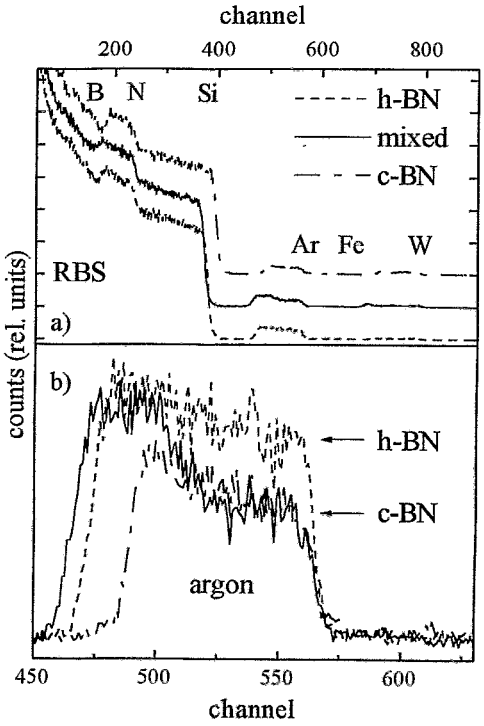

Fig. 3:

RBS spectra of the samples: The lower part is an enlargement of the Ar peak.

We have shown that, besides TEM, RBS or PIRR can be used to resolve the layered growth of c-BN containing films. The alteration point of the Ar incorporation can only give semi-quantitative results, as density and layer thickness are interdependent values during the data analysis. The simulation of the PIRR spectra with a c-BN on h-BN layer model yields the layer thicknesses and the cubic fraction of the toplayer. Both values enable a depth characterisation of the c-BN containing films, in contrast to the established ratio of the cubic to non-cubic IR peak intensities.

Acknowledgements

The authors acknowledge S. Mändl for helpful discussion. This work is supported by the SMWK (No. 4-7514.83-FZR/405).

References

[1] D.J. Kester, K.S. Ailey, D.J. Lichtenwalner, R.F. Davis, J. Vac. Sci. Technol. A12 (1994) 3074
[2] W.-L. Zhou, Y. Ikuhara, M. Murakawa, S. Watanabe, T. Suzuki, Appl. Phys. Lett. 66 (1995) 2490
[3] M.F. Plass, W. Fukarek, A. Kolitsch, U. Kreißig, Surf. Coat. Technol. (accepted)
[4] W. Fukarek, R.A. Yankow, W. Skorupa, Surface and Interface Analysis (accepted)
[5] J.A. Woollam, W.A. McGahan, B. Johs, Thin Solid Films 241 (1994) 44
[6] R. Geick, C.H. Perry, G. Rupprecht, Phys. Rev. 146 (1966) 543

Writing FIB Implantation and Subsequent Anisotropic Wet Chemical Etching for Fabrication of 3D Structures on Silicon

L. Bischoff, J. Teichert and B. Schmidt

Three-dimensional structures in silicon for micromechanical devices have been successfully fabricated by means of deep anisotropical etching [1,2]. Conventionally, etch-resistant oxides, nitrides, or photoresist masks are used to form such patterns on silicon wafers. An alternative etch-stop effect can be utilized with p^+ layers when silicon is doped at a sufficiently high concentration of boron. The same effect has been found for gallium [3] which is also a p-type dopant. In this way thin membranes can be formed using ion implantation of boron or gallium.

A focused ion beam (FIB) of Ga^+ ions offers unique possibilities to form such patterns. Its high level of flexibility in pattern shapes and implantation dose makes it especially important for research projects. The combination of FIB implantation and anisotropic etching results in a much more effective fabrication process than direct FIB sputter etching. Some work using the etch-stop effect of FIB implanted gallium has been carried out by La Marche *et al.* [3], Berry *et al.* [4], Steckle *et al.* [5], Chen *et al.* [6], and Edenfeld *et al.* [7].

The implantation experiments have been performed at the Research Center Rossendorf using the FIB system IMSA-100 [8]. A liquid metal ion source of gallium has been applied. Two ExB filters, built with permanent magnets, separate the two isotopes extracted from the gallium source. A $^{69}Ga^+$ beam of about 1.5 nA, an ion energy of 35 keV and a spot size between 100 and 300 nm has been employed. The beam can be positioned in a 4096 x 4096 pixel array on the wafer surface with a minimum dwell time of 1 µs/pixel. Full computer control of the beam allows to write patterns of arbitrary shape designed with AUTOCAD. Changing the dwell time and/or the repetition rate, the implantation dose has been varied between 1×10^{14} Ga^+ cm^{-2} and 3×10^{16} Ga^+ cm^{-2}. All implantations have been performed on (100) silicon wafers.

Subsequent wet chemical selective and anisotropic etching transfers the as-implanted 2D patterns into 3D structures. The selectivity between implanted and nonimplanted surface areas is given by the dependence of the etch rate in <100> - direction on the acceptor doping concentration, N_A. According to [9], the etch rate $R_{<100>}$ is constant up to $N_A \approx 1 \times 10^{19}$ cm^{-3} and decreases approximately by two orders of magnitude at $N_A \approx 1 \times 10^{20}$ cm^{-3}. Such a concentration in the maximum of the implanted profile corresponds to a gallium dose of $D = 5 \times 10^{14}$ cm^{-2}.

The variety of possible 3D Si structures is considerably large taking into account all possible orientations of a pattern in the (100)-plane and the undercutting of the pattern, especially at convex corners. Two examples of possible pattern orientations are shown in Fig. 1a: an orientation of the pattern boundary lines parallel to the <110>-directions, and an orientation parallel to the <100>-directions. The corresponding etched structures are shown in Fig. 1b. Due to the high etch rate ratio $R_{<100>}/R_{<111>} \approx 40$ for the given etch conditions (30% KOH/-H_2O solution at T = 80°C) trapezoidal or V-groove structures arise in the case A-A. In the case B-B, on the other hand, the (100)-crystal planes are perpendicular to the surface plane, and rectangular grooves can be etched. The undercut etch rate of the pattern boundary lines is the same as the etch rate $R_{<100>}$ perpendicular to the wafer surface. Under the given condi-

tions the etch time for full undercut of a FIB line of 1 µm width is about 1 min. Also, when a n-type silicon substrate is used the Ga^+ implant is electrically insulated from the supporting substrate by a pn-junction. This might lead to a new design of electrically driven micromechanical devices.

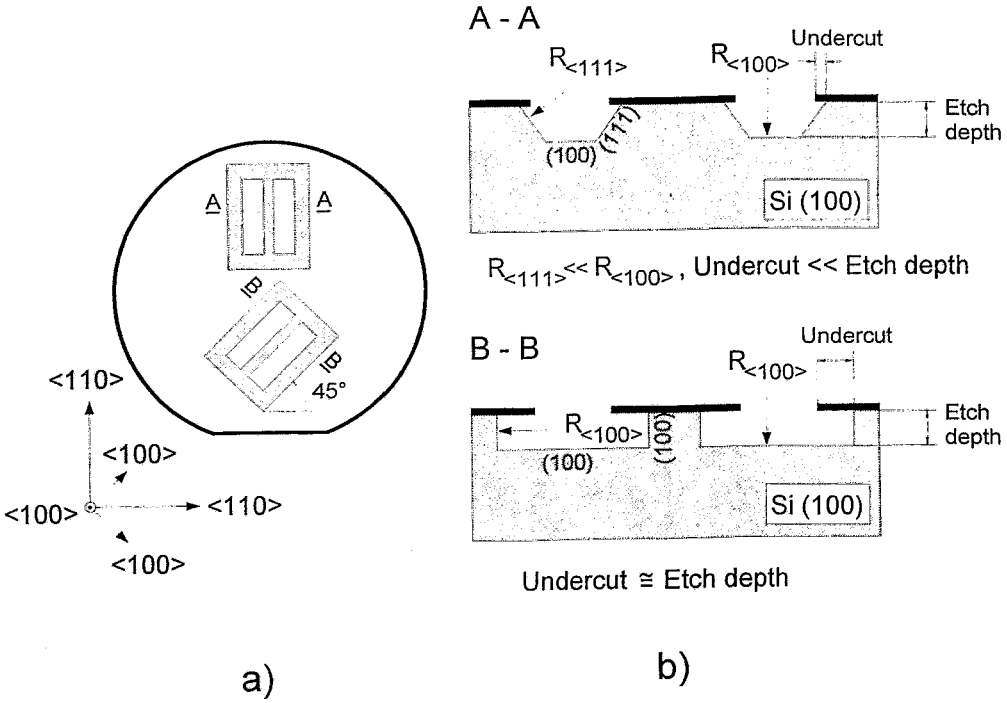

Fig. 1: FIB patterning by Ga^+ - implantation into <100>- oriented silicon wafers marked by shaded areas (a), and corresponding 3D silicon structures after selective anisotropic wet chemical etching(b).

Two examples of FIB patterned and etched test structures are shown in Figs. 2 and 3. In the SEM-image of Fig. 2, quadratic line structures oriented parallel to main wafer flat (<110>-direction) demonstrate the convex corner underetch of 8 µm after 4.5 min etch time leading to an etch depth in <100>-direction of 5 µm. Taking into account the convex corner underetch rate, well defined one-side supported strips can be fabricated. In case of a line orientation of 45° to the <110>-direction, as seen in Fig. 4, fully underetched bridge-like structures can be produced. The etch time was 3 min and the corresponding etch depth 3.5 µm. The free standing band thickness is approximately 50 nm.

A combination of FIB patterning and subsequent anisotropic etching has resulted in various ultra thin 3D structures. First examples of this technique have been presented in this report. Further investigations will focus on possible micromechanical applications.

Acknowledgements

The authors wish to thank Mrs. Dr. R. Müller and Mrs. E. Christalle for SEM analysis.

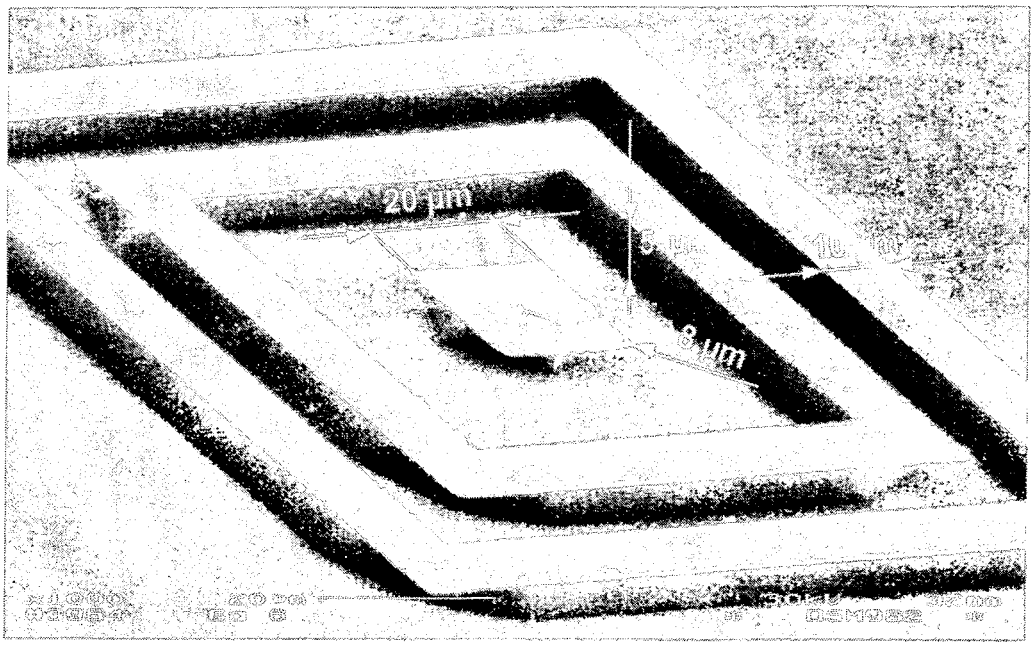

Fig. 2: SEM-image of quadratic line structure demonstrating the undercut at convex corners. The corner underetch rate is about 1.7 x $R_{<100>}$. The lines are oriented parallel and orthogonal to the main wafer flat.

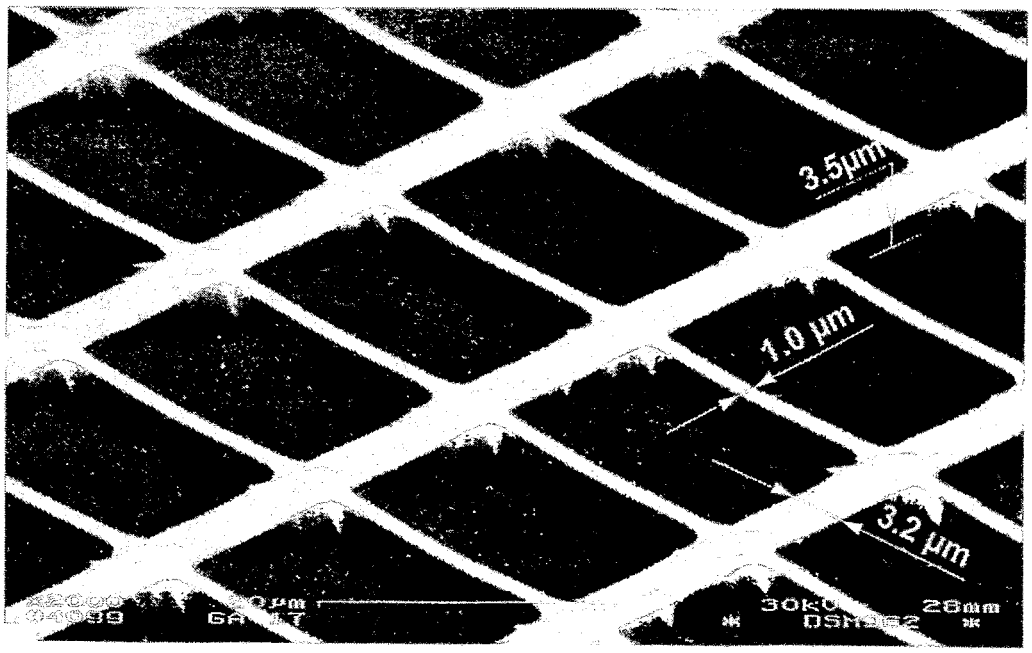

Fig. 3: SEM-image of a free standing grid pattern. The grid is oriented under 45° to the main wafer flat.

References

[1] K.E. Peterson, Proc. of IEEE 79 (1982) 420

[2] G. Kaminsky, J. Vac. Sci. Technol. B3 (1985) 1015

[3] P.H. La Marche, R. Levi-Setti, Y.L. Wang, J. Vac. Sci. Technol. B1 (1983) 1056

[4] I.L. Berry and A.L. Caviglia, J. Vac. Sci. Technol. B1 (1983) 1059

[5] A.J. Steckl, H.C. Mogul, S. Mogren, Appl. Phys. Lett. 60 (1992) 1833

[6] W. Chen, P. Chen, A. Madhukar, R. Viswanathan, J. So, Mat. Res. Soc. Symp. Proc. 279 (1993) 599

[7] K.M. Edenfeld, K.F. Jarausch, T.J. Stark, D.P. Griffis, P.E. Russell, J. Vac. Sci. Technol. B12 (1994) 3571

[8] L. Bischoff, J. Teichert, E. Hesse, D. Panknin, W. Skorupa, J. Vac. Sci. Technol. B12 (1994) 3523

[9] A. Heuberger (ed.), Mikromechanik, Springer Berlin 1989

Ion Drift in Borosilicate Glasses during Anodic Bonding to Silicon or Metals

K. Lange, S. Grigull, U. Kreissig, B. Schmidt, H. Huber* and W. Assmann*
*Sektion Physik, Universität München, Beschleunigerlabor, D-85748 Garching

By anodic bonding [1] adhesive-free hermetic glass-to-silicon or glass-to-metal seals can be produced at low temperatures below the glass transition point. Especially in microsystem technology, anodic bonding of silicon and glass wafers is established as a reliable standard process [2]. However, in spite of broad application and diverse scientific work, the actual mechanisms of anodic bonding are not yet clarified in detail. In particular a better knowledge of corresponding rate processes would be useful to optimize anodic bonding steps with respect to contradictory requests as, for example, low thermomechanical stress and quick, reliable bonding [3]. A key mechanism of anodic bonding is the thermal and, possibly in addition, electric field assisted activation of ions and their drift in the electric field applied during bonding [4-6]. Due to the low thermal activation energies of alkali ions in glasses, their drift is recognized to determine the rate of bonding in general [6]. For blocking anode materials [4] (e.g., silicon or aluminum), that is for negligible migration of anode cations into the glass, this drift results in a polarized depletion layer in the glass at the compound interface. The consequent high electric field within the depletion region leads to a strong electrostatic attraction at the interface and, therefore, to the intimate contact enabling reliable, laterally homogeneous bonding. As well, a high-field assisted movement of more toughly bonded atoms can become possible. Especially the drift of oxygen ions and subsequent anodic oxidation was discussed as reaction pathway which governs the formation of chemical bonds at the compound interface [2,6].

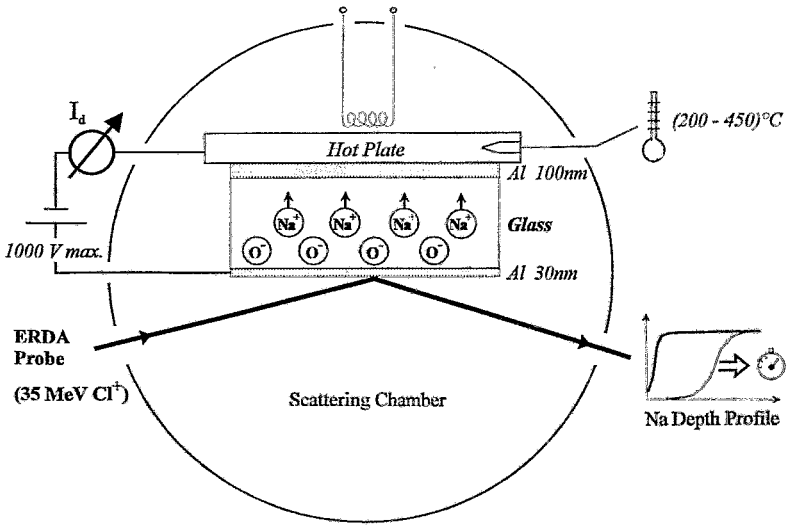

Fig. 1:
In situ ERDA of the electric field induced drift of thermally activated ions.

In the present work, the ion drift behaviour is investigated by quantitative depth profiling using Elastic Recoil Detection Analysis (ERDA) [7]. ERDA is particularly well suited for the objectives of the studies described here because of its ability to measure depth resolved contents of the various atomic components of technical glasses simultaneously [8]. Besides, the non-destructive character of ERDA is used for an in situ diagnostic of drift processes during anodic bonding. As indicated in Fig. 1, glass samples coated with thin aluminum layers were examined in the experiments. Real compounds of glass and thick bulk silicon or metals are unsuitable for ERDA due to the limited accessible depth depending on the range of the respective recoils to be

observed and the special detector system. The ERDA measurements were mainly carried out at the Rossendorf 5 MV tandem accelerator using 35 MeV ^{35}Cl incident ions. Essentially the sodium-borosilicate glass TEMPAX (Schott 8330; identical with PYREX, Corning #7740) was investigated, which is most common in microsystem technology because of its thermal expansion coefficient close to that of silicon. In addition, a microstructurable Li_2O-B_2O_3-SiO_2-glass ("glass A"), especially developed for anodic bonding to silicon, was examined [8]. To increase the analyzable depth, some additional measurements of TEMPAX with 210 MeV ^{127}J as projectiles were made at the 14 MV tandem accelerator of the University of Munich.

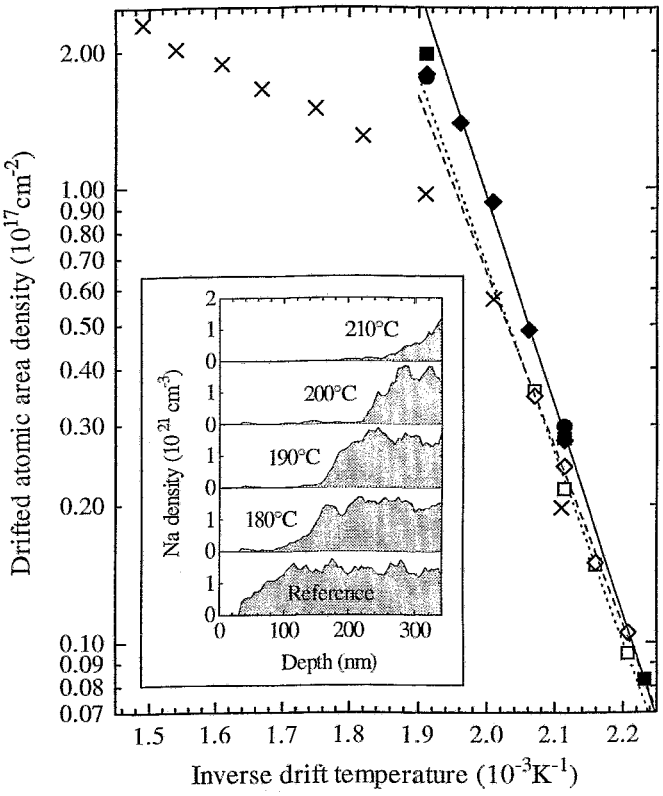

Fig. 2:
Arrhenius plots for the amount of sodium and lithium that is transferred in fixed drift time periods. Data for the lithium drift in glass A are indicated by closed symbols, sodium data for TEMPAX by open symbols and crosses. All data were extracted from ex situ ERDA depth profiles. Examples of sodium depth profiles after drift treatments at various temperatures but fixed voltage of 250 V and 20 min drift time are shown in the insert. The values for TEMPAX plotted as open symbols and those for glass A are not directly comparable due to different drift parameters. The samples of glass A as well as the TEMPAX samples analyzed at the Munich university (crosses) were treated at higher voltage (400 V) and reduced time (10 min).

For the determination of activation energies and drift rates of alkali ions, Al-coated glass samples were treated by drift processes at various temperatures but fixed voltage and period using a commercial anodic bonder and then analyzed ex situ (for details, see [8]). The formation of the depletion layer in TEMPAX at increasing temperatures is shown in the insert of Fig. 2. Due to the recoil detection by a Bragg ionization chamber the accessible depths for sodium and lithium were about 350 nm and 1000 nm, respectively. The density fluctuations in the depth profiles are mainly caused by the statistical errors of the ERDA measurements. The amount of alkali atoms, which the anodic near-surface glass region are depleted of, is given by the difference between the integrated depth distribution of the untreated reference and the treated sample. These atomic area densities are plotted in Fig. 2 on logarithmic scale as function of the reciprocal value of the drift temperature. It has to be emphasized that an Arrhenius-like activation behavior, indicated by the linear fit curves, is expected to be observed by this kind of measurement only for sufficiently small depletion depths as discussed below. In that way, thermal activation energies for sodium of 0.82 eV and 0.77 eV with a standard deviation of 0.04 eV are obtained for the two independent series of samples marked by different open symbols. These energy values agree with the activation energy of 0.80 eV already published for sodium self-diffusion in PYREX #7740 [9]. For the lithium drift in glass A an activation energy of 0.91 eV ± 0.02 eV was found. This value close to that of sodium in TEMPAX points to

similar ionic alkaline bonds in both glasses. The rates of lithium drift, however, are higher compared to the sodium drift rates for identical drift parameters. As main reason the different alkali contents can be considered but phase separations known for glass A could play a role, too. For large depletion layer thicknesses the drift is slowed down due to the reduction of the electric field strength within the layer. In Fig. 2 this saturation effect can be seen at high temperatures. Clear evidence of the drift saturation independently of the thermal activation was given by correspondent in situ measurements. The drifted sodium area density at a temperature of 400°C ($T^{-1} = 1.49 \cdot 10^{-3}\ K^{-1}$ in Fig. 2) corresponds to a depletion layer thickness of about 1.6 µm. Investigations of the bond strength of glass-silicon-compounds joined with full-area electrodes have shown a maximum strength already at a temperature of about 325°C using the same bonding parameters otherwise (400 V for 10 min). In this case, the depletion layer thickness amounts to about 1.2 µm. It should be remarked that, nowadays, temperatures around 450°C are typically used in full-wafer anodic bonding of silicon and TEMPAX for applications in micromechanics. Such high temperatures have their roots in the sufficiently quick bonding despite nonoptimized electrode geometries (e.g., needle cathodes) but they are undesirable with respect to the majority of further requirements on microsystem devices.

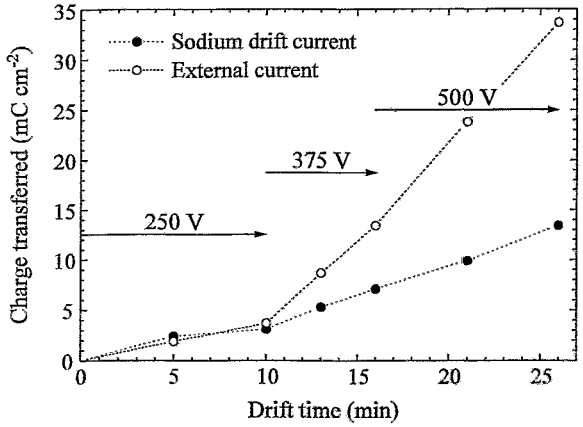

Fig. 3:
Comparison of the transferred charge carried by sodium ions and the total charge moved in the external circuit during a sequence of drift treatments with various drift voltages. Time periods at certain voltages are indicated by the arrows. TEMPAX glass at a fixed temperature of 210°C was used for this in situ experiment. The statistical measurement errors are of the magnitude of the symbol size or smaller.

Further detailed information about the ion drift processes during anodic bonding can be obtained by the in situ ERDA experiments described schematically by Fig. 1. To increase the accessible depth range for heavier recoils like sodium a time-of-flight detector system was installed for these experiments. In the following, an in situ investigation of the influence of the external bias on the ion activation and drift will be discussed as an example. The results shown in Fig. 3 allow to look especially at the electric field assisted activation of charge carriers. For this experiment a TEMPAX sample was heated up to a temperature of 210°C and then treated by a drift process with stepwise increasing voltage. The samples were always glued on to the heated plate to ensure optimal thermal contact. Mainly for the reason of ion beam effects, the ERDA measurements were not performed dynamically in the present case, that is the data were not taken continously during the drift treatment. The ion beam effects had turned out to be mainly due to a local heating of the sample surface which can be controlled by the beam current density and suitable breaks between drift and analysis periods. Therefore, the ion beam analyses were carried out during periods without external bias but still heated sample. The negligible influence of this procedure on the drift was checked by comparison with ex situ experiments. The total charge transported through the external electric circuit was determined as function of the drift time by integrating the external current monitored during the experiment. The part of this charge carried by sodium ions was deduced from ERDA data taken after drift times which are indicated in Fig. 3 by the symbols. From the comparison of the sodium drift current and the total external current, sodium ions can be concluded to be the main charge carriers for a drift voltage of 250 V

at a temperature of 210°C. For the higher voltages applied in this experiment only less than half the external current is caused by the sodium ion drift. In principle, other alkaline or alkaline earth metals (K, Ca), aluminum and oxygen ions as well as electrons might contribute to the total drift current. However, other alkali ions than sodium, alkaline earth metals and further impurities do not contribute significantly due to the low contents. As well, a major contribution from the anodic aluminum coating can be also excluded in the present case from the ERDA results, although the drift of aluminum from the top layer into the glass was already shown by ex situ ERDA measurements of TEMPAX samples treated under comparatively excessive conditions (e.g., T = 450°C, U = 500 V, Δt = 30 min). On the other hand, due to a still unsufficient mass resolution (for Al and Si) a negligible drift could not be inferred for the about 1.1 at% aluminum bulk content in TEMPAX, which has to be compared with the sodium concentration of about 2.4 at%. Moreover, an oxygen drift could not be observed in the present in situ experiment but can also not be excluded because local changes in the oxygen concentration small compared to the bulk concentration of about 64 at% are difficult to detect. As for aluminum, also oxygen ion drift, leading to an oxidation of the aluminum coating, was already proven by ex situ experiments at the same excessive conditions listed above. In particular the oxygen drift needs to be clarified by refined experiments because of its relevance for the formation of chemical bonds in anodic bonding. By further investigating all relevant ions, finally, also the still open question might be answered whether electron conductivity, which is negligible for unmodified TEMPAX under the same conditions, plays a role within the modified high-field depletion layer.

Acknowledgements

This work is supported by the BMBF (contract 13MV0266/8).

References

[1] G. Wallis, D. Pomerantz, J. Appl. Phys. 40 (1969) 3946
[2] H. Baumann, S. Mack, H. Münzel, in: Proceedings of the "3rd International Symposium on Semiconductor Wafer Bonding", edited by C.E. Hunt, H. Baumgart, S.S. Iyer, T. Abe, U. Gösele, Proceedings Volume 95-7 (The Electrochemical Society, Inc., Pennington, New Jersey, 1995) p. 471
[3] A. Cozma, B. Puers, J. Micromech. Microeng. 5 (1995) 98
[4] D.E. Carlson, K.W. Hang, G.F. Stockdale, J. Am. Ceram. Soc. 55 (1972) 337
[5] Y. Kanda, K. Matsuda, C. Murayama, J. Sugaya, Sensors and Actuators A21-23 (1990) 939
[6] K.B. Albaugh, D.H. Rassmussen, J. Am. Ceram. Soc. 75 (1992) 2644
[7] S. Grigull, R. Behrisch, U. Kreissig, M. Harz, Fresenius J. Anal. Chem. 353 (1995) 578
[8] K. Lange, S. Grigull, M. Harz, U. Kreissig, B. Schmidt, in: Proceedings of the "3rd International Symposium on Semiconductor Wafer Bonding", edited by C.E. Hunt, H. Baumgart, S.S. Iyer, T. Abe, U. Gösele, Proceedings Volume 95-7 (The Electrochemical Society, Inc., Pennington, New Jersey, 1995) p. 371
[9] C.G. Wilson, A.C. Carter, Phys. Chem. Glasses 5 (1964) 111

Interpretation of Depth Sensing Hardness Measurements

T. Chudoba

Recently, depth sensing hardness measurements with Vickers or Berkovich indenters have been established as one of the most important tools for the investigation of the mechanical properties of surfaces and thin layers. This was made possible by the development of instruments which are able to measure the loading force and indentation depth continuously with a high resolution. Along with the improvement of the experimental base, a theory was developed by Loubet et. al. [1] and Doerner and Nix [2], and improved by Oliver and Pharr [3], that allows the calculation of hardness values and Young's modulus from the loading and unloading parts of the load-depth function. But up to now the shape of the load-depth function is not fully understood and it cannot be derived from simple material constants. Therefore a model has been developed that allows a better understanding of the elastic part of the deformation. It describes the elastic part of an impression with Vickers or Berkovich indenters by a virtual spherical indenter the radius of which is determined by the E-modulus and the contact area of the elastoplastic deformation [4]. In this way the loading and unloading curve of a homogeneous material can be derived from two parameters, i.e. hardness and E-modulus. The calculations are compared with experimental results.

All measurements presented here were performed with an ultramicrohardness tester DUH-202 from Shimadzu. The instrument has a load range from 0.1mN to 2000mN. The load and displacement resolutions are 0.02mN or 1% of the measuring range and 1nm, respectively. Specially selected Vickers indenters (pyramids with quadratic base) with a tip radius of about 0.1μm were used. Eight to ten indentations were made at each load, averaged and, if necessary, smoothed. By this procedure a standard deviation of 4.7nm could be reached for ten indentations into fused silica at 30mN. For the data handling and the calculation of the results a software was developed that includes corrections of the machine frame deformation and of deviations of the indenter tip from the ideal shape. Different samples from steel, hard metal, silicate glass and silicon were measured in a load range between 1mN and 2000mN.

According to its normal static definition, the hardness H is the quotient of the peak load F_{max} and the projected area A of the impression after unloading

$$H = \frac{F_{max}}{A}. \qquad (1)$$

The area is calculated from the diagonal length (Vickers hardness) or the side length (Berkovich hardness), assuming that the edges are straight lines. The geometry of the elastoplastic penetration of a conical or Vickers indenter into a flat surface is shown in Fig. 1. Under the action of the load F the indenter reaches the maximum depth h which can be divided into the contact depth h_c below the contact area A_c and the depth h_s of the surface deformation outside the contact area. After unloading the surface deflection goes back and the bottom and the walls of the indentation show a certain amount of recovery connected with a change of the shape so that the final depth is h_0. If a depth is calculated from the diagonal of the indentation remaining after unloading, using the known geometry of the indenter, a depth h_p is obtained that is named the plastic depth. It is assumed in the figure that no elastic recovery in the surface plane takes place.

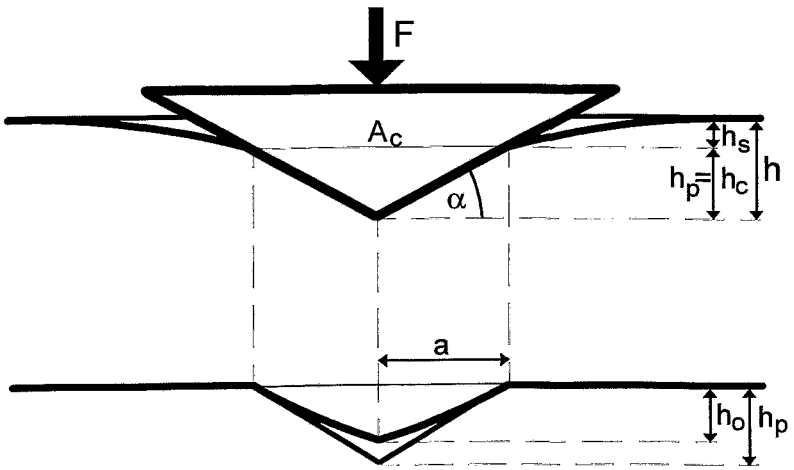

Fig. 1: Geometry of a hardness impression with a Vickers indenter under load (upper part) and after unloading (lower part).

To compare the results of depth sensing hardness measurements with static hardness definitions, it is necessary to establish a relationship between the measured indentation depth h, the contact area under load A_c and the projected area after unloading A, so that the hardness can be computed from its normal definition (1). According to the model of Oliver and Pharr [3] the contact stiffness S as the first derivative of F(h) for pure elastic deformation is required for the separation of the elastic surface deformation h_s and the plastic deformation h_p. It can be shown that the relation between S and the contact area A_c

$$S = \beta \frac{2}{\sqrt{\pi}} E_r \sqrt{A_c} \tag{2}$$

is valid for any axissymmetric indenter and even for a disturbed surface after a hardness impression [5], [6]. The correction factor β depends on the pressure distribution below the indenter and deviates only markedly from 1 for a strongly asymmetric indenter shape [7]. Therefore, equation (2) can be used for the description of an elastoplastic Vickers impression. The elastic deformation of the diamond indenter itself can be easily included by defining a reduced modulus E_r:

$$\frac{1}{E_r} = \frac{1-\nu_i^2}{E_i} + \frac{1-\nu_s^2}{E_s} \tag{3}$$

(subscript i indicates the indenter, s the substrate, E is the Young's modulus and ν the Poisson ratio). The contact stiffness S can be determined at peak load by fitting the unloading curve with a suitable function and calculating the tangent at this point. Then it is possible to determine the elastic surface deformation. Because of $F=C\cdot h^n$ and $S=dF/dh$, the quotient F/S is always a linear function of h. The exponent n depends on the indenter shape. It is 2 for a cone and 1.5 for a sphere. In the pure elastic case the ratio h_s/h is known and with

$$h_s = \varepsilon \cdot \frac{F}{S} \tag{4}$$

a corrected hardness is finally obtained, that is comparable with the Vickers hardness:

$$H = \frac{F_{max}}{K \cdot \left(h - \varepsilon \frac{F_{max}}{S} \right)^2} . \tag{5}$$

K is a constant factor depending on the shape of the indenter. If the indenter tip deviates from the ideal shape, K is a function of the depth h_p and requires the determination of an area function [4].

The value ε in equation (4) was originally derived by Oliver and Pharr [3] to be ε=0.72 for a pure elastic indentation of a cone. In the following it will be shown, that a correct deduction of ε for an elastoplastic deformation is possible, using the model of a virtual spherical indenter (see Fig. 2). It gives ε=0.75 as a reasonable value for the hardness measurement of many materials with Vickers or Berkovich indenters [4]. The basic assumption of the model is, that the elastic deformation above and below the contact area can be calculated using the elastic equations of a sphere. Further it is assumed, that the contact area A_c is equal to the projected area A of the plastic hardness impression after unloading $A_c=A$ with $A=F/H$ (see Fig.1 and 2). The radius of the sphere is calculated on the assumption that the contact area of an elastic impression of the sphere into an undisturbed flat surface is equal to the projected area of the hardness impression:

$$R = \frac{4}{3} \frac{E_r}{F} \left(\frac{A}{\pi} \right)^{3/2} . \tag{6}$$

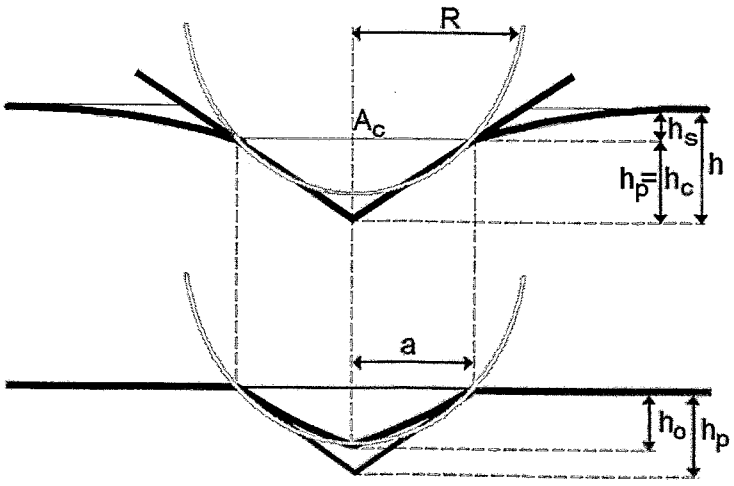

Fig. 2: Geometry of the model of a virtual spherical indenter under load (upper part) and after unloading (lower part) in comparison to Fig. 1.

The model allows to calculate the loading as well as the unloading curve of the load-depth-function by using the known equations for the plastic deformation by a Vickers indenter and the equations for the elastic penetration of a sphere with radius R into an isotropic half-space (see [8]). The $h \propto F^{1/2}$-proportionality assumed hitherto for the loading curve is replaced by

$$h = h_s + h_p = \frac{C_s\sqrt{H}}{E_r}F^{1/3} + \frac{C_p}{\sqrt{H}}F^{1/2}, \qquad (7)$$

with C_s and C_p as constants. An analysis of the measured data of all homogeneous materials investigated in this work shows that this function gives the best fit. One example for the fit of the loading curve of a Vickers impression into synthetic silica with a peak load of 5mN is shown in Fig. 3 (here no values for H and E_r are assumed).

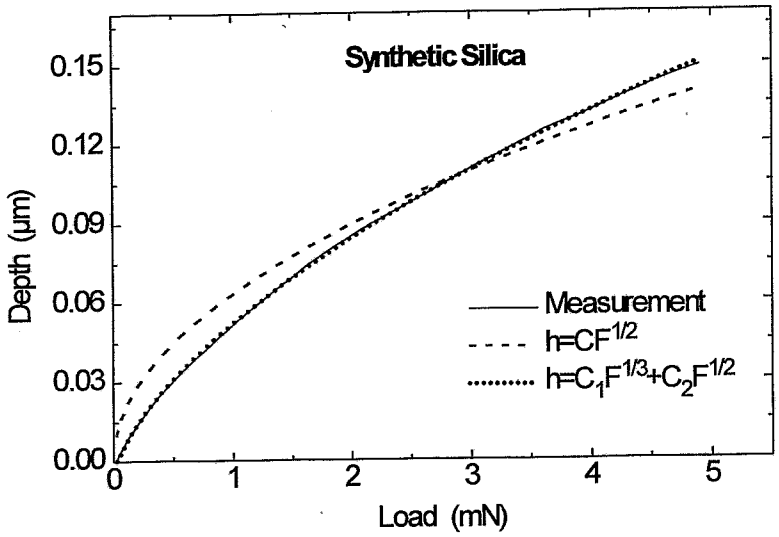

Fig. 3: Comparison of the measured loading curve of a Vickers impression into synthetic silica with two different fit functions.

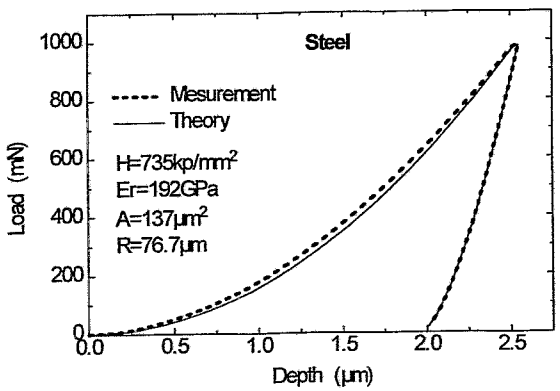

Fig. 4: Measured (dashed line) and calculated (solid line) load-depth function for steel at a peak load of 1000mN using the model of a virtual spherical indenter.

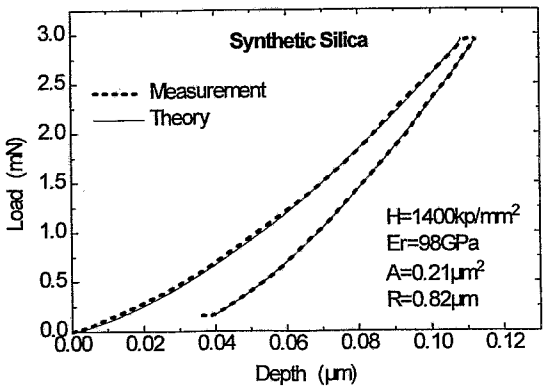

Fig. 5: Measured (dashed line) and calculated (solid line) load-depth function for synthetic silica at a peak load of 3mN using the model of a virtual spherical indenter.

Fig. 4 and 5 compare the measured and calculated (not fitted) load-depth functions of a steel sample (hardness reference plate no. 744-214 from Shimadzu) and of synthetic silica. Input parameter were the known hardness and E-modulus of the materials. It is evident, that the model allows an accurate description of loading and unloading curves for a broad load range. The differences in the loading curves of the steel sample are due to a hardness increase at the surface. Similar results are obtained for the other investigated materials.

For inhomogeneous materials, especially for layer systems or ion implanted samples, the calculation of a depth dependent hardness is more complicated. Here the best way for the interpretation of depth sensing hardness measurements is the calculation of a ratio of hardness between the pure substrate and the modified surface layer.

References

[1] J. L. Loubet, J. M. Georges, J. Marchesini, G. Meille, J. Tribology 106 (1984) 43
[2] M. F. Doerner, W. D. Nix, J. Mater. Res. 1 (1986) 601
[3] W. C. Oliver, G. M. Pharr, J. Mater. Res. 7 (1992) 1564
[4] T. Chudoba, submitted to J. Mater. Res. (1995)
[5] G. M. Pharr, W. C. Oliver, F. R. Brotzen, J. Mater. Res. 7 (1992) 613
[6] H. Gao, T.-W. Wu, J. Mater. Res. 8 (1993) 3229
[7] B. C. Hendrix, J. Mater. Res. 10 (1995) 255
[8] K. L. Johnson, Contact Mechanics, Cambridge University Press, Cambridge 1985

Tritium Depth Profiling in Carbon by Accelerator Mass Spectrometry

M. Friedrich, G. Sun, R. Grötzschel, R. Behrisch*, C. García-Rosales* and M. L. Roberts+
*Max-Planck-Institut für Plasmaphysik, Euratom, Garching, Germany
+Lawrence Livermore National Laboratory, Livermore, USA

For the measurement and depth profiling of hydrogen isotopes in the surface layers of solids several methods have been developed. In Rossendorf both methods Elastic Recoil Detection Analysis (ERDA) and Nuclear Reaction Analysis (NRA) have been successfully applied [1,2]. For the detection of very small amounts of tritium in carbon, such as deposited on the vessel walls of DD fusion experiments, the sensitivities of these techniques are not sufficient. A very sensitive method is the Accelerator Mass Spectrometry (AMS). In this technique the materials to be investigated are sputtered with a Cs ion beam and the particles released as negative ions are accelerated and analysed with an electrostatic tandem accelerator. Contrary to conventional Secondary Ion Mass Spectrometry (SIMS) any interference from molecular ions is suppressed by dissociation of the molecules in the stripper and by use of stopping foils in front of the detector [3]. For tritium detection any background of ^{3}He is negligible because no negative He ions are generated in a Cs sputter ion source.

A test facility for tritium detection by AMS was built up at the 30 deg. beam line of the Rossendorf 3 MV Tandetron [4]. The Cs sputter ion source model 860-C is applied for generation of the negative ions by sputtering the carbon tiles to be investigated. The negative tritium ions are selected with the 82.5 deg. deflecting magnet and are accelerated using the Tandetron at a terminal voltage of 1.5 MV. After acceleration and analysis with the switching magnet the tritium ions are counted with a surface barrier detector. The residual HD and heavier ions are stopped in an Al foil in front of the detector. The facility was optimised by using Ti targets from a tritium contaminated ion getter pump. For this material no single count was measured for tritium with ERDA within one hour, while in our AMS measurements 20,000 counts/s were obtained. For well defined depth profiling the sample to be sputtered is screened by the holder with an 1.5 mm diameter opening and is mechanically scanned over a 3.0 mm diameter area by two off-axis disks rotating at different speeds. Due to this scanning the bell shaped sputter crater is changed into a more cylindrical shape (Fig. 1). After 3 hours sputter time a crater depth of about 20 μm was measured.

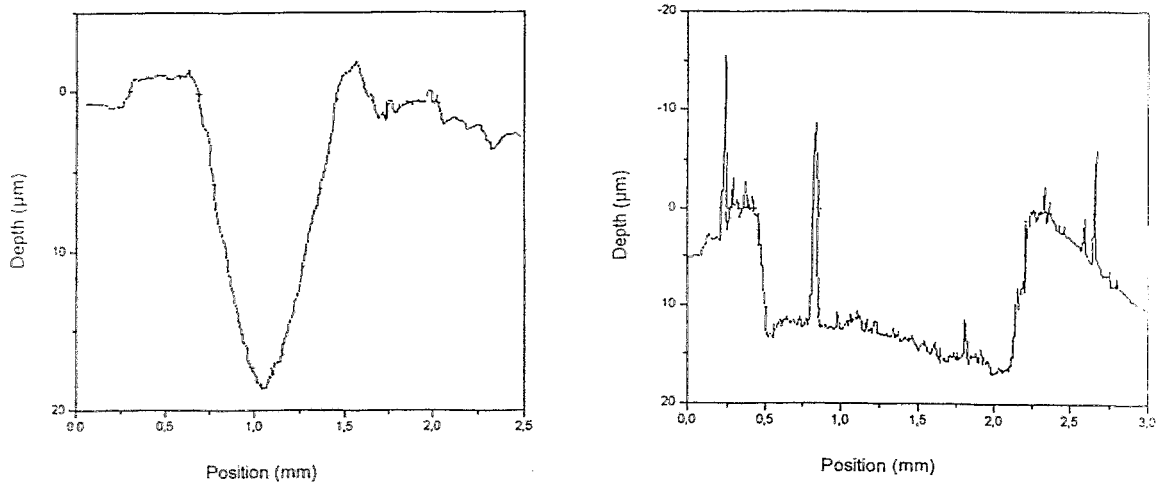

Fig. 1: Measured shape of sputter craters in carbon samples without (left) and with (right) mechanical scanning of the sputter target.

The tritium and deuterium depth profiles measured at a carbon tile from the divertor of the fusion experiment ASDEX-upgrade at the Max Planck Institut für Plasmaphysik Garching are shown in Fig. 2.

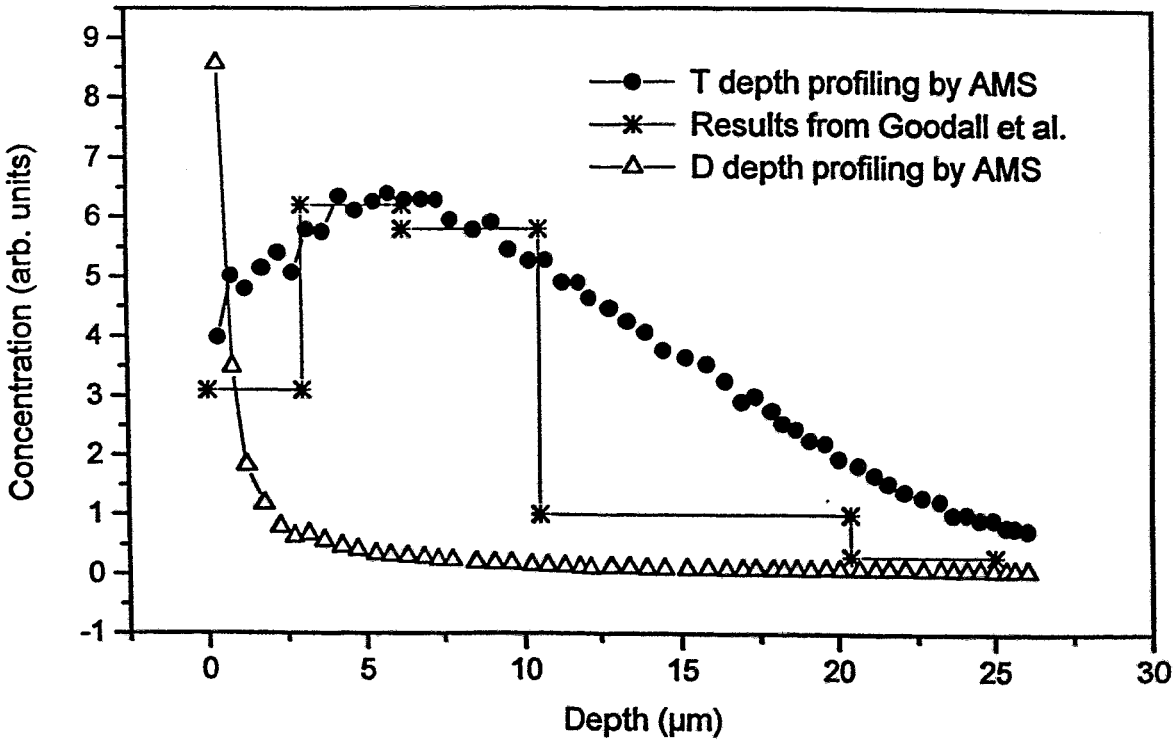

Fig. 2: Depth profiles of deuterium and of tritium in a carbon tile from the Garching ASDEX-upgrade fusion experiment. In comparison the results of Goodall et al. measured at samples from JET are shown.

During the experiment the ion currents of deuterium and carbon are measured in a Faraday cup at the accelerator entrance, while the tritium ions are counted with a surface barrier detector after acceleration. In the figure the tritium profile measured with a different technique [5] at a carbon wall tile of the Joint European Plasma Experiment JET in Culham, England, is also shown. The relatively large depth of the tritium found in the measurements is likely due to the generation of tritium in DD reactions in the plasma with an energy of about 1 MeV. Due to the adsorption of the atmospheric water vapour the hydrogen ion currents of carbon samples from the fusion experiment and of blank samples are of the same order of magnitude. Therefore, these currents give only less information on the fusion plasma.

The absolute isotope ratios T/H including the isotope fractionation are obtained by calibration using a standard sample from the Center for Accelerator Mass Spectrometry of the Lawrence Livermore National Laboratory. The range of the isotope ratios T/H or T/D, which can be measured at our facility is at present about 10^{-6} to 10^{-13}. It is limited by the maximum counting rate of the detector and by the tritium contamination of the ion source, respectively. For exact quantitative calculations of the tritium and deuterium isotope concentration some calibration samples will be prepared by high energy implantation of H and D into carbon.

Acknowledgements

The authors wish to thank Mrs. Romy Aniol for surface profile measurements and the staff of the accelerator department for construction of the beam line, sample preparation and ion source modification. This work is supported by BMFT KKS 06 DR 666 I / TP: 8.

References

[1] U. Kreissig, R. Grötzschel, R. Behrisch, Nucl. Instr. and Meth. B85 (1994) 71
[2] W. Rudolph, C. Bauer, P. Gippner, D. Grambole, C. Heiser, F. Herrmann, H.-J. Thomas, J. Radioanalytical and Nucl. Chem. 83/1 (1984) 99
[3] R. Middleton, J. Klein, D. Fink, Nucl. Instr. and Meth. B47 (1990) 409
[4] M. Friedrich, W. Bürger, D. Henke, S. Turuc, to be published in Nucl. Instr. and Meth. A
[5] D. H. J. Goodall, G. M. McCracken, J. P. Causey, G. Sadler, O. N. Jarvis, J. Nucl. Mat. 162-164 (1989) 1059

Fundamentals of Ion-Solid-Interaction

R. Mathar

Influence of the first-order polarization on point charge stopping in the jellium

Adding the contribution of the next higher order of the density parameter to the random phase approximation (the zeroth-order, non-interacting approximation to the susceptibility) improves the linear dielectric function of the jellium model. The Lindhard-Winther theory of the electronic energy loss is extended by the insertion of the corresponding results by Holas et al. [Phys. Rev. B 20, 4912 (1979)] in a straightforward manner. As known from static approximations to the local-field correction, the low velocity electronic stopping is enhanced. Above the stopping power maximum the first-order dielectric function delivers a correction of the opposite sign.

supported by BMBF

M. Posselt
T. Frei
*C.S. Murthy**

Three-dimensional modeling of low-dose BF_2^+ implantation into single-crystalline silicon

The prediction and control of channeling effects is an important issue in applications of BF_2^+ implants in order to realize ultra-shallow and compact doping profiles. The binary collision code Crystal-TRIM was used to simulate 1D, 2D and 3D boron and fluorine range profiles and damage distributions for 15 keV BF_2^+ implantation into (100) Si. At the relatively low dose of 10^{13} cm^{-2} damage accumulation can be neglected. For a given area at the wafer surface irradiated by the ion beam, it is therefore possible to determine 3D and 2D profiles in an efficient manner by the superposition of point response profiles. Point response profiles are obtained by irradiating a sufficiently small area, e.g. a side of an unit cell of the silicon lattice. The influence of axial and planar channeling, dechanneling and rechanneling on the implantation profiles was studied in detail both for channeling and tilt-angle implants. Considerable lateral channeling branches were found.

Collaboration: * IBM Semiconductor Research and Development Center East Fishkill, USA

*V. Konoplev**
K.-H. Heinig

Mechanisms of silicon self-interstitial formation and diffusion studied by molecular dynamics simulation

Si self-interstitial equilibrium configurations and the collective mechanisms of their random diffusional walk have been studied by MD simulations using the Stillinger-Weber many-body potential. New methods for the search for these configurations and the investigation of the diffusion have been employed. The search of the equilibrium configurations is based on a phase space sampling procedure which imitates the process of the self-interstitial formation in an end-of-range collision cascade. Two <110>-dumbbell-like self-interstitial configurations have been found, the well-known <110>-dumbbell and an extended dumbbell structure (the ground state). The random diffusional walk of self-interstitials consists of single-step and double-step jumps of typical durations and jump distances of 0.3 ps, 3.8 Å and 1 ps, up to 8 Å, respectively. The long distance jumps were found to be composed of two well-resolved stages: the excitation of the lowest energy extended <110>-dumbbell configuration of the self-interstitial in its first excited state, the normal <110>-dumbbell, followed by its deexcitation after some time. The calculated self-interstitial diffusivities have been compared with recently published experimental data.

supported by SMWK

Collaboration: * Institute of Electronics Tashkent, Uzbekistan

K.-H. Heinig

Cellular-automaton-based kinetic Monte-Carlo program for the study of diffusion, nucleation, growth, ripening, and coalescence at ion beam synthesis

Ion beam synthesis of buried layers and nanoclusters is a very complex technique where many physical processes like diffusion, nucleation, growth, Ostwald ripening and coalescence are involved simultaneously and/or successively. For this reason it is very hard to model ion beam synthesis. So far theoretical studies consider only the ripening process as well as the formation of as-implanted impurity profiles taking into account processes like swelling, sputtering and diffusion. Here, the difficulties with analytical models have been avoided by the development of a cellular-automaton-based kinetic Monte-Carlo program. This program considers all physical processes mentioned above simultaneously. First simulations of the ion beam synthesis of $CoSi_2$ nanoclusters as well as of buried $CoSi_2$ and SiO_2 layers give very promising results.

K. Albe

Bonding and structure of boron nitride: First principles calculations

Free energy calculations at T=0 K have been performed with advanced nonlocal-DFT methods (LCAO, Pseudopotential/Planewave) to derive precisely static lattice energies, bulk moduli and lattice parameters for several phases of boron nitride. Recent experimental pressure-volume data for the cubic and hexagonal phase could be reproduced with high accuracy improving former DFT calculations, where the bulk modulus of h-BN was highly overestimated. Regarding the phonon energy in Debye approximation, the zincblende structure has been identified as stable phase at room temperature. An empirical interatomic potential was proposed, combining a modified Tersoff expression and a Coulomb potential with effective charges depending on the interatomic distance. First-principles results were used for parametrization of the proposed potential, which is a promising candidate for MD-simulations.

supported by SMWK

*A.V.Dvurechenski**
R. Grötzschel
K.-H. Heinig
*V.A. Markov**
*V.A. Zinovyev**
*A.F. Zinovyeva**

Effect of low-energy noble gas ion pulses on MBE layer-by-layer growth of Si (111) surfaces

The dependence of the effect of low-energy Kr ion pulses (80-135 keV, 0.5 sec) on the top layer surface coverage during epitaxial growth of Si (111) surfaces has been studied. The Kr pulses lead to an increasing mean intensity of RHEED oscillations, which depends strongly on the mean surface coverage at the moment of the ion pulse. The maximum intensity enhancement was found for nearly completely filled surface layers, whereas the enhancement for a half filled top layer is small. A model has been suggested which takes into account an ion-assisted decay of two-dimensional adatom ions as well as sputter processes. Using input parameters found by our MD calculations, simulations with the set of reaction-diffusion equations of MBE growth have demonstrated qualitatively that surface smoothness is improved by low-energy ion pulse action. A quantitative understanding demands more sophisticated kinetic MC simulations, which are in progress.

supported by BMBF

Collaboration: * Institute of Semiconductor Physics Novosibirsk, Russia

V. Heera
T. Henkel
R. Kögler
W. Skorupa

Evidence for diffusion-limited kinetics of ion-beam-induced epitaxial crystallization in silicon

The theoretical predictions of point defect related models for ion beam induced epitaxial crystallization (IBIEC) with reaction- or diffusion-limited kinetics are compared to each other and with experimental results. It is shown, that the diffusion model provides the correct nuclear energy deposition and dose rate dependence of the IBIEC rate, whereas striking differences are observed for the reaction model. A compilation of several experimental data sets indicates a uniform diffusion regime for IBIEC in a wide range of defect generation rates from $6x10^{17}$ to $2x10^{22}$ $cm^{-3}s^{-1}$. In this range the IBIEC rate can be estimated by a simple formula. The expected layer thickness dependence of the IBIEC rate is verified by in-situ time resolved reflectivity measurements. From these results it can be concluded that point defects originating from both the amorphous and the crystalline side contribute to IBIEC. It is speculated that divacancies are the defects which diffuse and stimulate the recrystallization at the amorphous/crystalline interface.

supported by
DFG and BMBF

T. Henkel
V. Heera
R. Kögler
W. Skorupa
*M. Seibt**

The temperature dependence of ion beam induced interfacial amorphization in silicon

The temperature dependence of the ion beam induced interfacial amorphization process (IBIIA) in silicon has been investigated at temperatures above 80 K using RBS and XTEM. Three regimes are observed: (i) above 320 K the IBIIA rate depends on temperature with an activation energy of about 0.6 eV (thermal regime), (ii) at lower temperatures the rate moves towards a saturation value (transition regime), (iii) below approximately 150 K IBIIA is nearly temperature independent (ballistic regime). The low temperature regime can be explained by an athermal transport of point defects like in ballistic mixing processes.

supported by
DFG

Collaboration: * Institut für Physik der Universität Göttingen

Ion Beam Analysis

R. Grötzschel
S. Grigull
U. Kreißig
M. Mäder
*W. Assmann**
*S. Parhofer***

Thin film analysis by a combined application of RBS and ERDA

Thin magnetic layers of Nd_xFe_yB were studied by a combined application of RBS with He ions (1.7 - 4 MeV) and ERDA with Iodine ions (200 MeV) or Cl ions (36 MeV). RBS provides the Nd and Fe depth profiles whereas ERDA gives the depth information for all light elements when using Z-resolving detectors for the recoils. For the quantification a mutual normalization for the results from the different experiments is necessary. Cross reference peaks of constituing elements or of specially prepared marker layers, which can be well separated with both methods, proved to be advantagoeus.

Collaboration: *Universität München, **Siemens AG Erlangen

D. Grambole
F. Herrmann
*J. Eschenbaum**
*M. Altmeyer**

Hydrogen depth profiling in proton conducting ceramics by the ^{15}N nuclear resonance reaction analysis

High temperature metal oxide proton conductors are useful for various electrochemical devices such as sensors, steam electrolysers and fuel cells. To investigate systematically the influence of different hydrogen loading conditions on the hydrogen content in the samples, the concentration and the depth distribution of hydrogen were measured by the 6.385 MeV resonance of

the nuclear reaction $^{1}H(^{15}N, \alpha\gamma)^{12}C$. The unloaded and hydrogen-loaded thin films of Yb-doped $SrZrO_3$ were obtained at sintering temperatures between 600 and 900 °C using the sol-gel method. The hydrogen content of loaded films was considerably higher then the natural one of the unloaded samples.
Collaboration: *Institut für Physikalische Chemie der Universität des Saarlandes, Otto-Schott-Institut Jena, Fachbereich Elektrotechnik der TU Chemnitz-Zwickau, Picolab Oberflächen- und Spurenanalytik GmbH München, Leybold AG Hanau

D. Grambole
F. Herrmann
*B. Herrmann**

Micro PIXE analysis on bone structures of medieval human femur

Bone structures, represented in the form of so-called lines of arrested growth, were observed in medieval human femur. Because process and causes of line formation are not yet understood multielement analysis on an about 300 µm thick cross section of a femoral bone of a 10 - 12 years old child from Thuringia (Germany), dated across the 8th -11th centuries, was carried out by micro PIXE. Previously the resin-embedded bone sample was polished using an aluminium oxid paste suspension and ultrasonically cleaned by water and alcohol. For the investigation the new nuclear microprobe at the 3 MV tandetron accelerator was used with 3 MeV protons focused to an adapted beam spot size of about 4 µm with a current of about 300 pA. A series of line profiles across the bone lines, elemental maps and point analyses show reproducibly increased concentrations of the trace elements Mn, Fe, Zn, Pb and Sr on the bone lines.

supported by BMFT, DFG, Stiftung Volkswagenwerk

Collaboration: *Institut für Anthropologie der Universität Göttingen

C. Neelmeijer
M. Mäder
*H.-P. Schramm**

The COST-G1 "Paint layers" research program

Since January 1995 groups from twelve European countries have been joined in a communal research program on the application of ion beam analysis to art and archaeological objects - COST (European Cooperation in the Field of Scientific and Technical Research), initiated by scientists of the Louvre (Paris). Coordinating the working group "Paint Layers" within this frame a set of multilayer painting arrangements with representative pigment combinations was prepared for nondestructive Round Robin analysis to select the advantages and limits of both the XRF technique and the IBA techniques with external proton beams. Of special interest are the characterization of the chromophoric and secondary elements of the painting materials including thin buried imprimaturs, and to identify paint layer sequences.

supported by BMBF

Collaboration: *Hochschule für Bildende Künste, Dresden

*B. Köhler**
L. Bischoff
J. Teichert

Investigation of the ion acoustic effect induced by a focused ion beam

The acoustic waves in solids induced by the irradiation with a modulated focused ion beam has been investigated. The aim of these investigations is the development of an ion-beam-acoustic microscope which would allow to image surface as well as buried structures with high lateral resolution. The experiments have been performed using a 35 keV beam of Ga^+ ions with a current of about 3 nA and a spot size of about 300 nm. The ion beam is pulsed with a variable frequency up to 200 kHz. To detect the acoustic radiation a piezoelectric transducer with an integrated preamplifier has been used ($U_{out} \approx$ 20 nV). The in-phase signal from the transducer synchronized with the pulsed

ion beam was measured by a look-in amplifier. Scanning the ion beam across a sample, it could be shown that the measured amplitude and phase signals give an image of the sample material distribution.
Collaboration: *FhG-Institut für zerstörungsfreie Prüfverfahren, Einrichtung für akustische Diagnostik und Qualitätssicherung Dresden

Ion Beam Surface Modification

Y. Pacaud
V. Heera
R. Kögler
W. Skorupa

Damage behaviour and annealing of germanium implanted 6H-oriented SiC
This project is running an ongoing study concerning the damage behaviour and damage annealing after room temperature implantation of Ge (200 keV, 10^{12}-10^{15} cm^{-2}) into 6H-oriented SiC-wafers. Conventonal furnace annealing was performed at 500 °C and 900 °C in a quartz tube and alternatively at 1500 °C in a vacuum chamber which was refilled after evacuation with pure Argon gas. A variety of methods was used to study the samples: RBS, TEM, EPR, Raman spectroscopy, Positron Annihilation Spectroscopy. In the as-implanted state three different stages of damage were defined in relation to the level of energy deposition into nuclear processes. For the given implantation conditions amorphization started at a fluence of $3x10^{14}$ cm^{-2} ($4.7x10^{21}$ $keVcm^{-3}$). Annealing of the ion induced damage in SiC is more complicated than for silicon. Especially, no perfect recrystallization of the amorphous layers is obtained employing annealing temperatures up to 1500°C. Applying IBIEC (Ion Beam Induced Epitaxial Crystallisation), the temperature for recrystallization -although not yet complete- could be decreased down to 1000 °C or less.
supported by EMRS-Network III: IBOS
Collaboration: EMRS-Network III: IBOS, Universität Erlangen

H. Weishart
H.J. Steffen
W. Matz
W. Skorupa

Ion beam synthesis of conductive layers by tungsten-implantation into 6H-SiC
We studied high-dose implantation of tungsten into 6H-silicon carbide to synthesize a conductive layer. The samples were implanted at 200 keV at 100 °C or 500 °C and subsequently annealed. The influence of implantation fluence and temperature as well as annealing process on the reaction of W with SiC was investigated. RBS, AES and X-Ray Diffraction was used to study structure and composition of the layer as well as chemical states of the elements. Sputtering of the target becomes significant at doses exceeding $1.0x10^{17}$ $W^{+}cm^{-2}$. Amorphous phases of tungsten carbide and silicide form already in the as-implanted samples. An implantation at 100°C and annealing at 950°C leads to the crystallization of W_2C; tungsten silicide, however, remains amorphous. After implantation at 500°C and subsequent annealing crystalline W_5Si_3 forms, while tungsten carbide remains amorphous.

V. Heera
H. Reuther

High dose co-implantation of aluminium and nitrogen into 6H-silicon carbide
Results are presented about the impurity distribution and phase formation after high dose co-implantation of aluminium and nitrogen into 6H-SiC at room temperature and subsequent annealing between 1300 °C and 1700 °C. The composition and structure of the implanted and annealed layers have been investigated by AES, RBS, RHEED and XTEM. Nanocrystalline material of 3C

polytype is formed after annealing below 1500 °C. At higher temperatures, transformation into single crystalline material is obtained. However, this process is accompanied by impurity losses. Therefore, it was not possible to produce single crystalline $(SiC)_{1-x}(AlN)_x$ phases.
Collaboration: Institut für Festkörperelektronik der TU Ilmenau, Department of Materials Science and Engineering, Case Western Reserve University Cleveland, USA

V. Heera
*J. Stoemenos**
R. Kögler
W. Skorupa

Complete recrystallization of amorphous silicon carbide layers by ion irradiation

Ion-beam-induced recrystallization of amorphous surface layers on single crystalline silicon carbide substrates (6H-SiC) at 500 °C and 1050 °C has been investigated at temperatures by XTEM and RBS in the channeling mode. It is shown, that ion irradiation reduces substantially the on-set temperature of both the epitaxial layer regrowth and the random nucleation of crystalline grains. Two recrystallization regimes have been found. At 500 °C ion-beam-induced random nucleation (IBIRN) of crystalline grains strongly competes with ion-beam-induced epitaxial crystallization (IBIEC) and polycrystalline material stops the epitaxial regrowth front in an early stage. At a temperature of 1050 °C IBIEC dominates over IBIRN and a complete, but disturbed epitaxial regrowth is obtained.

supported by EMRS-Network III: IBOS

Collaboration: *Aristotle University of Thessaloniki, Physics Department, Thessaloniki, Greece

*P. Werner**
R. Kögler
*G. Mariani***
W. Skorupa

TEM imaging of C-Si defects in carbon-implanted silicon

Buried carbon-implanted layers in silicon were produced by high energy implantation of carbon ions into (100) CZ-Si. The depth distribution of carbon and the morphology of the implanted layer as well as the agglomeration and precipitation of carbon was investigated as a function of thermal annealing (700-1150 °C, 30 s) by TEM and SIMS. The outstanding properties of the carbon-implanted layer (effective impurity gettering, no formation of extended defects as loops or dislocations, and trapping of silicon self interstitials by carbon) can be related to the formation of special C-Si defects. The TEM images show agglomerates of such C-Si defects with a diameter of about 1 nm. For temperatures higher than 800 °C the density of these defects rapidly decreases and small incoherent SiC precipitates with a diameter of about 5 nm are formed.
Collaboration: *MPI Mikrostrukturphysik Halle; ** MATOP, CNRS Marseilles, France

R. Kögler
W. Skorupa
D. Panknin
F. Eichhorn

Impurity gettering in damaged regions of silicon produced by high energy ion implantation

The impurity gettering behaviour of buried ion implanted layers in Si was investigated for thermal short time treatment (700-1150 °C, 30 s). It was demonstrated that the gettering can be separated into a part resulting from the implant and a part resulting from the damage created by the implantation. The gettering effect of the implantation damage may be much higher than those of the implant, and the gettering region is located far outside the buried ion implanted layer. The damage gettering is unstable under a thermal treatment because the gettering sites vanish by defect annealing. Complete annealing of the implantation damage is necessary to certainly concentrate all impurities inside the gettering layer. But, also at a high temperature of 1000 °C in the region between the surface and projected range of the implant there are damage related "point" defects acting as gettering sites of high efficiency which are not yet

detected by the usual analysis methods (TEM, RBS). Therefore, the investigation of the gettering behaviour is also a tool to detect very small defects and defect agglomerates formed during the damage evolution to study the process of damage annealing.

W. Skorupa
N. Hatzopoulos
R.A.Yankov

Proximity gettering of transition metals in SIMOX (separation by implanted oxygen) structures

The gettering behaviour of Cu and Fe in ion beam synthesized silicon on insulator (SOI) material incorporating a buried oxide layer was investigated before and after the formation of deep gettering zones by either C or He implantation. Secondary ion mass spectroscopy (SIMS) analysis was employed to obtain information as to the C, O, Fe and Cu depth distributions. It is shown that the proximity gettering approach using C and He renders the possibility of removing and stabilizing metal contaminants not only away from the near surface region, but also remote from the buried oxide/substrate interface to which they usually segregate in the absence of efficient implantation induced gettering sinks. C implants are found to have better gettering efficiency as they getter both Cu and Fe whereas He implants getter Cu only. In addition, the C implant fluence needed to achieve one and the same gettering effect is an order of magnitude lower than the He fluence.

Collaboration: Center for Analysis of Substances Moscow, Russia

R. Weber
W. Skorupa

Ostwald-Ripening in oxygen implanted silicon substrates

During precipitation of oxygen in silicon the change from the growth to the ripening stage is continuous. As a consequence, no definite starting configuration for the ripening of SiO_2 precipitates can be found experimentally. Therefore, to follow the development of this precipitation process a series of different ripening stages was investigated. Oxygen was implanted into Cz-Si (100) at 300 keV to a fluence of 1×10^{17} $O^+ cm^{-2}$. The substrate temperature was varied from 230 °C to 650 °C. Annealing was carried out at 1300 °C for 1, 2, 4 and 8 hours. From Secondary Electron Microscopy at bevelled samples the diameter, position and density of the precipitates were obtained in dependence on the depth. The measured data provide informations about the interaction potential between the precipitates, which can be compared with theoretical models. The results from Transmission Electron Microscopy carried out on similar samples support the SEM data.

supported by
BMBF

*L.M. Maksimov**
*A.I. Ryazanov**
K.-H. Heinig
S. Reiss

Self-organization of precipitates during Ostwald ripening

Spontaneous pattern formation of precipitates is analysed using the diffusion interaction between precipitates. An analytical model for the study of the instability of the Ostwald ripening process is proposed. It is shown that, in contrast to homogeneous systems, the diffusion interaction between precipitates can result in self-organization of spatial structures. The mean distance between self-organized precipitate layers is found to be proportional to the diffusional screening length of the system.

supported by
BMBF

Collaboration: * Kurchatov Institute Moscow, Russia

*V. Borodin**
K.-H. Heinig
S. Reiss

The effect of system size on self-organization in finite precipitate ensembles

During heat treatment, a precipitate ensemble within a finite (in particular spherical) volume has a tendency to self-organization forming layered structures (shells) of precipitates. Using a statistical description of an initially equal-sized precipitate system we found that (i) the driving force for the (finite!) system evolution is present from the very beginning, no initial fluctuations are necessary, (ii) the patterning can be observed only for sufficiently large systems with system radius $R_s > \lambda_s$, where λ_s is the screening length, (iii) the patterning results from the dynamical self-resembling layer-by-layer "slicing" from still undisturbed precipitates.

supported by BMBF

Collaboration: * Kurchatov Institute Moscow, Russia

H. U. Jäger

Point defect-based modeling of transient diffusion of boron implanted in silicon along random and channeling directions

The difference in boron diffusion enhancement between channeled implants and random implants was simulated within the framework of a point defect-based model for boron diffusion and activation. In the case of implantation along channeling direction, the self-interstitials enhancing boron diffusion are distributed over a deeper region of the silicon crystal, and longer annealing times are necessary for their outdiffusion to the surface. The amount of anomalous diffusion during post-implantation annealing is therefore computed to be 10 - 50% higher in the implants along the [100] channeling direction than along the random direction. These model predictions are in good agreement with the data reported by Chu *et al.* [Nucl. Instr. Meth. B37/38 (1989) 365].

Collaboration: FhG-Institut für Mikroelektronische Schaltungen und Systeme (IMS2) Dresden

H. U. Jäger

An explanation of trap-limited self-interstitial diffusion and enhanced boron clustering in boron doped silicon superlattices

The time evolution of boron diffusion and electrical activation at low temperatures (670°C) was analyzed for B-doped crystalline Si superlattices which were grown by low-temperature molecular beam epitaxy and subsequently implanted with Si ions. We showed that the two effects found recently by the AT&T Bell Labs group [Appl. Phys. Lett. 66 (1995) 568] and denoted as *trap- limited interstitial diffusion* and *enhanced B clustering* can be explained provided that the transient deactivation of boron is modeled by the first-order reaction $I + B_s \Longleftrightarrow B_i$. Boron atomic and electrical profiles as well as self-interstitial profiles were calculated which reproduce the experimental results.

J. von Borany
*W. Füssel**
D. Panknin
B. Schmidt

Influence of MeV- implantation on silicon bulk and gate oxide properties

Bulk and oxide properties of MOS-capacitors after high energy ion implantation (B^+,P^+; 10 MeV, 10^{11}-10^{15} cm^{-2}; R_p=4.5 / 11.8 µm) through 100 nm gate oxide into n- or p- silicon has been investigated by CV measurements and SR profiling. The interface state density and oxide charge density after annealing is below $3x10^{10}$ $cm^{-2}eV^{-1}$ and $2x10^{10}$ cm^{-2}, respectively, applying subsequent annealing at 600°C ($\leq 10^{12}$ cm^{-2}) or 900 °C (10^{15} cm^{-2}). Observed changes of the bulk properties in the near surface region (≤3 µm) can be characterized as follows: (i) the carrier concentration is remarkle increased, if the implantation fluence (in cm^{-2})

is in the same order of magnitude compared to the substrate doping level (in cm^{-3}), (ii) after implantation of 10^{15} cm^{-2} and 900 °C annealing the minority carrier lifetime significantly increases up to milliseconds for both phoshorous and boron implantation due to gettering of impurities in the buried implanted layer.
Collaboration: *Hahn-Meitner Institut, Außenstelle Berlin Adlershof

W. Skorupa
R.A.Yankov
I.E. Tyschenko
*T. Böhme**
*H. Fröb**
*K. Leo**

Room-temperature, short-wavelength (400 - 500 nm) photoluminescence from silicon-implanted silicon dioxide films

A first experiment was performed to explore the possibility of using low temperature, multiple energy Si^+ ion implantation into thin silicon dioxide films on single crystalline silicon substrates and subsequent short-time thermal processing (Rapid Thermal Processing and Flash Lamp Annealing) to form silicon nanostructures capable of yielding a high-intensity emission in the short-wavelength part of the visible spectrum. The results showed a room temperature photoluminescence band of high intensity at about 450 nm (blue light) with subpeaks at 417, 438 and 467 nm. The blue photoluminescence band was observed using the following implantation conditions: 200 keV, $3x10^{16}$ cm^{-2} +100 keV, $1.8x10^{16}$ cm^{-2}, both implanted at -20°C, followed by an annealing step at 400°C for 0.5 h in forming gas. Flash Lamp Annealing at 1050° C for 20 ms was the only condition to keep this luminescence peak but with a intensity reduction of about 40%.

supported by DAAD (I.E.T.)

Collaboration: *Institut für Angewandte Photophysik der TU Dresden

*M. Palard**
K.-H. Heinig
*M.-O. Ruault**
*H. Bernas**

Study of the ion beam synthesis of $CoSi_2$ nanoclusters

The formation of $CoSi_2$ nanoclusters during 60 kV Co^+ ion implantation into heated Si targets has been observed at the CSNSM-CNRS Orsay by *in-situ, in-beam* TEM observations, i.e. the samples were implanted within the TEM facility. The experimentally found particle radius distributions (PRD) as well as results related to the nucleation and growth processes of $CoSi_2$ precipitate ensembles were compared with computer simulations using the cellular-automaton based kinetic Monte-Carlo program of the Research Center Rossendorf. The combination of this unique experimental technique with the powerful simulations give detailed information about the dose, dose rate and temperature dependence of the PRD as well as about the underlying physical processes.

supported by DAAD

Collaboration: *CSNSM-CNRS Orsay / Paris, France

M. Dobler
H. Reuther
M. Betzl
A. Mücklich

Investigation of iron silicides

200 keV Fe^+ ions were implanted into silicon at 350°C to investigate the phase formation of α-, β-$FeSi_2$ and ϵ-FeSi. Fluences of 1, 3, 5, and $7x10^{17}$ cm^{-2} were used to produce the silicides in different depth (buried layers at the lowest fluence, and surface layers at the highest fluence due to sputtering). The structures were characterized by RBS, CEMS, X-ray diffraction, XTEM, SEM, and AES. α-$FeSi_2$ is formed at the lowest fluences. β-$FeSi_2$ can be detected at each fluence and dominates at the fluences (3 and $5x10^{17}cm^{-2}$) which are connected to the maximum concentration near the stoichiometric value. ϵ-FeSi is formed at the highest fluence. Subsequent annealing of three samples (1, 3, and $7x10^{17}$ cm^{-2}) at 1150°C for 30 s leads to β→α phase transitions and changes in the silicide fractions in the CEM spectra. The sample implanted with $5x10^{17}$ cm^{-2} Fe was additionally irradiated with 3 MeV Si at room temperature, and shows significant changes in the phase composition, too.At all samples, the final

phase composition is nearly the same and indicates an equilibrium state for the formation process of the phases. Depending on the implantation, annealing and irradiation parameters Ostwald ripening, thermal diffusion or ballistical mixing dominates and determines the changes in the silicide layers.

supported by DFG

F. Brenscheidt
E. Wieser
W. Matz

Improvement of the mechanical properties of silicon nitride ceramics by metal ion implantation

An engineering silicon nitride ceramic doped with yttria and alumina was implanted with chromium ions to a fluence of 10^{17} ions/cm^2. The implantation energies varied from 200 keV to 3 MeV according to mean projected ion ranges from 100 nm to 1300 nm as predicted by TRIM simulations. X-ray diffraction measurements show no new chromium containing phases, but a reduction of the Bragg peak intensity. This effect is attributed to the amount of amorphized material in the surface which increases with increasing implantation energy. The wear behaviour of the material was tested with a pin-on-disc wear tester. For a relatively low load of 2 N wear is reduced for all implantation energies. For smaller energies no wear groove is formed and material obviously abraded from the pin sticks on the non-destroyed surface. This behaviour is accompanied by a slight increase in pin wear and friction coefficient with respect to the non-implanted state. Only for the 2 and 3 MeV implantations a wear track is observed which is very shallow compared with the unimplanted sample. Considering the load dependence of the wear behaviour we observed that above a critical load the wear of samples implanted with lower energies becomes higher compared with the unimplanted state. Samples implanted with 2 MeV show a remarkable wear reduction even above this critical load.

T. Chudoba

Improvement of hardness, wear and corrosion of Magnesium by Ti^+ and Mn^+ ion implantation

The mechanical and corrosive surface properties of Mg were studied after 180keV Ti^+ or Mn^+ ion implantation with a fluence ranging from $5x10^{16}$ cm^{-2} to $3x10^{17}$ cm^{-2}. The sputter coefficient was about five times lower than predicted by the Yamamura formula. Implantation depth and ion concentration were investigated by AES and RBS. The measured mean projected range of about 190 nm agrees well with TRIM calculations for both ion species. In the implanted peak maximum a concentration ratio Mn:Mg=1:1 has been obtained at a fluence of $3x10^{17}$ cm^{-2}. The implantation results in a hardness increase close to the surface up to 2.5 compared with an unimplanted sample. At the highest fluence of $3x10^{17}$ cm^{-2} the hardness is lower than that for $2x10^{17}$ cm^{-2}. The reason is seen in a growth of the precipitate radius beyond a critical dimension. An improvement of the wear behaviour was observed for both Ti^+ and Mn^+ implants, caused by a reduction of the adhesive wear. The corrosion was measured by cyclovoltametry. At a fluence of $2x10^{17}$ cm^{-2} the open circuit potential shifts markedly in the anodic direction which indicates a better corrosion behaviour. The shift for Ti^+ is higher than that for Mn^+.

P. Nitzsche
L. Bischoff
J. Teichert
E. Hesse

Focused ion beam sputtering yield measurements for cobalt ions on silicon and related materials

In the case of high fluence focused ion beam implantation or ion milling at energies of about 50 keV the sputtering process determines the limit of deposited ion concentration and the amount of eroded material. In order to measure the deposition a charge- and mass-selected focused ion beam of 35 keV Co^+ ions (IMSA-100) was used to sputter holes of micrometer dimensions into crystalline, amorphous and poly-silicon, as well as SiO_2 and 6H:SiC. For crystalline silicon targets, the sputtering yield was also measured as a function of the incident angle of the ion beam and the substrate temperature. The sputtered holes were analyzed by SEM and surface profiling. The sputtering yields, determined by the volume loss method, were in a good aggreement with theoretical calculations. As $CoSi_2$ has a low specific resistivity it is widely used to fabricate conducting paths on topographically structured surfaces. The results of these investigations will help to improve the quality of such strutures.

supported by SMWK

Ion- and Plasma Assisted Depositon

N.P. Barradas
D. Panknin
E. Wieser
M. Betzl
A. Mücklich

Formation of β-$FeSi_2$- layers by IBAD

Using the IBAD (Ion Beam Assisted Deposition) technique Fe was deposited on silicon at 700°C to form β-$FeSi_2$ while being irradiated with Ar ions. The Ar energy E_{Ar} was varied between 200 and 1000 eV, and the Ar ion to Fe atom ratio I_{Ar}/A_{Fe} between 0.14 and 0.71. The samples grow in a columnar way with pin-holes and their surface is rough. A soft IBAD process with low Ar energy (200 eV) and low I_{Ar}/A_{Fe} ratio (0.14) improves the layer structure in comparison to samples pepared without Ar irradiation. Less pin-holes are formed, and the roughness shows a minimum. The roughness increases for larger E_{Ar} and larger I_{Ar}/A_{Fe}. All samples are polycrystalline but with a pronounced texture. The preferential orientation $FeSi_2(110,101)\|Si(001)$ with a few degrees misorientation and $FeSi_2(010)\|Si(001)$ is found by X-ray diffraction and TEM. The prefered grain orientation is also enhanced by the soft IBAD process. Samples optimized in this way were implanted with Co to fluences between 1.9 and 7.9×10^{16} cm^{-2} to change the bandgap.

supported by EU-program: HCM

A. Kolitsch

Implantation into a-C films

Hard amorphous carbon films prepared by neon ion beam assisted carbon deposition on silicon wafers were investigated before and after modification by 20 keV carbon ion beams of different fluences ranging from 1×10^{15} to 1×10^{18} C^+/cm^2. The microstructure of the as-deposited and post-treated films were characterized by electron energy loss spectroscopy (EELS), in particular obtaining changes of the C-K-edge in the spectra. The results show a well correlated increase of the sp^3-content with rising fluence of 20 keV carbon ions. Ion implantation with enhanced carbon energies e.g. at 200 keV in films thinner than the projected carbon ion range results only in a weak electronic interaction of the ions with the films and improves the adhesion of the films due to interface mixing. Dramatical changes of the mechanical properties such as an hardness increase of such films were not found.

supported by SMWK

Collaboration: TU Chemnitz-Zwickau and TU Dresden

A. Kolitsch
U. Kreißig

Synthesis of carbon nitride containing films by IBAD

The C_xN_y film formation by nitrogen ion beam assisted deposition of carbon was investigated. Comprehensive experiments were devoted to the influence of the nitrogen to carbon transport ratio during the deposition process on the resulting nitrogen content and the composition of the films. The film stoichometry was analyzed by ERDA and the state of chemical bond by XPS. The largest nitrogen content of the carbon films was found using transport ratios of N/C=1-1.2. A further increase of the N_2^+ ion current results in an enhanced resputtering of the film. The variation of the deposition temperature (RT to 450°C) has shown a nitrogen maximum in the films at 200°C. The N-1s core level analysis (XPS) shows a remarkable decrease of the area of the 398 eV binding energy peak (β-C_3N_4?) and an increase of the 400eV (α-C_3N_4, sp^2-structure?) peak with increasing deposition temperature.

supported by SMWK

Collaboration: TU Dresden

N. Schell
W. Matz
F. Prokert

X-ray reflectivity for determination of layer and interface parameters

Investigations of the reflectivity of X-rays of IBAD prepared carbon layers on Si and BN layers were performed with synchrotron radiation in Grenoble and Hamburg. The reflectivity at angles below 3° allows the non-destructive determination of the densities, thicknesses, and interface roughnesses of single or multiple near-surface layers up to an accuracy of less than 1 %.

Post-implantation of C in carbon layers results in a thickness growth rather than in a densification. The unrealistic thickness of the SiC interlayer determined pointed to heavy metal incorporation which was later confirmed by RBS.

In December a laboratory X-ray reflectometer was commissioned in Rossendorf. So this method is now permanently available.

Collaboration: ESRF, Grenoble, University of Lausanne, HASYLAB, Hamburg

R. Küchler

Influence of texture on the velocity of acoustic surface waves

In TiN coatings deposited by ion assisted processes a weak [111] texture is preferred. The influence of any texture on the velocitiy of acoustic surface waves was calculated using the Hamiltons principle (the time average of kinetic and potential energy is equal). The change of the elastic coefficients by such textures was detemined. The phase vecolity was calculated as a function of the present texture. The calculation shows that the velocity of the acoustic surface waves decreased with increasing texture.

supported by DFG

Sensors and Microsystems

J. von Borany,
R. Grötzschel
B. Schmidt
*E. Verbitskaya**

Heavy ion response of silicon high field region detectors

High energy ion implantation of phosphorous (10 MeV, 10^{11}-10^{12} cm^{-2}) has been applied to realize silicon detectors with shallow regions (~5 µm) of high electric field strength ranging from 10 to 150 kV/cm. The detectors were tested for ^{15}N, ^{16}O and ^{35}Cl ions of 1-10 MeV in a backscattering arrangement. With increasing field strength the high energy edge of the backscattering spectra is shifted towards higher channels and an increased slope indicates a better energy resolution. This result is mainly caused by a field dependent decrease of the

effective detector window down to 35 nm. For an electric field of about 50 kV/cm, an excellent energy resolution of 65 keV has been measured for 2-10 MeV ^{15}N ions nearly independent on the ion energy, which is contrary to conventional pn-junction detectors ($\delta E \sim E^{1/3}$). The investigations give rise to the conclusion that the electron-hole creation energy for charged particles is a function of the stopping power, which differ to about 1% between α-particles (150 keV/µm - 3.620 eV) and ^{35}Cl-ions (3500 keV/µm - 3.585 eV).
Collaboration: *PTI St. Petersburg, Russia

J. von Borany
*A. J. H. Maas**
*S. S. Klein**

Modified silicon detector structure for particle discrimination
High field region detectors with MeV- implanted buried n^+- layers (R_p=4.5 µm) have been tested investigating the discrimination between α-particles and light ions (C,N,O) in an ERDA-experiment. The detectors operate in a mode where the depletion is limited in the surface region down to the buried layer. Therefore, the α-particles generate only a dE-signal. The discrimination between scattered α-particles and recoils is realized by a pulse shape discrimination technique. The α-particle component in the two dimensional spectra is suppressed very well, considerably better than in a conventional PIPS-detector made from low resistivity silicon. This result can be explained as follows: (i) the contribution of hole diffusion from the undepleted bulk into the depletion zone to the α-signal amplitude is reduced due to the enhanced recombination in the buried n^+-layer, (ii) despite the low depletion depth the electric field strength is above 20 kV/cm, which is advantegeous for charge carrier collection from the recoils.
Collaboration: *Eindhoven University of Technology, Department of Physics

H. Seifarth
J. von Borany
K.D. Butter

Amorphous Ge films for blocking contacts of high purity (HP) Ge-detectors
Amorphous a-Ge films and hydrogen doped a-Ge:H films were prepared by rf-magnetron sputtering at room temperature in an Ar and Ar (7 % H_2) plasma, respectively. Depending on the temperature, the films exhibit different types of electrical conduction with activation energies of about 0.35 eV, 0.2 eV and 0.1eV. Annealing or hydrogen incorporation reduce the density of localized states and changes their distribution within the energy gap.This leads to an irreversible increase of the sample resistivity and to a shift of the temperature ranges with dominant conduction type.The properties of contacts depend on the energy band profile of the junction between the amorphous Ge film and the HP-Ge crystal. Electrical contacts formed by amorphous Ge films on HP-n-Ge crystals exhibit blocking behaviour for both majority and minority charge carriers.

J. Hüller
M. T. Pham
D. Möller
W. Matz

Preparation and properties of miniaturized thin film planar copper electrodes

The electrode preparation is based on a Si wafer substrate covered with SiO_2 and/or Si_3N_4 layers. The top layer is coated with a thin 50 nm Cu deposit which is converted into CuS by treatment in H_2S. The existence of CuS was shown by X-ray diffraction spectrometry and the complete conversion by the absolute value of the electrode potential. For sensitivity measurements the chip electrode of 5x5 mm^2 in size was coupled to a fluidic microcell using a chip clip technology. The effective electrode area in liquid contact with the flow channel was about 4 mm^2. Nernstian response of 29 mV/pCu between pCu5 and pCu1 has been measured in Cu nitrate and sulphate solutions. This behaviour is in quantitative agreement with reference measurements carried out with a commercial macro-ISE, containing a CuS/Ag_2S pellet.

supported by AiF

J. Hüller
M. T. Pham
D. Möller
M. Mäder
H. Reuther

Ion beam synthesis of thin chalcogenide films: formation of buried arsenic sulphide and copper sulphide in SiO_2

Different, but nearly stoichiometric ratios of S and As / Cu ions (20 keV < E_{ion} < 115 keV) were implanted into SiO_2 up to fluences of about 10^{17} cm^{-2}. Under optimal conditions up to 95% of the implanted fluences could be incorporated. The existence of arsenic sulphide within the SiO_2 matrix by means of AES and XPS. Thermal treatment between 500 and 1000°C leads to strong losses of As, Cu and mainly S down to residual contents of only a few percent, independent of the annealing regime used (RTA or 10 min furnace). Nearly Nernstian Cu^{2+} ion sensitivity has been found only between pCu3 and pCu1.

supported by AiF

Collaboration: Institut Fresenius für Angewandte Festkörperanalytik Dresden

V. Beyer
B. Schmidt

Electrochemical etch stop on buried phosphorous implanted layers for thin Si membrane formation

The buried n-type layers in p-type substrates have been formed by P^+ implantation with E = 5, 10, 15 MeV, D = (1 - 10)x10^{13} and subsequent annealing. Anisotropic window etching from the front side, additional low energy P^+-implantation and annealing and finally Al-layer deposition have been carried out for contacting the buried n-type layers. Using the 3-electrode electrochemical configuration and anisotropic etching in 30% KOH/H_2O solution at 80 °C from the substrate rear side, the etch stop behaviour at the buried n^+-type layers was investigated. Thickness measurements show that at P^+-energies of 5, 10 and 15 MeV c-Si membranes with thicknesses of 4.7 - 8.7 µm can be fabricated. However, the etching stops about 1 - 2 µm before the metallurgical pn-junction. This behaviour is comparable to that found in earlier investigations on low energy implanted shallow junctions and deep diffused pn-junctions.

T. Gehring
*S. Howitz**
*T. Wegener**

Applications of a silicon-based valve-free micropump

The silicon micro membrane pump is based on nozzle-diffuser-elements as fluid restrictions on the in- and outlet. The fluidic structure and the pump membrane are produced by one single etch step. Due to the missing valves the fill-up with fluid is very easy.

Five different applications have been developed and tested. All of them require two pump structures, realized on a single chip. To increase the pump pressure and the flux rate two pumps were serially connected. The parallel pumping structure has similar properties. A double pump combination with two fluid inlets and one outlet allows to mix two different fluids in a variable ratio. Another layout with one inlet and two outlets splits a fluid stream into two channels. Bidirectional pumping is possible with a serial combination of two pumps, working in different directions.

Collaboration: *GeSiM, Technology Transfer Center ROTECH, Rossendorf

M. Harz

Calculation of the curvature of anodically bonded Silicon and TEMPAX

An analytical model basing on the theory of plates and shells has been developed to calculate the stress induced by the anodic bonding process in silicon and TEMPAX-glass. The model considers the bend and stress state of the untreated wafers as well as the mechanical and thermal load conditions during the anodic bonding process. Restrictions of the model are given by the viscoelastic and structural relaxation of TEMPAX-glass. The viscoelastic relaxation allows the linear-elastic calculation up to a temperature of 480°C. The structural relaxation has to be noticed even at lower temperatures of 300°C and, therefore, acting inside the whole bonding temperature range. Taking the glass relaxation processes into consideration the validity of the linear-elastic model is verified experimentally. It turned out that the main reason of stress is the mismatched thermal expansion of silicon and TEMPAX-glass.

Neutron Scattering

A. Hempel
F. Eichhorn

The influence of temperature and air humidity on the mesostructure of cement paste studied by small-angle neutron scattering

Technically important properties like strength, permeability for liquids and gases, thermal insulation and corrosion resistance of hydrated cement as the main component of concrete are determined by its mesostructure. The most important external conditions which influence the development of this structure during the hydration process are temperature and humidity. Small-angle neutron scattering was used to study the structure changes of hydrating Portland cement paste in the size range between 100 and 2000 nm for temperatures between 10 °C and 50 °C and a humidity from 11 % to 100 %, respectively. A maximum of the particle size distribution function is found at a particle radius of about 450 nm. With increasing temperature the growth of hydrates is accelerated. Already after a hydration time of 10 hours the structure tends to a nearly final state. A more compact structure was found after a hydration at low temperature or high humidity. Scanning electron microscopic investigations support these results. The compactness is correlated with the highest strength of the concrete material.

supported by BMBF

Collaboration: HMI Berlin, Institute for Nuclear Physics, Řež near Prague, JINR Dubna, IzfP Saarbrücken/Dresden

K. Walther
K. Ullemeyer
J. Heinitz
M. Betzl

Texture and internal stress studies by neutron time-of-flight technique

In cooperation with other groups the texture of geological samples of quartzites, muscovite-quartzites, calcites (naturally and experimentally deformed samples), granulites and calcit-mylonit-quartzites have been measured. In order to improve the texture machine a new detector arrangement has been designed.

The new experimental facility for internal stress investigations, commissioned in 1995, allows to measure stress depth profiles with minimal scanning steps of 2,5 μm in translation (x,y,z) and 0,0025° in rotation (ψ, ϕ). The investigated volume is 1x1xh mm^3 (h is the height of the neutron beam, 1-10 mm, depending on the sample). This new instrument was tested by experiments with Fe75Cu25 and Zr2.5Nb. A second test experiment was the strain investigation in a bent Al bar. This sample with the dimension 20x15x200mm^3 was bent in a 4-point bending device. From the experimental results of the unbent sample and from the compression and extension zones of the bent sample the strains $\epsilon_c=2.5\cdot10^{-3}$ and $\epsilon_e=3.5\cdot10^{-3}$ are obtained.

supported by BMBF

Collaboration: Joint Institute of Nuclear Research, Dubna, TU Dresden, Universität Göttingen, TU Clausthal-Zellerfeld, Institut of Physics of Earth, Moscow, IFS Moscow, MIFI Moscow, University of California, Berkeley

Ion Beam and Analytical Equipment

M. Friedrich
S. Turuc
W. Bürger

Operation and development of the electrostatic accelerators

The ***2 MV VdG*** has been operated reliably exclusively for RBS measurements. The old electrostatic lens and corrector power supply units have been replaced by new devices. A disruption of the Wennerlunds charging belt after only about 300 hours of operation caused a serious destruction of mechanical parts of the charging system.

The ***5 MV Tandem*** has been applied to ion beam analysis, high energy implantation, surface modification, basic ion-solid interaction research and detector development. No opening of the accelerator vessel due to technical problems was necessary in 1995. The supply and control system of the sputter injector has been completely reconstructed. On the basis of the industrial modular programmable logic controller SIMATIC S5 (Siemens) a remote control of all relevant parameters of the ion source is now available. The power supply system of the duoplasmatron ion source (H, N) has been also modernised.

The ***3 MV Tandetron*** has been used for high energy ion implantation, ion beam synthesis and ion beam analysis including the microprobe facility. Optimized handling procedures of the sputter ion source increased the typical lifetime between necessary source cleaning to more than 500 h. The availibility of He ions was restricted due to heat flow problems at the Li charge exchange channel. A wide variety of ions (H...Au) has been accelerated very reliably at terminal voltages between 0.1 and 3.0 MV. Only one pressure vessel opening due to a defective needle bearing was necessary.

H. Tyrroff
D. Henke
*R. Friedlein**
*G. Zschornack**

Optimization of the ECR ion source and the retardation system with respect to high current ion densities

The charge distribution of ions inside an ECR plasma is substantially influenced by the energy distribution function F(E) of the plasma electrons. We determined F(E) from the Bremsstrahlung spectra emitted from the ECR discharge. The investigations reveal, that the high energy part of F(E) consists of a warm component at about 3 keV and an additional second contribution at about 30 keV for a 7.5 GHz discharge. For a 14.7 Ghz discharge the corresponding components were obtained at 3 keV and 70 keV. The intensity of both components depends on discharge parameters as UHF power, mirror field excitation, gas pressure and gas composition. The ion charge distributions inside the plasma and the extracted beam are different, characterized by the presence of higher charge states inside the plasma.

The optimization of the retardation system results in ion energies between (0.01-10) keVxq depending on the charge state q. The low energy level was determined from the measured plasma popential. For a given q/M, approximately 90 % of the ions, emitted from the source into an acceptance angle of 37 mrad, are transferred to the target onto a spot of 5 mm diameter. Particle fluxes between 10^9 and 10^{13} $cm^{-2}s^{-1}$ are realized for a large spectrum of ions (e.g. 10 nA of Ne^{9+}).

supported by SMWK

Collaboration: *Technische Universität Dresden

J. Teichert
L. Bischoff
E. Hesse
*P.D. Prewett**
*J. G. Watson**
*I. Loader**

A new achromatic ExB mass separator for focused cluster beams

An achromatic ExB mass separator was implemented and tested in the focused ion beam system FIB-50 at the Rutherford Appleton Laboratory. The designed mass resolution of about 35 has been obtained. It was shown that the ExB filter implementation does not reduce the lateral resolution. The FIB-50 system has now the capability for the application of alloy ion sources and the investigation of cluster emission.

The cluster emission of a Cobalt-Neodymium liquid alloy ion source has been investigated. The measurements show an about 10 times higher cluster production than observed for a gallium source. The distribution of the large clusters has a maximum at about 1400 AMU. The mass separator of the Rossendorf IMSA-100 focused ion beam system was able to separate single charged pure cobalt clusters up to a size of about 10 atoms. Focused beams of light cobalt clusters have been produced.

supported by DAAD

Collaboration: *Central Microstructure Facility, Rutherford Appleton Laboratory Chilton, Didcot, UK

E. Hesse
J. Teichert
L. Bischoff

Improvement of the retarding field analyzer

At a retarding field analyzer the ion current passing the retarding electrode is measured in dependence of the retarding voltage. Until now, our experimental arrangement for the characterization of liquid metal ion sources (LMIS) enables only the measurement of energy distributions, but the exact ion energy could not be determined precisely enough to allow conclusions about the energy deficit of the ions. The reason was the use of different high-voltage supply units for the potentials of emitter and retarding electrode, which was necessary for

high voltage stability. This problem has solved by changing the potentials with respect to the earth potential. Now, the emitter is on earth potential and the potential of the retarding electrode is varied around the earth potential. For a Ga-LMIS a energy deficit of 5.5 V was measured for an emission current ranging from 0.7 to 7 μA. A concept for inserting a mass separation system was made.

J. Brutscher
R. Günzel
S. Mändl

Plasma source ion implantation (PSII)

A new facility to carry out plasma source ion implantation (PSII) was constructed and put into operation. Compared to the first facility, developed by the Research Center Rossendorf, several improvements could be achieved. The basic pressure of the new facility was reduced to $5*10^{-4}$ Pa, thus oxygen contamination of the top layer of the PSII treated samples could be considerably decreased below the detection limit of Rutherford backscattering analysis. The high voltage unit of the new facility was constructed for voltages up to 100 kV, switching voltage pulses with a frequency ranging from single shot up to 1 kHz and a pulse duration between 2 μs and 100 μs. The maximum current during the pulse is 10 A. The plasma is produced by an ECR plasma source with a working pressure ranging from 0,1 Pa up to several Pa. In order to investigate the basic processes of PSII an experimental setup for the measurement of the mass and energy distribution of ions extracted from the plasma boundary during the application of the high voltage pulse was installed. First measurements of the plasma parameters could be carried out using Langmuir probes. The probe measurements offered in the pressure range of 0.2 ... 0.5 Pa a plasma density of 10^9 to 10^{10} cm^{-3}, an electron temperature of about 5 eV and a plasma potential of 10 to 15 V.

H. Weishart
R. Kliemann
W. Skorupa

Operation of a heated target chamber for implantation

In 1994 a halogen lamp based heatet target chamber was purchased from Fraunhofer-Institut für integrierte Schaltungen (IIS), Erlangen. This UHV chamber enables implantations at enhanced target temperatures up to 1200°C. The requested mobility of the chamber for coupling to different implanters required a replacement of the cryopump by a turbomolecularpump. For correct fluence measurements, a new heat resistant aperture system directly in front of the substrate holder was designed and installed into the chamber.

W. Matz
F. Prokert
N. Schell
M. Betzl
F. Eichhorn

Project of a synchrotron radiation beam line at the ESRF (ROBL)

The final specification of the beam line optics was made. There will be available a X-ray beam in the energy region 5-35 keV with an intensity of $5x10^{10}$ phot./sec at the sample. The beam may be focussed to a spot less than 0.4x0.4 mm^2. The optics accept 2.8 mrad of the horozontal radiation fan from the storage ring. The design of the goniometer for the materials science experiments was revised and agreed with future users from universities. The general layout of the beam line (hutches, cabins, communication, safety systems) was finally defined and approved by the FZR and the ESRF. The contract between ESRF and FZR for the construction phase of ROBL was approved by the ESRF council and signed by the directors.

Collaboration: Institut für Radiochemie, Zentralabteilung Forschungs- und Informationstechnik, ESRF, Grenoble, SNBL CRG, Grenoble

A. Mücklich

Transmission Electron Microscopy

The Philips CM 300 TEM was commissioned in spring. The 300 keV microscope is equipped with a LaB_6-cathode, a Super-Twin-alpha objective lens and a CompuStage sample goniometer. The resolution test with a gold foil gave a line resolution of about 0.14 nm for the (220) lattice planes. High resolution imaging is possible with the instrument but will not be the standard application. The useful TEM magnification range is 57 to 1000 k. Additionally, the STEM operation mode is possible. The analytical equipment is a energy dispersive detector system EDAX. Elemental analysis down to Z=5 (boron) is possible. The performance of the EDX was testet with BN films produced by IBAD.

Collaboration: TU Bergakademie Freiberg

Publications

Bischoff, L., Teichert, J., Hesse, E., Panknin, D., Skorupa, W.,
$CoSi_2$ microstructures by means of a high current focused ion beam,
J. Vac. Sci.Technol. B12 (1994) 3523

Bischoff, L., Teichert, J., Hesse, E.,
Interconnection lines following the surface topography fabricated by writing focused ion beam implantation,
Microelectronic Engineering 27 (1995) 351

Bürger, W.,
A fast and precise generating voltmeter for the control of the acceleration voltage of electrostatic accelerators,
Proc. 7th Int. Symposium on High Voltage Engineering, Graz, Austria (1995) 4499-1

Dvurechenskii, A.V., Grötzschel, R., Herrmann, F., Karanovich, A.A., Kögler, R., Rybin, A.V.,
Point defects depths distribution in Si implanted with high energy ions,
"Ion Implantation Technology-94" S.Coffa, G.Ferla, F.Priolo, E.Rimini (eds.), Elsevier Science B.V. (1995) 763

Engelhard, M., Jacob, W., Möller, W., Koch, A. W.,
New calibration method for determining the absolute density of CH radicals by laser-induced fluorescence,
Appl. Optics 34 (1995) 4542

Eremin, V.K., Ilyashenko, I.N., Strokan, N.B., Schmidt, B.,
Nonequilibrium charge carrier recombination in heavy ion tracks in silicon,
Fisika i Tekhnika Poluprovodnokov 29 (1995) 79

Friedlein, R., Herpich, S., Lehnert, U., Tyrroff, H., Wirth, H., Zippe, C., Zschornack, G.,
X-ray spectra on ECR plasmas,
Nucl. Instr. Meth. B98 (1995) 585

Friedlein, R., Herpich, S., Hiller, H.,Tyrroff, H., Wirth, H., Zschornack, G.,
Experimental study of the hot and the warm electron populations in an ECR argon-oxygen-hydrogen plasma,
Physics of Plasma 2 (1995) 1

Fukarek, W., Jacob, W., von Keudell, A.,
Role of Hydrogen Ions in Plasma-enhanced chemical vapor deposition of hydrocarbon films, investigated by in situ ellipsometry,
Appl. Phys. Lett. 66 (1995) 1322

Fukarek, W., von Keudell, A.,
A novel set-up for spectroscopic ellipsometry using an acousto-optic tuneable filter,
Rev. Sci. Instr. 66 (1995) 3545

Gärtner, K., Stock, D., Weber, B., Betz, G., Hautala, M., Hobler, G., Hou, M., Sarite, S., Eckstein, W., Jimenez-Rodriguez, J.J., Perez-Martin, A.M.C., Andribet, E.P., Konoplev, V., Gras-Marti, A., Posselt, M., Shapiro, M.H., Tombrello, T.A., Urbassek, H., Hensel, H., Yamamura, Y., Takeuchi, W.,
Round Robin computer simulations of ion transmission through thin crystalline targets,
Nucl. Instr. Meth. B102 (1995) 183

Große, M., Eichhorn, F., Böhmert, J., Brauer, G., Haubold, H.-G., Goerigk, G.,
ASAXS and SANS investigations of the chemical composition of irradiation-induced precipitates in nuclear pressure vessel steels,
Nucl. Instr. Meth. B97 (1995) 487

Harz, M.,
Der Einfluß der Elektrodengestaltung auf die Geschwindigkeit und die Qualität des anodischen Bondens,
Sensor Magazin 1 (1995) 24

Hatzopoulos, N., Panknin, D., Fukarek, W., Skorupa, W., Siapkas, D.I., Hemment, P.L.F.,
Electrical and optical characterisation of double SIMOX structures formed by sequential high energy oxygen implantation into silicon,
Microelectronic Engineering 28 (1995) 415

Häußler, F., Hempel, M., Eichhorn, F., Hempel, A., Baumbach, H.,
Hydrating Cement Pastes as a Complex Disordered System,
Physica Scripta T57 (1995) 184

Heera, V., Stoemenos, J., Kögler, R., Skorupa, W.,
Amorphisation and recrystallisation of 6H-SiC by ion-beam irradiation,
J. Appl. Phys. 77 (1995) 2999

Heera, V., Stoemenos, J., Kögler, R., Skorupa, W.,
Complete recrystallisation of amorphous silicon carbide layers by ion irradiation,
Appl. Phys. Lett. 67 (1995) 1999

Heera, V., Henkel, T., Kögler, R., Skorupa, W.,
Evidence for diffusion-limited kinetics of ion beam induced epitaxial crystallisation in silicon,
Phys. Rev. B52 (1995) 15776

Henke, D., Tyrroff, H., Grötzschel, R., Wirth, H.,
Slow, highly charged ions from a 7.25 GHz ECR ion source,
Nucl. Instr. Meth. B98 (1995) 528

Herrmann, F., Grambole, D.,
The new Rossendorf nuclear microprobe,
Nucl. Instr. Meth. B104 (1995) 26

Hesse, E., Bischoff, L., Teichert, J.,
Angular distribution and energy spread of a lithium liquid metal ion source,
J. Appl. Phys. 28 (1995) 1707

Hüller, J., Pham, M.T., Vopel, T., Albrecht, J.,
Ion-beam modification of ISFET membranes for copper ion detection,
Sensors and Actuators B24-25 (1995) 225

Hytry, R., Möller, W., Wilhelm, R.,
Running discharge for PECVD inner coating of metal tubes,
Surf. Coat. Technol. 74-75 (1995) 43

Jäger, H. U.,
Point defect-based modeling of diffusion and electrical activation of ion implanted boron in crystalline silicon,
J. Appl. Phys. 78 (1995) 176

Jäger, H.U.,
Point defect-based modeling of transient diffusion of boron implanted in silicon along random and channeling directions,
Mat. Res. Soc. Symp. Proc. 389 (1995) 71

Jentschel, M., Thess, A., Bahr, U.,
Lyapunov exponents and the merger of point-vortex clusters,
Phys. Rev. E51 (1995) 5120

Katsidis, C.C., Siapkas, D.I., Panknin, D., Hatzopoulos, N., Skorupa, W.,
Optical characterisation of doped SIMOX structures using FTIR spectroscopy,
Microelectronic Engineering 28 (1995) 439

Katsidis, C.C., Siapkas, D.I., Skorupa, W., Hatzopoulos, N., Panknin, D.,
Study of the high energy doping in Si and the formation process of doped high energy SIMOX structures using FTIR spectroscopy,
Ion Implantation Technology-94" S.Coffa, G.Ferla, F.Priolo, E.Rimini (eds.), Elsevier Science B.V. (1995) 959

Kögler, R., Borany, J. von, Panknin, D., Skorupa, W., Baither, D.,
Reverse currents of p^+/n diodes after high energy implantation of carbon and germanium ions and annealing,
"Ion Implantation Technology-94" S.Coffa, G.Ferla, F.Priolo, E.Rimini (eds.), Elsevier Science B.V. (1995) 814

Kolitsch, A., Richter, E., Drummer, H., Roland, U., Ullmann, J.,
The effect of a post-treatment of amorphous carbon films with high energy ion beams,
Nucl. Instr. Meth. B106 (1995) 511

Krause, P., Sporys, M., Obermeier, E., Lange, K., Grigull, S.,
Silicon to silicon anodic bonding using evaporated glass,
Proc. 8th Int Conf. on Solid-State Sensors and Actuators and Eurosensors IX, vol. 1, Royal Swedish Academy of Engineering Sciences, IVA, Stockholm, (1995) 228

Lange, K., Grigull, S., Harz, M., Kreissig, U., Schmidt, B.,
Ion drift behaviour in borosilicate glass during anodic bonding to silicon or metals,
Proc. 3rd Int. Symp. on Semiconductor Wafer Bonding, Proceedings-Volume 95-7
The Electrochemical society, Inc., Pennington, New Jersey (1995) 371

Liu, Q.K.K., Biersack, J.P., Posselt, M.,
Comparison of channeling trajectories and ranges calculated by the continuum potential approximation and Crystal-TRIM,
Nucl. Instr. Meth. B102 (1995) 3

Mathar, R., Posselt, M.,
Effective charge theory for the electronic stopping of heavy ions in solids: Stripping criteria and target-electron models,
Phys. Rev. B51 (1995) 107

Mathar, R., Posselt, M.,
Electronic stopping of heavy ions in the Kaneko model,
Phys. Rev. B51 (1995) 1578

Moll, H., Matz, W., Schuster, G., Brendler, E., Bernhard, G., Nitsche, H.,
Synthesis and characterization of uranyl orthosilicate $(UO_2)_2SiO_4 \cdot 2H_2O$,
Journ. Nucl. Mat. 227 (1995) 40

Möller, D., Pham, M.T., Hüller, J., Albrecht, J.,
Ag^+ sensitive membrane of sub-µm thickness prepared by ion implantation,
Analytica Chim. Acta 396 (1995) 1

Möller, W., (invited)
Grundlagen des ionenunterstützten Schichtwachstums,
Vakuum-Beschichtungstechnik I, Hrsg. E. Frey, VDI-Verlag, Düsseldorf (1995)

Möller, W., Fukarek, W., Lange, K., v. Keudell, A., Jacob, W.,
Mechanisms of the deposition of hydrogenated carbon films,
Jap. J. Appl. Phys. 34 (1995) 2163

Murthy, C.S., Posselt, M., Frei, Th.,
3-D modeling of low-dose BF_2^+ implantation into single-crystalline silicon,
in Proc. of the 3rd Int. Workshop on the Measurement and Characterization of Ultra-Shallow Doping Profiles in Semiconductors, p. 15.1, J. Ehrstein, R. Mathur G. McGuire, Editors, Research Triangle Park, NC (1995)

Neelmeijer, C., Wagner, W., Schramm, H.P., Thiel, U.,
De re metallica (G. Agricola) - IBA on air,
Nucl. Instr. Meth. B99 (1995) 390

Neelmeijer, C., Wagner, W., Schramm, H.P.,
Diagnose von Kunstwerken am Teilchenbeschleuniger - Fortschritte am Luft-Protonenstrahl,
Restauro 5 (1995) 326

Nikitin, A.N., Sukhoparov, W.A., Heinitz, J., Walther, K.,
Investigations of texture formation in geomaterials by neutron diffraction with high pressure chambers,
High Pressure Research 14 (1995) 155

Nomura, K., Reuther, H., Richter, E., Ujihira, Y.,
Magnetic structure of Fe-Si-Al films implanted with Al and N ions,
Radioanal. Nucl. Chem. 190 (1995) 299

Nomura, K., Shiozawa, H., Takada, T., Reuther, H.,
Gas sensor properties of SnO films implanted with Au and Fe ions,
Proc. 20th Chem. Sensor Symp., Tokyo (1995) (published)

Perez-Rodriguez, A., Serre, C., Calvo-Barrio, L., Romano-Rodriguez, A., Morante, J.R., Pacaud, Y., Kögler, R., Skorupa, W.,
Ion beam induced amorphisation and recrystallisation processes in SiC: Raman scattering analysis,
"Optical Diagnostics of Materials and Devices for Opto-, Micro-and Quantum Electronics",
S.V.Svechnikov and M.Ya.Valakh, (eds.), SPIE Proceedings Series 2648 (1995) 481

Pham, M.T.,
Analysis of the time dependence of interfacial potentials at ion-conducting membranes coupled to field effect devices,
J. Electroanal. Chem. 388 (1995) 17

Posselt, M.,
3-D modeling of ion implantation into crystalline silicon: influence of damage accumulation on dopant profiles,
Nucl. Instr. Meth. B96 (1995) 163

Posselt, M.,
Dynamic simulation of damage accumulation during implantation of BF_2^+ molecular ions into crystalline silicon,
Nucl. Instr. Meth. B102 (1995) 167

Posselt, M.,
Dynamic simulation of ultra-shallow implantation profiles in single-crystalline silicon,
Mat. Res. Soc. Symp. Proc. 389 (1995) 227

Posselt, M., Heinig, K.-H.,
Comparison of BC and MD simulations of low-energy ion implantation,
Nucl. Instr. Meth. B102 (1995) 236

Prokert, F., Savenko, B.N., Balagurov, A.M.,
Thermal Diffuse Scattering in Time-of-Flight Neutron Diffraction Studies on SBN and TSCC Single Crystals,
Acta Cryst. 51 (1995) 124-129

Prokert, F., Ihringer, J., Ritter, H.,
X-ray diffraction study of phase transition in $Sr_{0.39}Ba_{0.61}Nb_2O_6$ between 20 and 500 K,
Ferroelectrics Letters 20 (1995) 73-82

Reiss, S., Heinig, K.-H.,
Computer simulations of mechanisms of the SIMOX process,
Nucl. Instr. Meth. B102 (1995) 256

Reiss, S., Ruault, M.O., Clayton, J., Kaitasov, O., Heinig, K.-H., Bernas, H.,
Nucleation, growth and Ostwald Ripening of $CoSi_2$ precipitates during Co ion implantation in Si,
Mat. Res. Soc. Symp. Proc. 354 (1995) 183

Reuther, H.,
CEMS study of silicon implanted iron,
Hyperfine Interactions 95 (1995) 161-173

Salzer, R., Roland, U., Drummer, H., Sümmchen, L., Kolitsch, A., Drescher, D.,
Charakterisierung dünner Kohlenstoffschichten durch Ramanspektroskopie,
Zeitschrift für Physikalische Chemie 191 (1995) 1-13

Scheibe, H.J., Drescher, D., Kolitsch, A., Mensch, A.,
Investigation of surface topography, morphology and structure of amorphous carbon films by AFM and TEM,
Fresenius J. Anal. Chem. 353 (1995) 690

Schell, N., Simmons, R.O., Kaprolat, A., Schülke, W., Burkel, E.,
Electronic Exitations in hcp ^4He at 61.5 MPa and 4.3 K Studied by Inelastic X-Ray Scattering Spectroscopy,
Phys. Rev. Lett. 13 (1995) 2535

Schülke, W., Kaprolat, A., Gabriel, K.-J., Schell, N., Burkel, E., Simmons, R.O.,
First inelastic x-Ray scattering spectroscopy measurements of the dynamic structure factor $S(q,\omega)$ of electrons in a solid noble gas (He),
Rev. Sci. Instr. 66 (1995) 1578

Serre, C., Perez-Rodriguez, A., Romano-Rodriguez, A., Morante, J.R., Kögler, R., Skorupa, W.,
Spectroscopic characterisation of phases formed by high dose carbon ion implantation in silicon,
J. Appl. Phys. 77 (1995) 2978

Skorupa, W., Yankov, R.A. (invited)
Carbon -mediated effects in silicon and in silicon-related materials,
Materials Chemistry and Physics, Eds.L.J.Chen, K.N.Tu and U.M.Gösele; Elsevier Sequoia, Lausanne, 43 (1995) 1

Skorupa, W., (invited)
Ion beam procecessing for silicon-on-insulator,
"Physical and Technical Problems of SOI Structures and Devices", NATO ASI Series, 3.High Technology 4 (1995) 67; edited by: J.P.Colinge,V.S.Lysenko and A.N.Nazarov, Kluwer Acad.Publ., Dordrecht-Boston-London (1995)

Skorupa, W., Hatzopoulos, N., Yankov, R.A., Danilin, A.B.,
Proximity gettering of transition metals in SIMOX structures,
Appl. Phys. Lett. 67 (1995) 2992

Teichert, J., Bischoff, L., Hesse, E., Schneider, P., Panknin, D., Geßner, T., Löbner, B., Zichner, N.,
Comparison of $CoSi_2$ interconnection lines on crystalline and noncrystalline silicon, fabricated by writing focused ion beam implantation,
Appl. Surf. Sc. 91 (1995) 44

Thomae, R.W., Seiler, B., Bender, H., Brutscher, J., Günzel, R., Halder, J., Klein, H., Müller, J., Sarstedt, M.,
High current ion implantation by plasma immersion technique,
Nucl. Instr. Meth. B99 (1995) 569

Wagner, W., Neelmeijer, C.,
External proton beam analysis of layered objects,
Fresenius J. Anal. Chem. 353 (1995) 297

Walther, K., Heinitz, J., Ullemeyer, K., Betzl, M., Wenk, H.-R.,
Time-of-Flight Texture Analysis of Limestone Standard: Dubna Results,
J. Appl. Cryst. 28 (1995) 503

Weishart, H., Schöneich, E., Steffen, H.J., Matz, W., Skorupa, W.,
Ion beam synthesis by tungsten implantation into 6H-SiC,
Mat. Res. Soc. Symp. Proc. 354 (1995) 177

Yankov, R.A., Komarov, F.F.,
Direct formation of thin film nitride structures by high intensity ion implantation of nitrogen into silicon,
"Physical and Technical Problems of SOI Structures and Devices", NATO ASI Series, 3.High Technology 4 (1995) 67; edited by: J.P.Colinge,V.S.Lysenko and A.N.Nazarov, Kluwer Acad.Publ., Dordrecht-Boston-London (1995)

Conference Contributions

Albe, K., Heinig, K.-H.,
MD simulation and superhard materials: An empirical potential for Boron Nitride?
CCP5 Annual Meeting 1995: Advanced Computer Simulation of Materials,
Daresbury, UK, Sept 20 - 22, 1995

Aldridge, L.P., Bertram, W.K., Sabine, T., Eichhorn, F., Hempel, A., Ioffe, A.,
SANS spectra from hydrated cement pastes,
6th' BENSC Users' Meeting, HMI Berlin, 10.11.1995

Biersack, J.P., Jung, W.-C., Li Gong, Frey, L., Skorupa, W.,
Reviewing high energy implantation: Range distributions of 1-10 MeV B, P, As and Sb ions in silicon,
9.Int.Conf."Ion Beam Modification of Materials" , Canberra, Australia, February 5-10, 1995

Bischoff, L., Teichert, J., Hesse, E., (invited)
Feinfokussierte Ionenstrahlen aus Flüssigmetall-Ionenquellen und ihre Anwendung,
Frühjahrstagung der Deutschen Physikalischen Gesellschaft, Berlin, March 20-24, 1995

Bischoff, L., Teichert, J., Hesse, E., Panknin, D., Skorupa, W.,
Ion beam synthesis of $CoSi_2$-microstructures by means of a high current focused ion beam,
9.Int.Conf."Ion Beam Modification of Materials", Canberra, Australia, February 5-10, 1995

Bischoff, L., Teichert, J., Hesse, E., Prewett, P.D., Watson, J.G.,
Cluster beams from a Co-Nd liquid alloy ion source,
Int.Conf.Micro-and Nanoengineering.`95, Aix-en-Provence, France, Sept.26-28, 1995

Bischoff, L., Heinig, K.-H., Teichert, J., Skorupa, W.,
Submicron $CoSi_2$-structures fabricated by focused ion beam implantation and local flash lamp melting,
E-MRS Spring Meeting: Symp.D "Purification, Doping and Defects in II-VI materials", Strasbourg,
France, May 22-26, 1995

von Borany, J., Schmidt, B., Grötzschel, R.,
The application of high energy ion implantation for silicon radiation detectors,
7th European Symposium on Semiconductor Detectors, Schloß Elmau, Germany, May 7-10, 1995

Bottyan, L., Deak, L., Gerdau, E., Gittsovich, V.N., Grof, A., Korecki, J., Nagy, D.L., Reuther, H.,
Szilagi, E., Uzdin, V.M.,
Hyperfine fields profile in oxidized and surface alloyed Fe films by synchrotron Mössbauer
reflectometry,
Int. Conf. Appl. Mössbauer Effect, Rimini, Italy, Sept 10-16, 1995

Brauer, G., Anwand, W., Pacaud, Y., Skorupa, W., Plazaola, F., Coleman, P.G., Knights, A.P.,
Stoermer, J., Willutzki, P.,
Positron studies of defects in ion implanted SiC,
Int. Symp. on Si heterostructures: from physics to devices, Kreta, Greece, Sept. 11-14, 1995

Brenscheidt, F., Matz, W., Wieser, E., Fischer, W.,
High Energy Ion-Implantation of Titanium in Engineering Silicon Nitride Ceramics,
SMMIB´95, San Sebastian, Spain, Sept 4-8, 1995

Brutscher, J., Günzel, R.,
Plasma Immersion Ion Implantation as a simple method of ion implantation into metals,
Advances in Materials and Processing Technologies '95, Dublin, Ireland, August 8-12, 1995

Brutscher, J.,
Randschichtdynamik bei der Plasmaimmersionsimplantation,
Projekttreffen PIII, Clausthal-Zellerfeld, Germany, 27.01.1995

Brutscher, J.,
Randschichtdynamik bei der Plasma-Immersions-Implantation,
Winterseminar des Instituts für Angewandte Physik, 2.3. 1995, Frankfurt, Germany
Meeting Niederdruckentladungen, Mühlleiten, Germany, 16.03.1995

Bürger, W.,
A fast and precise generating voltmeter for the control of the acceleration voltage of electrostatic accelerators,
9th Int. Symposium on High Voltage Engineering, Graz, Austria, August 28-September 1, 1995

Chudoba, Th.,
Messung und Interpretation elastoplastischer Vickers Eindringkurven an ionenimplantierten Schichten,
59. Physikertagung und Frühjahrstagung der DPG, Berlin, Germany, March 20-24, 1995

Chudoba, Th., Schneider, M., Richter, E.,
Study of corrosion behaviour of pure magnesium after implantation of oxygen ions,
SMMIB'95, San Sebastian, Spain, Sept 4-8, 1995

Chudoba, Th., Schöneich, A., Richter, E.,
Modification of hardness and wear of pure magnesium by ion implantation,
SMMIB'95, San Sebastian, Spain, Sept 4-8, 1995

Chudoba, Th., Richter, E., Wieser, E.,
Improvement of hardness, wear and corrosion behaviour of light elements by ion implantation,
Interaction of radiation with solids, Minsk, Belarus, October 16-19, 1995

Chudoba, T., Richter, E., Schneider, M.,
Improvement of hardness, wear and corrosion behaviour of magnesium by ion implantation,
9th Int. Conf. "Ion Beam Modification of Materials", Canberra, Australia, Feb. 5-10, 1995

Deshkovskaya, A., Richter, E.,
Wear improvement of silicate glass surfaces by ion implantation,
European Workshop on Large Area Coating, Würzburg, Germany, June 26-28, 1995

Deshkovskaya, A., Richter, E.,
Improvement of strength of silicate glasses by ion implantation,
Interaction of radiation with solids, Minsk, Belarus, October 16-19, 1995

Deshkovskaya, A., Makova, L., Pinchuk, T., Richter, E.,
Microhardness and surface topology of silicates glasses after ion beam modification,
Interaction of radiation with solids, Minsk, Belarus, October 16-19, 1995

Dobler, M., Reuther, H.,
Investigations of ion beam synthesized buried iron disilicide layers by conversion electron Mössbauer spectroscopy,
Int. Conf. Appl. Mössbauer Effect, Rimini, Italy, Sept 10-16, 1995

Dobler, M., Reuther, H.,
CEMS-Untersuchungen an Fe-ionenimplantiertem Silizium,
Frühjahrstagung der DPG, Berlin, Germany, March 20-24, 1995

Dobler, M., Reuther, H., Barradas, N.P., Panknin, D., Wieser, E., Lange, H.,
Conversion Electron Mössbauer Spectrometry studies of FeSi and $FeSi_2$,
10th Int.Conf.Hyperfine Interactions, Leuven, Belgium, Aug. 28-Sept.1, 1995

Eichhorn, F., Hempel, A., Reichel, P., Boede, W.,
A neutron double-crystal diffractometer with an extended momentum transfer range,
International Conference on "Interference Phenomena in X-Ray Scattering" (IPX-95), Moscow,Russia,
August 14-19, 1995

Eichhorn, F., Prokert, F., Kögler, R., Wolf, K.,
Doppelkristalldiffraktometrische Untersuchungen an Silizium-Germanium-Schichten auf Silizium,
Herbstschule "Röntgenstreuung an Grenzflächen und dünnen Schichten", Petzow , Germany ,
Nov 15-18, 1995

Friedlein, R., Herpich, S., Küchler, D., Tyrroff, H., Zippe, C., Zschornack, G.,
Energy Dispersive X-Ray Spectroscopy for ECR Plasma Diagnostics,
1st Euroconference on Atomic Physics with Stored Highly Charged Ions, Heidelberg, Germany,
March 20-24, 1995

Friedlein, R., Tyrroff, H., Henke, D., Zippe, C., Zschornack, G.,
Hot and Warm Electron Energy Distribution at Different ECR Ion Source Operation Regimes,
6th International Conference on Ion Sources, Whistler, Canada, September 10-16, 1995

Friedlein, R., Tyrroff, H., Zippe, C., Zschornack, G., Barnitzke, W.,
Characteristic X-Rays and Electron Energy Distribution Function in Anisotropical Hot Plasmas,
6th International Conference on Ion Sources, Whistler, Canada, September 10-16, 1995

Friedrich, M., Bürger, W., Henke, D., Turuc, S.,
The Rossendorf 3 MV Tandetron: a new generation of heavy ion implanters,
7th Int. Conf. on Heavy Ion Accelerator Technology, Canberra, Australia, September 18-22, 1995

Friedrich, M., Bürger, W., Turuc, S.,
Operation and development of the Rossendorf electrostatic accelerators,
Workshop on electrostatic accelerator operation, University of Melbourne, Australia,
September 25-27, 1995

Fukarek, W.,
In situ ellipsometrische Untersuchungen zum Verständnis des Wachstums von polymerartigen C:H-Schichten,
Tagung "Niederdruckentladungen zur Oberflächenbehandlung", Mühlleiten, Germany,
March 13-17, 1995

Fukarek, W.,
In situ Ellipsometrie,
Frühjahrstagung des AK Plasmaoberflächentechnologie, Chemnitz, Germany, May 15, 1995

Fukarek, W., (invited)
Plasma surface interactions during the deposition of amorphous hydrogenated carbon films,
"Modelling and characterisation of industrial plasmas", Meeting of the Vacuum Group of The Institute of Physics, Salford, UK, June 28, 1995

Fukarek, W.,
In situ ellipsometric investigation of a-C:H film growth,
Woollam - Spektralellipsometrie - Anwenderseminar, Fraunhofer-Institut für Werkstoffphysik und Schichttechnoloogie, Dresden, Germany, Sept 12, 1995

Grambole, D., Herrmann, F., Herrmann, B.,
Multielement analysis on bone structures of medieval human femur,
7th Int. Conf. on Particle-Induced X-ray Emission and its Analytical Applications,
Padua,Italy, May 26 - 30, 1995

Große, M., Hempel, A., Eichhorn, F., Böhmert, J.,
SAXS investigation of structural changes in the plastic zone ahead of a crack tip in ductile metals,
Conference on "Horizons in small angle scattering from mesoscopic systems", Stromboli, Italy,
September 27.-30, 1995

Günzel, R., Kolitsch, A., Plass, M.F., Richter, E.,
Erzeugung von Hartstoffschichten mittels Ionenstrahltechniken,
Oberflächen und Wärmebehandlung, Chemnitz, Germany, May 16-17, 1995

Günzel, R., Mändl, S., Brutscher, J., Möller, W.,
Sheath Dynamics in Plasma Source Ion Implantation,
2nd International Workshop on Plasma-Based Ion Implantation, Sydney, Australia,
February 12-15, 1995

Günzel, R.,
Grundlegende anlagentechnische Fragestellungen bei der Plasmaimmersionsionen-implantation,
Projekttreffen PIII, Clausthal-Zellerfeld, Germany, Jan 27, 1995

Harz, M., Brückner, W.,
Thermally induced bend change of anodically bonded silicon and pyrex glass,
3rd International Symposium on Semiconductor Wafer Bonding, Reno , Nevada, USA,
May 21-26, 1995

Harz, M.,
Einfluß der strukturellen Relaxation von TEMPAX-Glas auf die Krümmung anodisch gebondeter Silizium-TEMPAX-Wafer,
1. Tagung Micro Materials, Berlin, Germany, Nov 28-29, 1995

Hatzopoulos, N., Panknin, D., Skorupa, W.,
Structural, optical and electrical characterisation of double SIMOX structures formed by sequential high energy oxygen implantation into silicon,
Frühjahrstagung der Deutschen Physikalischen Gesellschaft, Berlin, Germany, March 20-24, 1995

Heera, V., Kögler, R., Skorupa, W., Stoemenos, J.,
Ion beam induced crystallization of 6H-SiC,
6th Int. Conf. on Silicon Carbide and Related Materials-1995 (ICSCRM-95), Kyoto, Japan,
Sept. 18-21, 1995

Heera, V., Petzold, J., Ning, X.J., Pirouz, P.,
High dose Co implantation of Aluminum and Nitrogen in 6H-Silicon Carbide,
Int. Symp. on Si heterostructures: from physics to devices, Kreta, Greece, Sept. 11-14, 1995

Heinig, K.-H., Bernas, H., Ruault, M.O., Reiss, S., (invited)
Mechanisms of ion beam synthesis,
9th Int. Conf. on Ion Beam Modifications of Materials (IBMM95), Canberra , Australia,
Feb. 5 - 10, 1995

Heinig, K.-H., Jentschel, M., Reiss, S., (invited)
Fundamentals of Ion Beam - Solid Interactions,
Int. Conf. on Physical Electronics (UzBEC-1) , Taschkent, Uzbekistan, Nov 1 - 3, 1995

Heinig, K.-H., Jentschel, M., Börner, H., (invited)
Untersuchungen von interatomaren Potentialen und Gitterlokalisierungen von Fremdatomen durch hochauflösende Gamma-Spektroskopie (Crystal-GRID-Methode),
XXVI. Arbeitstreffen für Kernphysik, Schleching, Germany, March 1 - 9, 1995

Heinitz, J., Isakov, N.N., Walther, K.,
Ein Multidetektorsystem für schnelle Polfigurmessungen mit der Neutronenflugzeitmethode,
Deutsche Neutronenstreutagung, Reinstorf/Lüneburg, Germany, Sept 18-21, 1995

Helming, K., Schmidt, D., Ullemeyer, K.,
Preferred orientations in polymineralic materials described by texture components,
International Workshop "Mathematical Methods of Texture Annalysis", Dubna, Russia,
March 21-24, 1995

Hempel, A., Eichhorn, F.,
SANS investigation of hydrating cement - the influence of temperature and humidity,
Conference on "Horizons in small angle scattering from mesoscopic systems", Stromboli, Italy,
September 27-30, 1995

Hempel, A., Hempel, M., Eichhorn, F., Häußler, F., Baumbach, H.,
SANS studies for a structural characterization of industrial materials,
6th BENSC Users' Meeting, HMI Berlin, Germany, Nov 10, 1995

Henke, D., Tyrroff, H.,
Ion Optical System for Transport and Deceleration of Highly Charged Ions,
6th International Conference on Ion Sources, Whistler, Canada, September 10-16, 1995

Henkel, T., Heera, V., Kögler, R., Skorupa, W.,
Ion beam induced interfacial amorphisation of silicon below room temperature,
9.Int.Conf."Ion Beam Modification of Materials" , Canberra, Australia, February 5-10, 1995

Henkel, T., Heera, V., Kögler, R., Skorupa, W.,
Ionenstrahlinduzierte planare Amorphisierung von Silicium unterhalb Raumtemperatur,
Frühjahrstagung der Deutschen Physikalischen Gesellschaft, Berlin, Germany, March 20-24, 1995

Herrmann, S., Mahnke, H.-E., Schumann, D., Spellmeyer, B., Sulzer, G., Bollmann, J., Reinhold, B., Rörich, J., Wienecke, M., Yankov, R., Gummlich, H.-E.,
Palladium as an impurity in ZnTe,
E-MRS Spring Meeting: Symp.D "Purification, Doping and Defects in II-VI materials", Strasbourg, France, May 22-26, 1995

Hüller, J., Pham, M.T., Möller, D.,
Sensibilisierung anorganischer Festkörpermembranen für ISFET-Anwendungen mittels Ionenimplantation,
2. Dresdner Sensor-Symposium der Forschungsgesellschaft für Meß- und Sensortechnik e.V.,
Dresden,Germany, 11.12.1995

Jäger, H.U.,
Point defect-based modeling of transient diffusion of boron implanted in silicon along random channeling directions,
MRS 1995 Spring Meeting, Symposium R: Modeling and Simulation of Thin-Film Processing, San Francisco, CA, USA, April 17 - 21, 1995

Jentschel, M., Heinig, K.-H., Börner, H.G., Jolie, J., Kessler, E.G.,
Atomic collision cascades studied with the Crystal-GRID method ,
16th Int. Conf. on Atomic Collisions in Solids (ICACS-16), Linz, Austria, July 17 - 21, 1995

Jentschel, M., Heinig, K.-H., Börner, H.,
GRID-Methode - Erste Ergebnisse der Messungen am ILL Grenoble,
Treffen des BMFT-Verbundes Festkörperphysik und Materialforschung mit nuklearen Methoden, Friedrich-Schiller-Universität Jena, Germany, Oct 4 - 6, 1995

Kögler, R., Skorupa, W., Eichhorn, F.,
Proximity gettering in silicon by MeV-implantation of isovalent impurities,
9.Int.Conf."Ion Beam Modification of Materials" , Canberra, Australia, February 5-10, 1995

Kögler, R., Heera, V., Panknin, D., Skorupa, W.,
Temperature dependence of the ion beam induced crystallisation of SiC,
9.Int.Conf."Ion Beam Modification of Materials", Canberra, Australia, February 5-10, 1995

Köhler, B., Bischoff, L., Teichert, J.,
Ionenakustischer Effekt als potentielle Signalquelle eines Bildsystems für Ionen-Feinstrahl-Anlagen,
1.Tagung Micro Materials (MicroMat'95), Berlin, Germany, Nov.28-29,1995

Kolitsch, A., Richter, E., Drummer, H., Roland, U., Ullmann, J.,
Effects of post-treatment of amorphous carbon films with high energy ion beams,
9.Int.Conf."Ion Beam Modification of Materials", Canberra, Australia, February 5-10, 1995

Kolitsch, A., Möller, W., Richter, E.,
IBAD and nitrogen post-implantation of films containing carbon nitride,
Diamond Films'95, The 6th European Conference on Diamond, Diamond-like and Related Materials, Barcelona, Spain, September 10-15, 1995

Kolitsch, A., Sümmchen, L., Ullmann, J., Falke, U., Heger, P.,
Post-ion-implantation into amorphous carbon films,
SMMIB'95, San Sebastian, Spain, September 4-8, 1995

Kolitsch, A.,
Dynamical hardness depth curves of post-implanted amorphous carbon films,
SMMIB'95, San Sebastian, Spain, September 4-8, 1995

Kolitsch, A., Strauch, U.,
Ion beam assisted deposition of super hard materials in the DANFYS 1090 system in the Research center Rossendorf, Inc.,
2nd User Seminar of DANFYS 1090 Implanters, San Sebastian, Spain, September 8-9, 1995

Kolitsch, A., Richter, E.,
Oberflächenmodifizierung durch Ionenstrahltechniken,
Neue Anwendungen für moderne Oberflächentechnologien - Präsentations- und Vortrags-veranstaltung, Stuttgart, Germany, November 20-21, 1995

Komar, V., Deshkovskaya, A., Sronyakov, I., Richter, E., Schöneich, J.,
Spectroscopical investigations of fused silica modified by implantation of Li^+, Na^+ and In^+,
Interaction of radiation with solids, Minsk, Belarus, October 16-19, 1995

Konoplev, V., Heinig, K.-H.,
Mechanisms of silicon self-interstitials formation and diffusion studied by Molecular Dynamics simulation,
Int. Conf. on Physical Electronics (UzBEC-1), Taschkent, Uzbekistan, Nov 1 - 3, 1995

Kruijer, S., Reuther, H., Nikolov, O., Brand, R.A., Keune, W., Liljequist, D., Weber, S., Scherrer, S.,
CEMS and DCEMS investigations of aluminium implanted iron,
Int. Conf. Appl. Mössbauer Effect, Rimini, Italy, Sept 10-16, 1995

Kruijer, S., Nikolov, O., Reuther, H., Brand, R.A., Keune, W., Liljequist, D., Weber, S., Scherrer, S.,
CEMS- und DCEMS-Untersuchungen an Al-implantiertem Eisen,
Frühjahrstagung der DPG, Berlin, Germany, March 20-24, 1995

Lange, K., Möller, W.,
Mass spectrometric dianostics of radical and ion fluxes from a methane plasma,
Frontiers in Low Temperature Plasma Dianostics, Les Houches, France, Jan 23-27, 1995

Lange, K., Grigull, S., Harz, M., Kreissig, U., Schmidt, B.,
Ion drift behaviour in borosilicate glass during anodic bonding to silicon or metals,
3rd International Symposium on Semiconductor Wafer Bonding, Reno, Nevada, USA,
May 21-26, 1995

Mändl, S., Brutscher, J., Günzel, R., Möller, W.,
Design considerations for plasma immersion ion implantation systems,
Spring Meeting E-MRS, Strasbourg, France, May 22–26, 1995

Mathar, R., Posselt, M.,
Electronic stopping of heavy ions in the Kaneko model,
16th Int. Conf. on Atomic Collisions in Solids, Linz, Austria, July 17-21, 1995

Möller, W., Brutscher, J., Günzel, R., Mändl, S.,
Dynamic sheath investigations for plasma immersion ion implantation,
IUVSTA Intern. Workshop on Plasma Sources and Surface Interactions in Materials Processing,
Fuji-Yoshida, Japan, Sept. 20 - 22, 1995

Möller, W., (invited)
Plasma-Immersions-Ionenimplantation,
Statusseminar des BMBF/VDI-TZ "Oberflächen- und Schichttechnologien", Mainz, Germany,
May 29 - 31, 1995

Murthy, C.S., Posselt, M., Frei, Th.,
3-D modeling of low-dose BF_2^+ implantation into single-crystalline silicon,
3rd Int. Workshop on the Measurement and Characterization of Ultra-Shallow Doping Profiles in Semiconductors, Research Triangle Park, NC, USA, March 20-22, 1995

Neelmeijer, C., Wagner, W., Schramm, H.P., (invited)
Proton-induced on-air analysis of art objects,
12th Int. Conf. on Ion Beam Analysis, Tempe, Arizona, USA, May 22-25, 1995

Nikolayev, D., Ullemeyer, K.,
The effect of smoothing on ODF reproduction,
International Workshop "Mathematical Methods of Texture Analysis", Dubna, Russia,
March 21-24, 1995

Nomura, K., Reuther, H., Richter, E., Ujihira, Y.,
CEMS study on magnetic structure of Fe-Si-Al films implanted with Al and N ions,
Int. Conf. Appl. Mössbauer Effect, Rimini, Italy, Sept 10-16, 1995

Pacaud, Y., Skorupa, W.,
Basic damage studies in ion implanted 6H-SiC,
Europ. IBOS-Meeting, Univ.of Surrey, UK, January 13-14,1995

Pacaud, Y., Skorupa, W., Perez-Rodriguez, A., Brauer, G., Stoemenos, J., Barklie, R.C.,
Investigation of the damage induced by 200 keV Ge+ ion implantation in 6H-SiC,
E-MRS Spring Meeting: Symp.D "Purification, Doping and Defects in II-VI materials", Strasbourg,
France, May 22-26, 1995

Pacaud, Y., Brauer, G., Perez-Rodriguez, A., Stoemenos, J., Barklie, R.C., Voelskow, M., Skorupa, W.,
Study of the different stages of damage induced by 200 keV Ge^+ ion implantation in 6H-SiC,
Int. Symp. on Si heterostructures: from physics to devices, Kreta, Greece, Sept. 11-14, 1995

Pacaud, Y., Skorupa, W.,
Ge-ion implantation into 6H-SiC: Damage formation and annealing,
European IBOS-Meeting, Univ.de Paris VI, Paris, France, Oct.27-28, 1995

Perez-Rodriguez, A., Kögler, R., Calvo-Barrio, L., Serre, C., Romano-Rodriguez, A., Heera, V.,
Skorupa, W., Morante, J.R.,
Ion beam assisted recrystallisation of SiC/Si structures,
E-MRS Spring Meeting: Symp.D "Purification, Doping and Defects in II-VI materials", Strasbourg,
France, May 22-26, 1995

Perez-Rodriguez, A., Serre, C., Calvo-Barrio, L., Romano-Rodriguez, A., Morante, J.R., Pacaud, Y.,
Kögler, R., Skorupa, W.,
Ion beam induced amorphisation and recrystallization processes in SiC: Raman scattering analyses,
Int. Conf.Optical diagnostics of Materials and devices for opto-, micro- and quantum electronics,
(OPTIM '95), Kiev, Ukraine, May 10-13, 1995

Pham, M.T., Hüller, J.,
Kinetische Untersuchungen an Silikatmembranen mit Schichtdicken unter 100 nm,
Physikalisch-Chemische Grundlagen elektrochemischer Sensoren:
62. Bunsen-Kolloquium der Humboldt-Universität Berlin, Belzig, Germany, February 1995

Plass, M.F., Fukarek, W., Kolitsch, A., Steffen, J., Kreißig, U., Möller, W.,
Growth and characterisation of boron nitride thin films,
SMMIB'95, San Sebastian, Spain, September 4-8, 1995

Plass, M.F., Fukarek, W., Kolitsch, A., Kreißig, U.,
Growth and characterisation of boron nitride thin films,
Diamond Films'95, Barcelona, Spain, September 10-15, 1995

Plass, M. F., Chudoba, T., Richter, E.,
Measurement of friction and wear of ion implanted surfaces with a vibrating diamand stylus,
SMMIB'95, San Sebastian, Spain, Sept 4-8, 1995

Posselt, M.,
Dynamic simulation of ultra-shallow implantation profiles in single-crystalline silicon,
MRS 1995 Spring Meeting, Symposium R: Modeling and Simulation of Thin-Film Processing,
San Francisco, CA, USA, April 17-21,1995

Posselt, M., Murthy, C.S., Frei, Th.,
3-D modeling of BF_2^+ implantation into crystalline silicon: influence of damage accumulation on channeling effects,
MRS 1995 Spring Meeting, Symposium R: Modeling and Simulation of Thin-Film Processing,
San Francisco, CA, USA, April 17-21, 1995

Reiss, S., Heinig, K.-H.,
Keimbildung, Keimwachstum und Ostwald-Reifung bei der Ionenstrahlsynthese vergrabener SiO_2- und $CoSi_2$-Schichten,
Frühjahrstagung der Deutschen Physikalischen Gesellschaft, Berlin, Germany, March 20-24, 1995

Reiss, S., Heinig, K.-H.,
Self-structuring of buried SiO_2 precipitate layers during IBS - a computer simulation,
EMRS 1995 Spring Meeting, Symposium C: Pushing the Limits of Ion Beam Processing - from Engineering to Atomic Scale Issues, Strasbourg, France, May 22 - 26, 1995

Reiss, S., Heinig, K.-H.,
Modeling of coarsening in open systems - a self-organization process found by computer simulations,
MRS Fall Meeting: Symposium P: Materials Theory, Simulations and Parallel Algorithms,
Boston, MA, USA, November 27- December, 1995

Reuther, H., Richter, E., Günzel, R.,
Comparative study of nitrogen implanted iron produced either by conventional beam line or plasma immersion ion implantation,
SIMMB'95, San Sebastian, Spain, Sept 4-8, 1995

Reuther, H., Kruijer, S., Nikolov, O., Richter, E., Keune, W.,
CEMS and DCEMS investigations of aluminium implanted iron,
SIMMB'95, San Sebastian, Spain, Sept 4-8, 1995

Reuther, H., Lange, H., Dobler, M.,
CEMS studies on iron silicides,
Int. Conf. Appl. Mössbauer Effect, Rimini, Italy, Sept 10-16, 1995

Reuther, H., Dobler, M.,
CEMS and AES investigations on iron silicides,
6th European Conf. on Appl. Of Surface and Interface Anal., Montreux, Switzerland, Oct 9-13, 1995

Richter, E., Kolitsch, A.,
Verbesserung von Standzeiten bei Umformwerkzeugen durch Ionenstrahltechniken,
Workshop Verschleißschutz von Umformwerkzeugen, Essen, Germany, May 10, 1995

Richter, E., Brutscher, J.,
Härtung von Werkzeugstählen durch Ionenstrahlen,
Oberflächen- und Wäremebehandlungstechnik, Chemnitz, Germany, May 16-17, 1995

Richter, E., Chudoba, T., Günzel, R., Schneider, M.,
Improvement of Hardness, Wear and Corrosion Behaviour of Magnesium by Ion Implantation,
9.Int.Conf."Ion Beam Modification of Materials", Canberra, Australia, February 5-10, 1995

Richter, E., Schöneich, J.,
Implantation in light metal alloys with the DANFYS 1090 implanter in Research Center Rossendorf, Inc.,
2nd User Seminar of DANFYS 1090 implanters, San Sebastian, Spain, September 8-9, 1995

Richter, E., Kolitsch, A.,
Verbesserung von Standzeiten bei Umformwerkzeugen durch Ionenstrahltechniken,
MEFORM'95, Umformwerkzeuge - Beanspruchung und Verschleiß, Freiberg, Germany,
February 22-24, 1995

Romano-Rodriguez, A., Perez-Rodriguez, A., Serre, C., Calvo-Barrio, L., Morante, J.R., Kögler, R., Skorupa, W.,
TEM characterisation of Beta-SiC synthesised by high dose carbon implantation into silicon,
9. Int. Conf. on Microscopy of Semiconducting Materials, Oxford, UK, March 20-23, 1995

Romano-Rodriguez, A., Serre, C., Calvo-Barrio, L., Perez-Rodriguez, A., Morante, J.R., Kögler, R., Skorupa, W.,
Detailed analysis of Beta-SiC formation by high dose carbon ion implantation in silicon,
E-MRS Spring Meeting: Symp.N "Carbon, Hydrogen, Nitrogen and Oxygen in Silicon and other elemental semiconductors", Strasbourg, France, May 22-26, 1995

Ruault, M.O., Clayton, J., Hardit, C., Kaitasov, O., Bernas, H., Reiss, S., Heinig, K.-H.,
Ion beam-induced Ostwald Ripening and silicide growth in Silicon,
9th Int. Conf. on Ion Beam Modifications of Materials (IBMM95), Canberra, Australia,
February 5 - 10, 1995

Saroun, J., Lukas, P., Mikula, P., Dubsky, J., Kolman, B., Hempel, A., Eichhorn, F.,
Investigation of porosity in plasma sprayed Al_2O_3 deposits by small-angle neutron scattering,
16th European Crystallographic Meeting (ECM-16), Lund, Schweden, August 6-11, 1995

Schmidt, B., Eremin, V.K., Ilyashenko, I.N., Strokan, N.B.,
Recombination of noneqilibrium charge carriers in heavy ion tracks in silicon,
7th European Symposium on Semiconductor Detectors, Schloß Elmau, Germany, May 7-10, 1995

Schneider, P., Bischoff, L., Teichert, J., Hesse, E., Panknin, D.,
Die Synthese von $CoSi_2$-Drähten auf topographisch strukturierten Oberflächen unter Verwendung des feinfokussierten Ionenstrahls,
Frühjahrstagung der Deutschen Physikalischen Gesellschaft, Berlin, Germany, March 20-24, 1995

Schneider, P., Bischoff, L., Teichert, J., Hesse, E., Panknin, D.,
The synthesis of $CoSi_2$-microwires following the surface topography by writing focused ion beam implantation,
27.Tagung, Deutsche Gesellschaft für Elektonenmikroskopie., Leipzig, Germany, Sept 10-15, 1995

Serre, C., Perez-Rodriguez, A., Calvo-Barrio, L., Romano-Rodriguez, A., Morante, J.R., Esteve, J., Acero, M.C., Skorupa, W., Kögler, R.,
Synthesis of thin membranes in Si technology by carbon ion implantation,
MRS Fall Meeting: Symp.A "Ion-Solid interactions for materials modification and processing",
Boston, USA, Nov. 27-Dec. 01, 1995

Skorupa, W., Eichhorn, F., Hatzopoulos, N., Kögler, R., Panknin, D., Yankov, R., Chu, C., Werner, P., Danilin, A.,
Proximity gettering of transition metals in silicon and SIMOX by ion beam processing,
Frühjahrstagung der Deutschen Physikalischen Gesellschaft, Berlin, Germany, March 20-24, 1995

Skorupa, W., (invited)
Ion beam proceessing of SiC-State of the art,
European IBOS-Meeting, Univ.de Paris VI, Paris, France, Oct. 27-28, 1995

Skorupa, W., Heera, V., Pacaud, Y., Weishart, H., (invited)
Ion beam processing of single crystalline silicon carbide,
XIII.Simposio Latino Americano de Fisica do Estado Solido (SLAFES), Gramado, RS, Brasilien, Nov. 5-10, 1995

Skorupa, W., Kögler, R., Yankov, R.A., Schmidt, B., (invited)
External gettering by buried ion-implanted carbon-rich layers,
II.International Workshop on Ion Implantation, Gramado, RS, Brasilien, Nov. 10-11,1995

Steffen, H.J., Hatzopoulos, N., Weber, R., Skorupa, W., (invited)
Growth of a buried oxide-silicon-oxide layer structure by oxygen ion implantation studied with electron spectroscopy,
Int. Conf. on Metallurgical Coatings and Thin Films(ICMCTF), San Diego, USA, April 24-28, 1995

Teichert, J., Bischoff, L., Hesse, E., Schneider, P., Panknin, D., Geßner, T., Löbner, B., Zichner, N.,
Comparison of $CoSi_2$ interconnection lines on crystalline and noncrystalline silicon fabricated by writing focused ion beam implantation,
Materials for Advanced Metallization '95, Radebeul, Germany, March 19-22, 1995

Tyrroff, H., Friedrich, M., Henke, D., Grigull, S., Mäder, M., Zschornack, G., Friedlein, R.,
The Rossendorf ECR ion source,
Workshop on electrostatic accelerator operation, University of Melbourne, Australia,
September 25-27, 1995

Uebele, P., Wiedenmann, A., Eichhorn, F., Hempel, A., Herrmann, M., Hermann, H.,
SANS study of silicon nitride ceramics,
6th BENSC Users' Meeting, HMI Berlin, Germany, November 10, 1995

Walther, K.,
Spannungsmessung mit der Flugzeitmethode im VIK Dubna,
Arbeitstreffen "Neutronographische Spannungsanalyse", Potsdam, Germany, 11.12.1995

Weber, R., Skorupa, W.,
Über den Präzipitationsverlauf von Sauerstoff in mit Sauerstoff implantierten Silicium-Substraten,
Frühjahrstagung der Deutschen Physikalischen Gesellschaft, Berlin, Germany, March 20-24, 1995

Weber, R., Skorupa, W.,
Statistical analysis of silicon dioxide precipitates in oxygen implanted silicon,
E-MRS Spring Meeting: Symp. C "Pushing the limits of ion beam processing:
From engineering to atomic scale issues", Strasbourg, France, May 22-26, 1995

Weishart, H., Matz, W., Skorupa, W.,
Ion beam synthesis by high dose tungsten implantation into 6H-silicon carbide,
ICSCRM - 95, Kyoto, Japan, Sept. 18 - 21, 1995

Weishart, H., Steffen, H.J., Matz, W., Skorupa, W.,
Ion beam synthesis by tungsten implantation into 6H-silicon carbide,
E-MRS Spring Meeting: Symp.D "Purification, Doping and Defects in II-VI materials",
Strasbourg, France, May 22-26, 1995

Weishart, H., Matz, W., Skorupa, W.,
Ion beam synthesis by high dose tungsten implantation into 6H-Silicon carbide,
Int. Symp. on Si heterostructures: from physics to devices, Kreta, Greece, Sept.11-14, 1995

Zorba, T.T., Mitsas, C.L., Siapkas, I.D., Terzakis, G.Z., Siapkas, D.I., Pacaud, Y., Skorupa, W.,
An infrared study of Ge+ implanted SiC,
Int. Symp. on Si heterostructures: from physics to devices, Kreta, Greece, Sept.11-14, 1995

Lectures

Chudoba, Th.,
Härtemessungen in oberflächenmodifizierten Schichten,
TU Dresden, Institut für Oberflächenphysik und Mikrostrukturphysik, Germany, May 1995

Harz, M.,
Spannungsreduzierung anodisch gebondeter Silizium-TEMPAX-Wafer durch thermische Nachbehandlung,
Statusbericht zum Teilvorhaben Si-Si-Fusion- und Si-Glas-Anodic-Bonding im Rahmen des BMFT-Verbundprojektes ANSYS, Förderkennzeichen 13MV0266, Berlin, Germany, Jan. 23, 1995

Harz, M.,
Relaxationseffekte in anodisch gebondeten Silizium-Glas-Wafern,
Institutseminar, TU Dresden, Institut für Halbleiter- und Mikrosystemtechnik, Dresden, Germany, Feb.15, 1995

Harz, M.,
Streßarmes anodisches Bonden von TEMPAX und Silizium,
3. Arbeitstagung der AG "Waferbonden" im Deutschen Verband für Schweißtechnik e.V.,
Chemnitz, Germany, March 28, 1995

Harz, M.,
Ursachen, Berechnung und Reduzierung thermomechanischer Spannungen beim anodischen Bonden,
Seminar, TU Berlin, Bereich Technologien der Mikroperipherik, Berlin, Germany, Nov. 16, 1995

Heera, V., Kögler, R., Skorupa, W., Stoemenos, J.,
Ion beam induced crystallization of 6H-SiC,
Electrotechn. Lab., Photon Process Section,Tsukuba, Japan, Sept. 25, 1995

Heinig, K.-H.,
Collision cascades and ion beam induced phase transitions,
University Newcastle, Australia, Feb.15, 1995

Heinig, K.-H.,
Computer simulation of ion-solid interaction,
University Fribourg, Switzerland, Mar. 1., 1995

Heinig, K.-H., Jentschel, M., Konoplev, V., Börner, H.G.,
Entwicklung einer neuen nuklearen Methode - molekulardynamische Rechnungen zur Simulation dieser Methode und zu Eigenschaften von Interstitials,
Kolloquium am Hahn-Meitner-Institut Berlin, Germany, Feb. 9, 1995

Heinig, K.-H.,
Molekulardynamische Simulation von Ionen-Festkörper-Wechselwirkungen und von Punktdefekten,
Seminar an der TU Dresden, FB Physik, Germany, Sept. 5., 1995

Heinig, K.-H.,
Ion beam - solid interactions studied by computer simulations,
Institute of Semiconductor Physics, Novosibirsk, Russia, Oct. 26., 1995

Heinig, K.-H.,
Computer simulation of sputtering,
University of La Laguna, Spain, Nov. 28., 1995

Heinitz, J.,
Fundamentals of texture measurements with neutrons on steady state and pulsed sources,
Lecture course for students: "Basic principles of modern texture analyses", Dubna, Russia,
March 6-11, 1995

Heinitz, J.,
Characterization and comparison of texture measuring facilities in several research centers,
Lecture course for students: "Basic principles of modern texture analyses", Dubna, Russia,
March 6-11, 1995

Jäger, H.U.,
Bor-Implantation in Silizium - Modellierung von Diffusion und Aktivierung bei niedrigen Ausheiltemperaturen,
15. Treffen der Benutzergruppe "Ionenimplantation", Fraunhofer-Institut für Integrierte Schaltungen, Abt. Bauelementetechnologie (IIS-B), Erlangen, Germany, April 27, 1995

Jäger, H.U.,
Boron ion implantation into crystalline silicon - modeling of diffusion and electrical activation for low annealing temperatures,
Seminar für Trainees, Fraunhofer-Institut für Mikroelektronische Schaltungen und Systeme (IMS2), Dresden, Germany, Nov. 29, 1995

Kögler, R.,
The process of IBIEC in Si,
Dept. of Appl. Phys., Univ. of Barcelona, Spain, May 12, 1995

Lange, K.,
Anodisches Glas-Silizium-Bonden und Silizium-Silizium-Waferbonden,
Bericht zum Gesamtprojekttreffen, BMBF-Verbundprojekt AN-SyS,
Förderkennzeichen 13MV0266, Daimler-Benz Aerospace AG, München, Germany, July 13, 1995

Lange, K.,
Mechanismen des Anodischen Bondens,
Bericht zum Gesamtprojekttreffen, BMBF-Verbundprojekt AN-SyS,
Förderkennzeichen 13MV0266, FhG-IMS, Duisburg, Germany, Nov. 9, 1995

Matz, W.,
Das Projekt der Rossendorfer Beam Line an der ESRF,
Seminar des Institutes für Physik der TU Chemnitz-Zwickau, Germany, Jan 8, 1995

Neelmeijer, C.,
Zerstörungsfreie Diagnose von Kunstwerken am Luft-Protonenstrahl,
Institutskolloquium im MPI Garching, Germany, Dec. 1, 1995

Pacaud, Y.,
Réalisation et modification de matériaux par l'implantation ionique,
Laboratoire des Composites Thermo-Structuraux, (LCTS), UMR-47CNRS-SEP-UB1, France,
June 1, 1995

Panknin, D.,
Buried $(Fe_{1-x}Co_x)Si_2$ layers with variable band gap formed by ion beam synthesis,
Dept. of Appl. Phys., Univ. of Barcelona, Spain, April 8, 1995

Posselt, M.,
Channeling effects and damage accumulation in ion implantation,
Microelectronics Research Center, University of Texas at Austin, TX, USA, Nov. 7, 1995,
Theory and Modeling Group, Lawrence Livermore National Laboratory, Livermore, CA, USA,
Nov. 17, 1995

Posselt, M.,
Theory and computer simulation of ion-beam-induced effects in solids,
Theory and Modeling Group, Lawrence Livermore National Laboratory, Livermore, CA, USA,
Nov. 15, 1995

Posselt, M.,
Ion-solid interaction,
TU Dresden, Institut für Theoretische Physik, Germany, Dec. 12, 1995

Schmidt, B., Lange, K., Grigull, S.,
Charakterisierung von Glasoberflächen mit Hilfe von Ionenstrahl-Analysemethoden,
1. Statusseminar des Verbundvorhabens "Anwendungsgerechte Systemintegration und Zuverlässigkeit für die intelligente mikromechanische Sensorik (AN-SYS)", Berlin, Germany, Jan. 24, 1995

Schmidt, B., Lange, K.,
Si-Oberflächenbehandlung vor dem Bonden und Driftverhalten von Na in TEMPAX,
Statusbericht zum Teilvorhaben Si-Si-Fusion- und Si-Glas-Anodic-Bonding im Rahmen des BMFT-Verbundprojektes ANSYS, Förderkennzeichen 13MV0266, Berlin, Germany, Jan 23, 1995

Schmidt, B.,
Si-Sperrschichtdetektoren mit MeV-implantierten Dotierungsprofilen: Herstellung, Eigenschaften und Anwendungen,
Institutseminar, Universität Hamburg, Institut für Experimentalphysik, Arbeitsbereich Nukleare Meßtechnik, Hamburg, Germany, May 24, 1995

Skorupa, W.,
Ionenstrahlprozesse für SiC,
TU Dresden, Institut für Mikroelektronik, March 1, 1995

Skorupa, W.,
High energy implantation into silicon-State of the art,
National Nano-Device Lab., and Dept.Mat.Sc.&Eng., National Tsing Hua Univ.,Hsinchu,Taiwan,
Feb.3, 1995

Skorupa, W.,
Recent activities at the Rossendorf Ion Beam Modification of Advanced Materials Group,
Dept. of Appl. Phys., Univ. of Barcelona, Spain, June 26, 1995

Skorupa, W.,
Ion beam processing of single crystalline SiC,
CEMES-CNRS, Toulouse, France, June 28, 1995

Skorupa, W.,
Recent activities at the Rossendorf Ion Beam Modification of Advanced Materials Group,
Electrotechn. Lab., Photon Process Section, Tsukuba, Japan, Sept 25, 1995

Skorupa, W.,
Carbon-related defects in ion beam processed silicon,
Instituto de Fisica, Universidade Federal do Rio Grande do Sul, Porto Allegre, Brasilien, Nov 13, 1995

Ullemeyer, K.,
X-ray texture analysis of rocks and its application in geology,
Lecture course for students: "Basic principles of modern texture analyses", Dubna, Russia,
March 6-11, 1995

Ullemeyer, K.,
Alternative methods of texture determination in geology,
Lecture course for students: "Basic principles of modern texture analyses", Dubna, Russia,
March 6-11, 1995

Walther, K.,
Progress Report for the Diffractometers NSHR and Epilon at the 7A beam line of the reactor IBR-2, 4th meeting of the Programme Advisory Committee, Dubna, Russia, Nov 13-14, 1995

Weishart, H.,
Kontaktierung von SiC-Hochtemperaturelektronik,
TU Dresden, Institut für Mikroelektronik, March 1, 1995

Reports

Aldridge, L.P., Sabine, T., Eichhorn, F., Hempel, A.,
SANS spectra from hydrated cement pastes,
BENSC Experimental Report 1994,
Berichte des HMI Berlin, HMI-B 525, May 1995, 346-347

Betzl, M., Gorski, N.,
Untersuchung der Weich-Weich-Wechselwirkung mit Hilfe der Neutronen-Kleinwinkelstreuung,
Abschlußbericht BMBF-Förderprojekt 03-Du3ROS TP03, Au-Nr. A.8-K16

Betzl, M., Walther, K.,
Betrieb eines Texturdiffraktometers hoher Auflösung (Spektrometer NSWR am Impulsreaktor IBR-2 des VIK Dubna),
Abschlußbericht BMBF-Förderprojekt 03-Du3ROS TP01, Au-Nr. F.4-K08

Eichhorn, F., Hempel, A.,
Modernisierung eines Doppelkristalldiffraktometers (das mit zylindrisch gekrümmten perfekten Kristallen arbeitet, für Neutronenkleinwinkelstreuungsuntersuchungen mittels ortsauflösendem Detektor),
Abschlußbericht Projekt 03-EI3ROS-3, F.2-K02

Große, M., Eichhorn, F., Hempel, A.,
SANS investigations of the through-the-thickness variation of the carbide structure in large forgings of the steel 15Kh2MFA,
BENSC Experimental Report 1994
Berichte des HMI Berlin, HMI-B 525, May 1995, 348-349

Große, M., Böhmert, J., Brauer, G., Eichhorn, F., Goerigk, G.,
ASAXS investigations of irradiation-induced precipitates in VVER-440-type reactor pressure vessel steel with high Cu contet,
Jahresbericht (Annual Report) 1994 Hamburger Synchrotronstrahlungslabor HASYLAB am Deutschen Elektronensynchrotron DESY, 535-536

Hempel, A., Eichhorn, F., Reichel, P.,
Methodic study of the double-crystal diffractometer S V-12,
BENSC Experimental Report 1994,
Berichte des HMI Berlin, HMI-B 525, May 1995, 350-351

Hempel, M., Häußler, F., Eichhorn, F., Hempel, A., Baumbach, H.,
Material research on hydrating cement paste and solid state nuclear tract detectors by SANS,
Annual Report 1994,
Frank Laboratory of Neutron Physics, Joint Institute for Nuclear Research, Dubna 1995,
67-70

Pham, M.T.,
Ion beam surface treatment of biomaterials,
FZR-Report, FZR-112, Nov. 1995

Pham, M.T., Howitz, S.,
Abschlußbericht: Entwicklung eines integrierten ISFET-Mikrosystems zur dynamischen iono-metrischen Meßwerterfassung,
Projekt-PT-Nr.0534/044, Nov. 1995

Podurets, K.M., Shilstein, S.S., Eichhorn, F., Hempel, A.,
Observation of the cold neutron refraction at the domain walls systems and at the individual domain walls in silicon iron,
BENSC Experimental Report 1994,
Berichte des HMI Berlin, HMI-B 525, May 1995, 354

Schmidt, B.,
Ionenstrahlsynthese von Nanoclustern,
FZR-Report, FZR-115, Nov. 1995

Skorupa, W.,
Hochenergieimplantation in Silicium,
Abschlußbericht zum BMFT-Fördervorhaben SK3ROS (KFA-PFR), 1995

Tyschenko, I.,
Physical and optical properties of nanocrystals formed by ion implantation,
Final Report for DAAD-Project , Ref. No. 325

Laboratory Visits

Betzl, M.,
JINR Dubna, Frank Laboratory for Neutron Physics, Russia, March 27-April 7, 1995

Boede, W.,
JINR Dubna, Frank Laboratory for Neutron Physics, Russia, March 27-April 7, 1995/Nov 13-24, 1995

Eichhorn, F.,
Russian Research Center, Kurchatov Institute, Moscow, Russia, Aug 13-29, 1995

Heera, V.,
Electrotechn. Lab., Photon Process Section, Tsukuba, Japan, Sept 24-26, 1995

Heinig, K.-H.,
University of Newcastle, Newcastle, Australia, Feb. 13-16, 1995

Heinig, K.-H.,
University of Fribourg, Fribourg, Switzerland, Feb. 26-28, 1995

Heinig, K.-H.,
Institute Laue-Langevin, Grenoble, France, May 10-13,1995

Heinig, K.-H.,
CSNSM Orsay, Paris, France, Sept. 25-28, 1995

Heinig, K.-H.,
Institute of Semiconductors, Novosibirsk, Russia, Oct. 22 - 30, 1995

Heinig, K.-H.,
Institute of Electronics, Tashkent, Uzbekistan, Oct. 29-Nov. 7, 1995

Heinig, K.-H.,
University of La Laguna, La Laguna, Spain, Nov. 23-30, 1995

Heinig, K.-H.,
Russian Research Center - Kurchatov Institute of Atomic Energy, Moscow, Russia,
Dec. 17-20, 1995

Hesse, E.,
Central Microstructure Facility, Rutherford Appleton Lab. Chilton, Didcot, UK, Feb 13-20, 1995

Kögler, R.,
Dept. of Appl. Phys., Univ. of Barcelona, Spain, May 7-13, 1995

Kögler, R.,
MPI für Festkörperforschung, Stuttgart, Germany, Oct 10-13, 1995

Matz, W.,
European Synchrotron Radiation Facility, Grenoble, France, Feb 15-17, 1995/Aug 21-23, 1995
HASYLAB at DESY, Hamburg, Germany, May 5-8, 1995

Pacaud, Y.,
Dept. of Physics, Univ. of Thessaloniki, Greece, April 3-12, 1995

Pacaud, Y.,
Laboratoire des Composites Thermo-Structuraux, (LCTS), UMR-47, CNRS-SEP-UB1, France, May 31-June 1, 1995

Panknin, D.,
Dept. of Appl. Phys., Univ. of Barcelona, Spain, April 23-29, 1995

Posselt, M.,
Intel Corporation, TCAD Department, Santa Clara, CA, USA, Apr. 21, 1995

Posselt, M.,
Institut für Integrierte Systeme der ETH Zürich, Zürich, Switzerland, Sep. 25-Oct. 1, 1995

Posselt, M.,
Theory and Modeling Group, Lawrence Livermore National Laboratory, Livermore, CA, USA, Oct. 16-Nov. 21, 1995

Posselt, M.,
Microelectronics Research Center, University of Texas at Austin, TX , USA, Nov. 6-7, 1995

Prokert, F.,
HASYLAB at DESY, Hamburg, Germany, May 1-8, 1995
Institut für Kristallographie, Universität Tübingen, Germany, March 10-18, 1995

Reichel, P.,
JINR Dubna, Frank Laboratory for Neutron Physics, Russia, March 27-April 7, 1995/
Nov 13-24, 1995
Institute of Nuclear Physics, Rez, Czech Republik, Dec 18-19, 1995

Schell, N.,
European Synchrotron Radiation Facility, Grenoble, France, April 3-13, 1995/Aug 21-23, 1995/
Nov 18-30, 1995
HASYLAB at DESY, Hamburg, Germany, May 1-8, 1995

Schmidt, Br.,
ETH, Zürich, Switzerland, Sept. 25-Oct. 6, 1995

Schmidt, Br.,
University of La Laguna, La Laguna, Spain, Dec. 7-21, 1995

Skorupa, W.,
National Nano-Device Lab., and Dept.Mat.Sc.&Eng., National Tsing Hua Univ., Hsinchu,Taiwan, Feb 2-4, 1995

Skorupa , W.,
Dept. of Appl. Phys., Univ. of Barcelona, Spain, June 26, June 30-July 1, 1995

Skorupa, W.,
CEMES-CNRS, Toulouse, France, June 27-29, 1995

Skorupa, W.,
Electrotechn. Lab.,Photon Process Section, Tsukuba, Japan, Sept 24-26, 1995

Skorupa, W.,
MPI für Festkörperforschung, Stuttgart, Germany, Oct 10-13,1995

Skorupa, W.,
Instituto de Fisica, Universidade Federal do Rio Grande do Sul, Porto Allegre, Brasilien,
Nov 11-14, 1995

Strobel, M.,
CSNSM Orsay, Paris, Fance, Nov. 7-20, 1995

Strobel, M.,
Russian Research Center - Kurchatov Institute of Atomic Energy, Moscow, Russia,
Dec. 4-15, 1995

Teichert, J.,
Central Microstructure Facility, Rutherford Appleton Lab., Chilton, Didcot, UK,
Jan 20-Feb 6, 1995, June 8-20, 1995

Walther, K.,
JINR Dubna, Frank Laboratory for Neutron Physics, Russia, March 13- April 7, 1995/May 24-June 18, 1995/Sept 25-Oct 1, 1995/Nov 13-Dec 1, 1995

Weishart, H.,
MPI für Festkörperforschung, Stuttgart, Germany, Oct 10-13, 1995

Wirth, H.,
MPI für Festkörperforschung, Stuttgart, Germany, Oct 10-13, 1995

Guests

Dr. C.Allen, Materials Science Division, Argonne National Lab., Argonne, IL, USA,
Sept 29-Oct 4, 1995

Prof. M. Behar, Dept. of Physics, Univ.Porto Alegre, Brazil,
Aug 1-Sept 2, 1995

Dr. V. Borodin,
Russian Research Center - Kurchatov Institute of Atomic Energy, Moscow,Russia,
Aug. 7 - Sept. 15, 1995, Nov. 9, - Dec. 23, 1995

L. Calvo-Barrio, Dept. of Physics, Univ. of Barcelona, Spain,
Nov 13-30, 1995

Dr. A. Claverie, CEMES-CNRS, Toulouse, France,
Sept 11-14, 1995

Dr. A. Deshkovskaya, University of Minsk, Belarus,
May 19-Dec 23, 1995

Prof. A. Dvurechenskii, Institute of Semiconductors, Novosibirsk, Russia,
Aug 21-Sept 30, 1995

Prof. G. Gilmer, AT&T Bell Laboratories, Murray Hill, USA,
May 27 - 31, 1995

Hatzopoulos, N., Dept. Electronic and Electrical Eng., Univ. of Surrey, Guildford, UK,
March 1-June 30, 1995

Dr. S. Intarasiri, Institute for Science and Technology, Chiang Mai, Thailand,
Oct 16, 1995-Jan 12, 1996

Dr. M. Jakas, Departamento de Fisica Fundamental, Universidad de la Laguna, Tenerife, Spain,
June 8-22, 1995, Aug. 31-Nov. 4, 1995

Dr. S. Kimura, Photophysics section, Electrotechnical Lab., Tokyo, Japan,
Nov 26-Dec 6, 1995

Dr. V. Klemm, TU Bergakademie Freiberg, Germany,
March 6-April 28, 1995

Dr. V. Konoplev, Institute of Electronics Tashkent, Usbekistan,
Feb. 20-May 19, 1995, Nov. 11-Dec. 21, 1995

Dr. F. Machalett, Dept. of Physics, Univ. of Jena, Germany,
Dec 11-15, 1995

Prof. G. L. R. Mair, Dept. of Physics, Univ. of Athens, Greece,
Sept 18-30, 1995

Prof. V. Magula, Welding Research Institute, Bratislava, Slowakia,
May 2 -14, 1995

Dr. Y. Makita, Photophysics section, Electrotechnical Lab., Tokyo, Japan,
Nov 26-Dec 6, 1995

M. Mařik, Tschechische Akademie der Wissenschaften, Inst. f. Kernphysik, Rež, Czech Republic,
Oct 16-27, 1995

I. Mrotchek, University of Minsk, Belarus,
Nov 1-Dec 23, 1995

Dr. Y. Mussichin, Akademie der Wissenschaften, Physikal.-Techn. Inst., St. Petersburg, Russia,
Nov 12-Dec 31, 1995

Dr. O. Nikolov, Institut für Kernforschung, Sofia, Bulgaria (z.Z. Universität Liverpool, UK),
Nov 5-11, 1995

Prof. A. Ovsjannikov, VIK Dubna, Russia,
Sept 25-Oct 12, 1995

M. Palard,
CSNSM - IN2P3 Orsay, Paris, France,
May 8-June 9, 1995, Nov. 13-Dec. 16, 1995

P. Pelicon, "Jožef Stefan"-Institute, Ljubljana, Slowenien,
Oct 1-31, 1995

Dr. A. Perez-Rodriguez, Dept. of Physics, Univ. of Barcelona, Spain,
Dec 12-19, 1995

Prof. P. Riviere, J. P., Dept. of Physics, Univ. of Poitiers, France,
March 15-19, 1995

Dr. A. Romano-Rodriguez, Dept. of Physics, Univ. of Barcelona, Spain,
Aug 12-31, 1995

J. Rožinek, Tschechische Akademie der Wissenschaften, Inst. f. Kernphysik, Rež, Czech Republic,
Oct 16-27, 1995

Prof. J. Solomon, Dept. of Physics, Univ. of Dayton, OH, USA,
Sept 25-30, 1995

Prof. A. Tolopa, Institute of Applied Physics, Sumy, Ukraine,
Sept 18-Dec 17, 1995

Prof. J. Trushin, Yoffe-Institut, St. Petersburg, Russia,
March 27-April 15, 1995/Oct 30-Nov 15, 1995

Dr. I. Tyschenko, I., Institute for Semiconductor Physics, Novosibirsk, Russia,
Jan 1-31, 1995/Nov 5, 1995-Feb 29, 1996

Dr. E. Verbitskaya, Physikalisch-Technisches Yoffe-Institut, St. Petersburg, Russia,
April 10-July 10, 1995

M. Vlassov, Universität St. Petersburg, Russia,
Nov 13-Dec 9, 1995

Dr. A. E. Volkov,
Russian Research Center - Kurchatov Institute of Atomic Energy, Moscow, Russia,
Sept. 4-Oct. 13, 1995

Dr. R. Yankov, Bulg.Acad.of Sciences, Institute for Electronics, Sofia, Bulgaria,
Feb 26-June 26, 1995/Sept 14-Dec 11, 1995

Dr. I. Zyganov, Staatliche Technische Universität Lipezk, Russia,
Oct 1, 1995- Oct 31, 1996

Awards

Reiss, S.,
Young Scientist Award
European Materials Research Society, Strasbourg, May 1995

PhD Theses

Küchler, R.
Der nichtlineare Einfluß hoher Eigenspannungen in Beschichtungen auf die Ausbreitungsgeschwindigkeit von Ultraschalloberflächenwellen,
TU Dresden, Dezember 1995

Mathar, R.,
Dielektrische Theorie des elektronischen Energieverlustes schwerer Ionen in Festkörpern,
TU Dresden, Juni 1995

Diploma Theses

Engwicht, D.,
Entwicklung von Visualisierungen und deren Umsetzung in Computeranimationen und Videosequenzen zur Darstellung evolutionärer physikalischer Prozesse mit Hilfe des Advanced Visualization System

Frei, T.,
Erweiterung der Funktionalität des Visualisierungssystems AVS durch die Entwicklung neuer Moduli zur Lösung wissenschaftlicher Visualisierungsaufgaben des Forschungszentrums Rossendorf

Meetings organized by the texture group in the Frank Laboratory of Neutron Physics, Dubna

Lecture course for students: "Basic principles of modern texture analyses",
Dubna, Russia, March 6-11, 1995

International Workshop "Mathematical Methods of Texture Analysis",
Dubna, Russia, March 21-24, 1995
Co-organizer: Institut für Metallkunde und Metallphysik der TU Clausthal-Zellerfeld

Workshop "Neutronographische Spannungsanalyse", Potsdam, Germany, Dec 11, 1995
Co-organizer: Abt. Recentes Spannungsfeld im GeoForschungszentrum Potsdam

Meetings organized by the institute

COST 515 WP1 Workshop, Rossendorf, Germany, October 12-13, 1995
38 participants of 10 European countries
Chairmen: W. Möller (FZ Rossendorf), M. Remy (University Nancy)
Local Organizer: A. Kolitsch, I. Heidel

Patents

Brutscher, J.,
Verfahren zur Implantation von Ionen in leitende bzw. halbleitende Werkstücke mittels Plasmaimmersionsionenimplantation (PIII) und Implantationskammer zur Durchführung des Verfahrens,
DP 195 38 903.4, offengelegt am19.10.95

Fukarek, W.,
Schnelles Spektroskopisches Ellipsometer,
DP 43 43 490.8-42, offengelegt am 22.6.1995

Howitz, S., Pham, M.T., Fiehn, H.,
Mikrokapillare mit integrierten chemischen Mikrosensoren und Verfahren zu ihrer Herstellung,
EP 0 633 468 A2, 11.01.1995

Howitz, S., Pham, M.T.,
Mikro-Fluiddiode,
DE 05 005 A1, 24.08.1995

Pham, M.T., Howitz, S.,
Mikrofluidik-Manipulator,
EP 0 672 834 A1, 20.09.1995

Pham, M.T., Howitz, S.,
Chemischer Mikro-Analysator,
EP 0 668 500 A2, 23.08.1995

Departments of the Institute

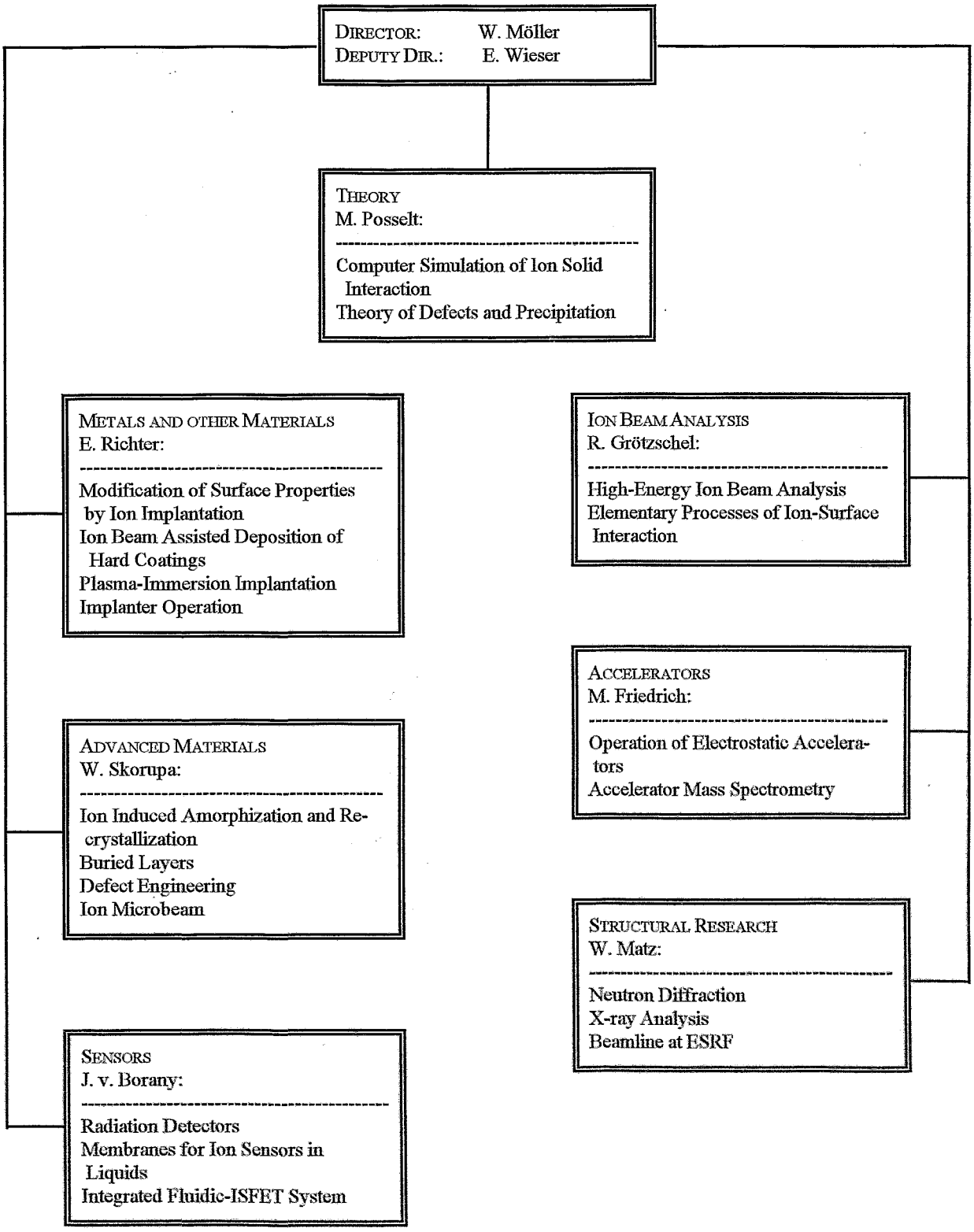

List of Personnel

Director: Prof. W. Möller **Deputy Director:** Prof. E. Wieser

Scientific Staff:
Permanent:

Dr. M. Betzl
Dr. L. Bischoff
Dr. J. von Borany
Dr. W. Bürger
Dr. F. Eichhorn
Dr. M. Friedrich
Dr. W. Fukarek
Dr. D. Grambole
Dr. R. Grötzschel
Dr. R. Günzel
Dr. V. Heera
Dr. K.-H. Heinig
Dr. H.-U. Jäger
Dr. A. Kolitsch
Dr. R. Kögler
Dr. U. Kreißig
Dr. W. Matz
Dr. A. Mücklich
Dr. C. Neelmeijer
Dr. D. Panknin
Dr. M.T. Pham
Dr. M. Posselt
Dr. F. Prokert
Dr. H. Reuther
Dr. E. Richter
Dr. B. Schmidt
Dr. J. Schöneich
Dr. H. Seifarth
Dr. W. Skorupa
Dr. J. Steffen
Dr. J. Teichert
Dr. H. Tyrroff
Dr. M. Voelskow

Post Docs:

Dr. J. Brutscher
Dr. N. Schell
Dr. M. Weiler
Dr. H. Weishart

Stipendiaries:

Dr. Y. Pacaud
Dr.N. Pessoa Barradas
Dr. G. Sene

Projects:

M. Bürger
Dr. H. Fiehn
M. Harz
D. Henke
Dr. E. Hesse
Dr. S. Howitz
Dr. J. Hüller
Dr. O. Kruse
R. Küchler
Dr. K. Lange
M. Mäder
P. Nitzsche
Dr. M. Seidel
T. Vopel
Dr. K. Walther

PhD Students:

K. Albe
F. Brenscheidt
T. Chudoba
M. Dobler
S. Grigull
A. Hempel
T. Henkel
M. Jentschel
W. Jiang
S. Mändl
R. Mathar
D. Möller
U. Müller
M.F. Plass
Br. Schmidt
M. Strobel
G. Sun
S. Reiß
R. Weber
H. Wirth

Diploma Students:

V. Beyer
D. Engwicht
T. Frei

Technical Staff:
Permanent:

J. Altmann
R. Aniol
G. Anwand
I. Beatus
W. Boede
K.-D. Butter
W. Gäßner
B. Gebauer
H.-J. Grahl
P. Hartmann
F. Herrmann
G. Hofmann
M. Iseke
S. Klare
R. Kliemann
L. Kumpf
A. Kunz
G. Küster
D. Maul
M. Mißbach
I. Morawitz
K. Müller
F. Nötzold
W. Probst
A. Protze
E. Quaritsch
P. Reichel
B. Richter
M. Roch
E. Rost
C. Rußig
B. Scheumann
H. Schluttig
E. Schmidt
G. Schnabel
J. Schneider
A. Scholz
J. Schröter
C. Schulenberg
H. Seifert
K. Sommerfeld
U. Strauch
K. Thiemig
S. Turuc
A. Vetter
A. Weise
G. Winkler
I. Winkler

Projects:

G. Franz
H. Hempel
A. Schneider